Physical Oceanography and Circulation

Tom Weingartner, Ying-Chih Fang, Peter Winsor
University of Alaska Fairbanks
Institute of Marine Science 115 O'Neill
Fairbanks, AK 99775
tjweingartner@alaska.edu

Abstract

We examined the time-varying circulation and water mass properties of the Chukchi Sea shelf surrounding Hanna Shoal using shipboard surveys and oceanographic moorings funded through the BOEM COMIDA program. The COMIDA data were complimented by other data sets whose collection was supported by Shell, ConocoPhilips, Statoil, the North Slope Borough, and other BOEM-supported projects in the region. We found that the sea ice and associated surface meltwaters are transported westward on average in response to the prevailing northeasterly winds. The vertically-averaged flow was eastward and parallel to the isobaths northwest of Hanna Shoal, in agreement with many circulation models but this flow component was negligible or slightly westward northeast of Hanna Shoal, in contrast to these same models. These observations imply that there should be, on average, zonal convergence in the flow north of Hanna Shoal. Presumably this convergence is associated with an off-shelf deflection of the eastward-flowing water observed to the northwest of Hanna Shoal. The near-bottom circulation flows clockwise around the northwest and northeast sides of Hanna Shoal on average, and this finding agrees with the numerical models. The circulation differences between the model and observations on the northeast side of Hanna Shoal are due to baroclinic pressure gradients. These oppose the barotropic forcing and tend to drive a counterclockwise flow, around the Shoal. This inference is consistent with the mean vertical velocity shear from the moorings and the fall hydrographic data. We also found that the water column on the shelf to the east of Hanna Shoal remains strongly stratified year-round with this stratification maintained by cold, dilute meltwater in the upper 15 – 20 m and near-freezing, salty winter water on the bottom. This winter water is advected into the region by the bottom flow. Its source is elsewhere on the Bering or Chukchi Sea shelves. It is transported into the area east of Hanna Shoal after being carried northward through the Central Channel and then around Hanna Shoal and or northward through Herald Valley and then eastward across the outer shelf. Some winter water may form locally over Hanna Shoal, especially in years when grounded ice atop the Shoal results in the formation of latent heat polynyas. Our results also imply that waters on the shelf east of Hanna Shoal are renewed much more slowly than elsewhere in the Chukchi Sea.

In summer and fall meltwater and winter water were the major water masses in the COMIDA study area. Bering Sea summer waters (Alaskan Coastal Water and Bering Sea Water) were often found south of ~71.5°N. The boundary separating the water masses to the north from those to the south consists, in most years, of a strong, surface front between the meltwater and the Bering waters and, perennially, by a sub-surface front between the winter and Bering water masses. The subsurface front is not necessarily contiguous with the surface front. The subsurface front appears to extend zonally from the southwest side of Hanna Shoal eastward to the head of Barrow Canyon. Very likely this front extends northward and parallel to the eastern side of the Central Channel along the west side of Hanna Shoal. The latter inference is consistent with

summer sea ice concentration maps, which effectively delineate the northward path of the Bering Sea Water in the Channel, COMIDA CTD sections collected along the northwest side of Hanna Shoal in August 2012 and 2013, which captured waters clearly influenced by BSW, and the September 2013 acrobat section that detected intrapycnocline eddies along the HSNW mooring line. The meltwater/Bering summer water fronts are baroclinically unstable, a process which leads to the formation of intrapycnocline, anticyclonic eddies that propagate across the front carrying Bering summer waters. The existence of these fronts (and the associated frontal processes) and the strength and depth of the pycnocline in the COMIDA sampling area depends upon the vertical and horizontal distributions of meltwater, winter water, and Bering Sea summer waters. In contrast to 2012 and 2013, there was no evidence of surface fronts in 2011 and the shelf stratification in that year was much weaker. These differences were attributed to the dearth of meltwater on the northeastern Chukchi shelf in 2011 compared to the other years.

The sub-surface front is likely a perennial feature of the shelf and it appears to be an effective barrier that prevents waters from south of Hanna Shoal from moving onto the shelf to the east of the Shoal. Consequently, north of the front, the shelf has an arctic-flavor insofar as it is heavily stratified due to surface meltwater and very dense winter waters over the bottom. The circulation also changes on either side of the front. South of the front the summer waters are carried northward over the shelf from Bering Strait and then into Barrow Canyon. Here the shelf circulation is engaged in the meridional transfer of Pacific Ocean waters into the Arctic Ocean. North of the front the exchange appears to be primarily zonal. Meltwater and sea ice are advected westward and dense bottom waters are transported eastward.

1. Introduction

There were two main goals of the COMIDA physical oceanography component. The first was to understand the time-varying circulation and water mass properties of the Chukchi shelf around Hanna Shoal. The second, and closely linked, goal was to provide the physical oceanographic context for the biological and chemical components of COMIDA. Numerical models (e.g., Winsor and Chapman, 2004; Spall, 2007) indicate that the mean circulation around Hanna Shoal includes a clockwise flow around the north and east sides of the Shoal (Figure 1). Until this study, however, there were no systematic observations available upon which to evaluate these model results. Thus an essential aspect of this study was to compare these model predictions with the observations. This report summarizes some of the results from the 2012 - 14 field programs.

The Hanna Shoal portion of the Chukchi Sea shelf is, as suggested by the models (Figure 1), intimately connected to the broader Chukchi Sea circulation field, including Bering Strait. From Figure 1, these connections include flow moving eastward across the outer shelf and shelfbreak which derives from Herald Canyon (or Valley). According to the model, the northward flow through the Central Channel rounds the western side of Hanna Shoal and joins the flow moving eastward from the Herald Valley. Some of this merged flow feeds the eastward-flowing shelfbreak current that continues into the Beaufort Sea (e.g. Pickart, 2004; Nikolopoulos et al., 2005) and some continues southward and back onto the northeastern Chukchi shelf east of Hanna Shoal. Eventually this component of the flow exits the shelf via Barrow Canyon. According to the model the mean flow on the shelf east of Hanna Shoal is very sluggish because the streamlines are far apart here) in comparison to the much swifter flow on the northwest side of Hanna Shoal (and Barrow Canyon and the Central Channel for that matter).

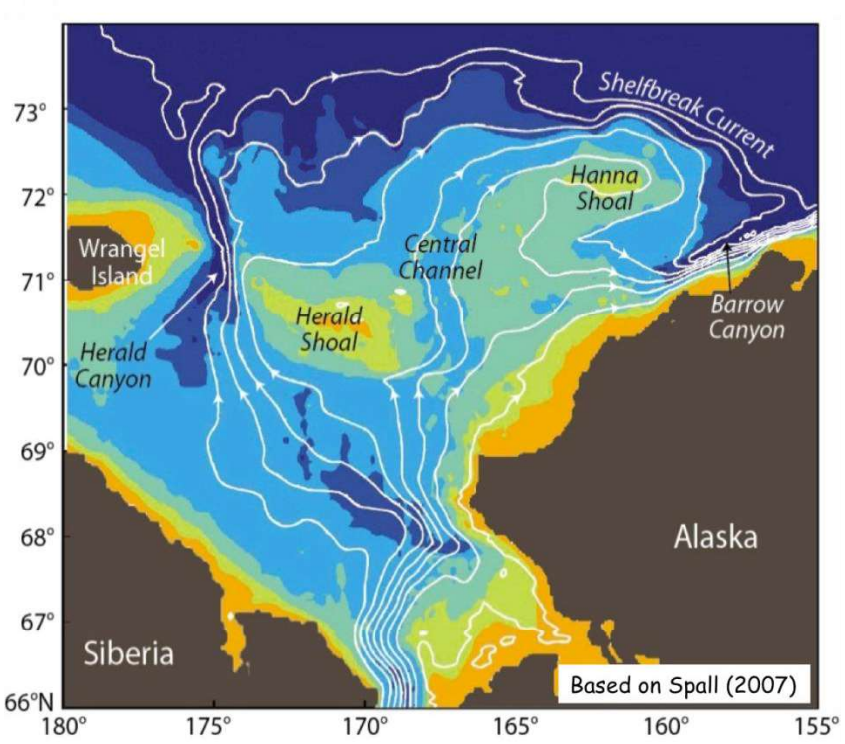

Figure 1. The mean, vertically-integrated flow over the Chukchi Sea shelf based on the model study of Spall (2007). Note the clockwise circulation around the northern and eastern sides of Hanna Shoal.

In addition one of the streamlines wraps nearly around the south side of Hanna Shoal before reflecting eastward. This implies that fluid is being carried from the north side of Hanna Shoal to the south side. In contrast, the streamlines farther south indicate a mean eastward flow that transports water across the central shelf from the Central Channel and the southern Chukchi Sea toward Barrow Canyon. The Hanna Shoal circulation affects regional ecosystem processes; including distribution of biogeochemical properties and benthic and planktonic organisms. Indeed, as will be evident, the circulation greatly affects the hydrographic properties around Hanna Shoal in the summer months, at the very least, when COMIDA sampling took place.

The physical oceanographic measurements supported by COMIDA included oceanographic moorings, shipboard CTDs and Vessel-Mounted ADCPs (VM-ADCP). There were, however, many additional data sets derived from other projects, including those supported by BOEM, the oil industry (primarily through the Chukchi Sea Environmental Studies Program; CSESP), the North Slope Borough-Shell Baseline Studies Program, and the Alaska Ocean Observing system. These data sets include additional oceanographic moorings and high-frequency radar (HFR) deployed along the Chukchi Sea coast (Weingartner et al., 2013a), satellite-tracked drifters (Weingartner et al., 2015), and shipboard CTD data sets (Weingartner et al., 2012, 2013b, 2014). Many of these data sets are still being analyzed and some have only recently become available. The expanded data sets allow us to extend the COMIDA results in time and space. The COMIDA data sets complement these other programs insofar as many of the COMIDA measurements were made in previously un- or undersampled regions of the Chukchi Sea shelf. In aggregate, these various data sets will allow a comprehensive synthesis of the physical

oceanography of the northeastern Chukchi Sea shelf. Although we include elements of these data sets herein, this synthesis will be part of the BOEM-supported NE Chukchi Circulation Study.

2. Methods

2.1 COMIDA Moorings

The COMIDA mooring component included 6 current meter moorings. These were initially deployed in August 2012 from the *USCG Healy*. They were then recovered and re-deployed in September 2013 from the *Norseman II* under the direction of Chief Scientist, Peter Winsor (UAF). The same vessel and Chief Scientist conducted the recoveries in September 2014. The moorings were targeted for deployment on the 40, 50, and 60 m isobaths to the northwest and northeast of Hanna Shoal. By choosing the same isobaths on either side of Hanna Shoal we could test for continuity of mass transport under the assumption that the mean flow is primarily geostrophic, as predicted by the models. In practice we deployed the deepest moorings on the 56 m isobath in 2012 and 2013 because heavy ice impeded *Healy* from reaching the deeper depths on the northwest side of Hanna Shoal in a timely manner. The mooring nomenclature is a combination of Hanna Shoal (HS) and the direction from the Shoal (northwest or northeast), the isobath depth, and the deployment year. For example, HSNW60-12 is the mooring deployed on the 56 m isobath northwest of Hanna Shoal in 2012.

The mooring positions and deployment times are listed in Tables I and II for the respective years. In both years each mooring had an ADCP and a MicroCat temperature/conductivity/pressure (T/C/P) recorder mounted about 3 m above bottom (Figure 2). Moorings HSNE50-12 and HSNE60-12 included an ISCAT at ~25 and 30 m depth, respectively. The ISCAT is a T/C/P sensor that records data internally and onto a data logger mounted to the mooring float 3 m above bottom. The ISCAT includes a weak link mechanism that allows it to detach from the mooring should a deep ice keel snare the ISCAT and begin dragging the mooring. The ISCAT and MicroCat pairs on these moorings were designed to measure changes in water column stratification.

Similarly configured moorings were deployed in 2013 using fresh equipment. Unfortunately the two ISCATs scheduled for re-deployment in 2013 were not functioning correctly and consequently were not deployed. Overall the data quality was very good, however, the ADCP on mooring HSNW60-12 failed about 1 month after deployment. Furthermore, this mooring could not be recovered in 2014 following its second deployment. The acoustic release did not respond to shipboard interrogations and a tight ship schedule and poor weather precluded undertaking extensive search and dragging operations for this mooring. It is quite possible that HSNW60-13 is still in position and that it can be recovered by a future dragging operation. Figure 3 shows a high-resolution map of the 2012-14 COMIDA mooring locations and Figure 4 shows the time lines of available data from each COMIDA mooring.

Figure 5 shows the locations of the COMIDA moorings in 2012 and 2013 along with the other moorings for which we have acquired data over the years from 2008-2009 through 2014-2015. Most of these moorings were sponsored by the oil industry. UAF recently obtained these data sets and will combine them with the Hanna Shoal moorings. There were also a comprehensive

Figure 2. A photograph of the assembled COMIDA ADCP and MicroCat TCP mooring. The ADCP electronics are housed in the center well on the syntactic foam float. The MicroCat sits in a separate well with only the sensors exposed.

set of moorings in Barrow Canyon (indicated by the prefix BC), which were jointly funded by industry and BOEM (2010-2012), then by BOEM (2012-2014), and finally by UAF (2014-2015). Under separate BOEM funding, Dr. Robert Pickart deployed an array of 6 moorings (CS1 – CS5; FM1) that extended across the shelfbreak and slope from the end of the COMIDA HSNE line. These moorings were deployed from the USCG *Healy* in October 2013 and recovered in fall 2014.

Of particular relevance to the COMIDA array is the 2011-2012 industry array, which included a set of three moorings to the NW of Hanna Shoal (HS01 – HS03). Data from these moorings will be valuable in comparing with the COMIDA array because, as we will show, the ice and water properties in late summer and fall of 2011 were quite different than in 2012-14. In addition the three industry moorings (HS04 – 06) on the southeast side of Hanna Shoal will be used to assess flow in here. Finally we note that the moorings in Central Channel (Crackerjack), Site 1 (or CPAI01) in Klondike, and Burger and Statoil all provide records that will be useful in addressing circulation around Hanna Shoal and interannual variations in the circulation over this shelf.

Table 1. 2012-2013 Mooring specifics. 2012 deployments were conducted in ice; recoveries were undertaken in open water.

Mooring	Deployment date 2012	Latitude (° ‘ N)	Longitude (° ‘ W)	Depth* (m)	Instruments
[2]HSNW56-12	August 16	72 41.745	164 31.935	56.2	ADCP/uCat
[1,2]HSNW50-12	August 16	72 31.517	164 5.944	50.3	ADCP/uCat
[2]HSNW40-12	August 16	72 16.85	163 32.034	40.7	ADCP/uCat
[3]HSNE40-12	August 21	72 07.267	160 29.735	40.4	ADCP/uCat
[4]HSNE50-12	August 21	72 09.749	159 07.346	49.7	ADCP/uCat/IC[6]
[4]HSNE56-12	August 21	72 10.88	158 33.092	56.2	ADCP/uCat/IC[6]

[1]Mooring was to include ISCAT (IC), but this was snagged on ice and broke from mooring during deployment. ISCAT was recovered and was used on NE moorings.
[2]Moorings were deployed in rotting broken ice, with local concentrations of ~40 – 60%.
[3]Mooring was deployed in rotting broken ice, with regional concentrations of ~70%.
[4]Moorings were deployed in rotting broken ice, with regional concentrations of ~50%.
[6]HSNE50 ISCAT was at 24.9 m below surface, or 24.8 meters above bottom (mab)
[6]HSNE56 ISCAT was at 29.5 m below surface, or 26.7 meters above bottom (mab)

Table 2. 2013-2014 Mooring specifics. All mooring operations in 2013 and 2014 were conducted in ice-free waters.

Mooring Name	Deployment Date 2013	Latitude (° ‘ N)	Longitude (° ‘ W)	Depth (m)	Instruments
HSNE-40-13	September 8	72°07.257'	160°29.540'	41	ADCP/uCat
HSNE-50-13	September 8	72°09.768'	159°07.297'	50	ADCP/uCat
HSNE60-13	September 8	72°10.892’	158°33.069'	57	ADCP/uCat
HSNW-40-13	September 9	72°16.852'	163°32.073'	41	ADCP/uCat
HSNW-50-13	September 9	72°31.514'	164°05.949'	51	ADCP/uCat
HSNW60-13	September 9	72°41.753'	164°31.943'	57	ADCP/uCat

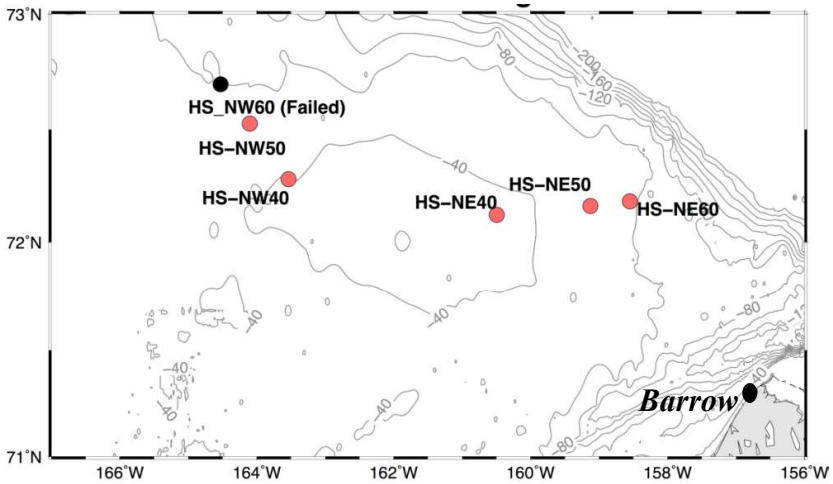

Figure 3. Bathymetric map showing the locations of the COMIDA current meter moorings in 2011 – 12 and 2013 – 14.

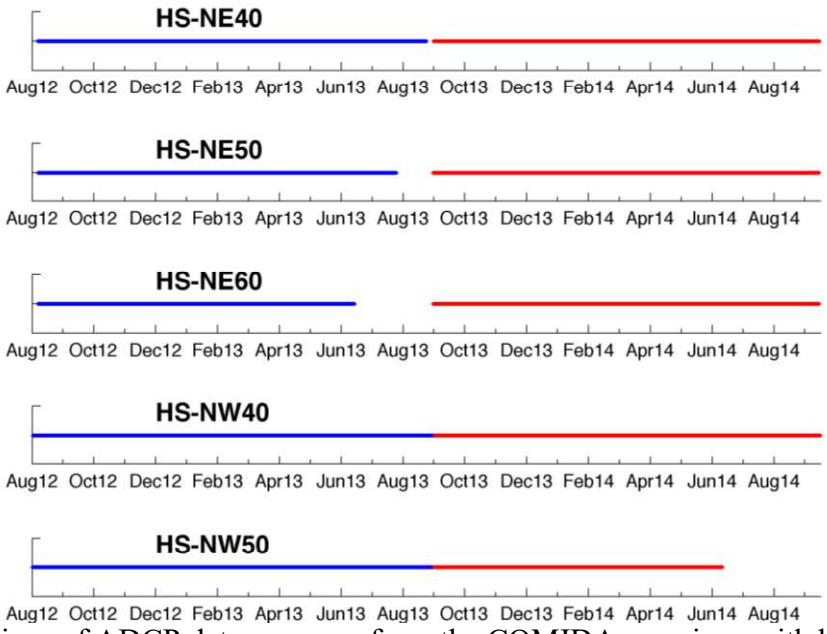

Figure 4. Timelines of ADCP data recovery from the COMIDA moorings with blue being for 2012-2013 and red for 2013-2014 deployments.

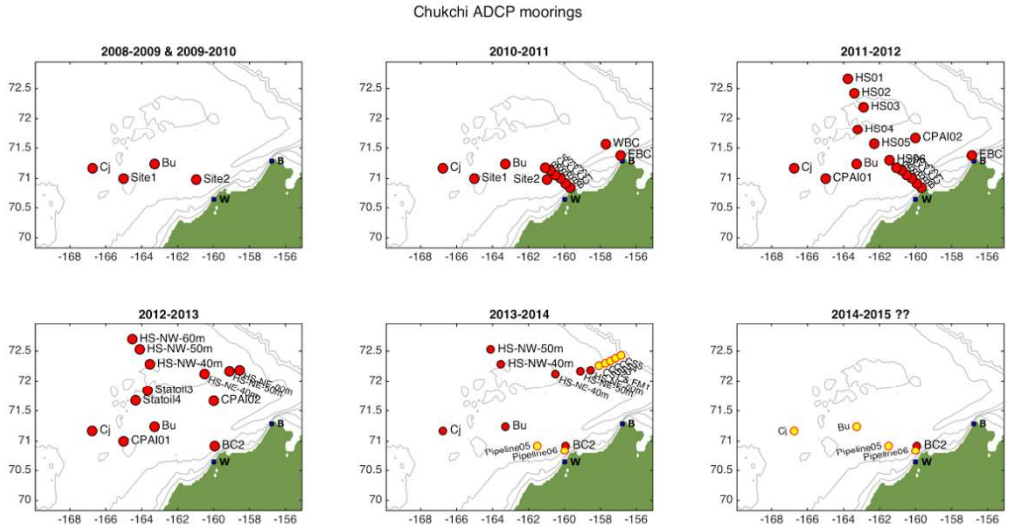

Figure 5. Maps of ADCP mooring locations in the northeastern Chukchi Sea shelf from 2008 – 2015. Yellow dots indicate moorings in which data processing is not yet complete.

2.2 CTD and VM-ADCP Data

The *Healy* COMIDA cruises enabled the collection of CTD and VM-ADCP data using a 150 kHz unit. Winsor's cruises, which serviced the COMIDA moorings, also occupied several CTD sections around Hanna Shoal and over the HSNW and HSNE and Chukchi slope array of Pickart. Data along these sections were collected with a towed-vehicle (Acrobat) that provides high resolution (~250 m in the horizontal and 1 m in the vertical) CTD data along the transect. Weather and schedule constraints did not permit sampling extensively over the slope array. The *Norseman II* also carries a 300-kHz vessel-mounted ADCP (VM-ADCP), which enabled us to

collect velocity data in both 2013 and 2014. Pickart also conducted CTD and VM-ADCP sections on either side of Hanna Shoal in summer 2014 from the USCG *Healy* as part of his NSF-funded program in the Chukchi Sea. All of these data sets are presently being processed.

We used the 3-hourly winds produced by NOAA's North American Regional Reanalysis (NARR) models (Mesinger et al., 2006) derived for gridpoints north (72.5°N, 161.5°W) and south (71.3°N, 161.5°W) of Hanna Shoal as a representation of the wind field over the northeastern Chukchi Sea. Ice-concentration maps for May, June, July, October, and November of 2011 - 2013, were prepared based on data obtained by the Special Sensor Microwave Imager (SSMI) satellite sensor and processed according to Spreen et al. (2008). More detailed maps of the ice edge for the August – September periods of each year were prepared based on analyses performed by the National Snow and Ice Date Center (NSIDC).

3. Results

3.1 Sea Ice

The annual formation and decay of sea ice exerts a tremendous influence on the circulation and water properties of the Chukchi Sea shelf. In general, ice begins forming in late October and effectively covers the entire shelf, including Bering Strait, by late December. Ice retreat commences in late April or early May with northward retreat in Bering Strait. By mid-July the ice edge is typically north of 70°N, with prominent embayments forming in Herald Valley, the Central Channel, and Barrow Canyon (Paquette and Bourke, 1981; Martin and Drucker, 1997). Ice continues to retreat through September, although it may remain over Hanna Shoal throughout the summer. In fact, the interannual variability in summer/early fall ice cover over Hanna Shoal is probably very large. To illustrate this we show maps of the seasonal evolution of ice retreat for May, June, and July 2011 - 2013 (Figures 6 – 8). Figure 9 has more detailed maps of the ice edge (defined by 15% ice concentration limit per NSIDC) in the northeastern Chukchi Sea for the August – September period of the same years.

The sequence of SSMI ice concentration maps provides a broader perspective of the seasonal evolution in sea ice retreat over the Chukchi shelf prior to the 2012 and 2013 surveys and also contrasts these years with 2011. In each year, substantial ice retreat began in Bering Strait by the third week of May. In 2011 (Figure 6), ice began retreating simultaneously from the northwest coast of Alaska in May, with a substantial fraction of the northeastern Chukchi Sea (south of 70°N) ice-free by the 3rd week of June. Ice continued to retreat northward through July, with the shelf effectively ice-free by the end of July. In contrast, ice retreated more slowly in 2012 and 2013. In 2012 (Figure 7), ice retreated in Bering Strait and along the northwest coast of Alaska through mid-June, but then the retreat stalled, or even reversed, into mid-July. At this time the ice-edge embayments in Herald Valley, the Central Channel and Barrow Canyon were evident, but substantial concentrations of ice remained over Hanna Shoal. In 2013 (Figure 8), the ice-edge embayments were evident by 1 July and the southernmost limit of sea ice in the northeastern Chukchi at ~70^{o}N by mid-June. By late July much of the western Chukchi Sea was ice-free, but heavy concentrations of ice remained over the northeastern shelf, particularly east of, and over Hanna Shoal.

The northeastern Chukchi Sea was, for all practical purposes ice-free in August and September 2011 (Figure 9, top). In 2012 ice remained over Hanna Shoal and portions of the shelf south of Hanna Shoal into mid-September (Figure 9, middle). This same basic pattern held in 2013 (Figure 9, bottom), except that the ice-edge retreated rapidly from south of Hanna Shoal on 1 September to north of the shelfbreak by mid-September. In both of the August COMIDA cruises visual observations from the bridge of the *Healy* indicated that thick ice was grounded atop Hanna Shoal. According to A. Mahoney [University of Alaska, Fairbanks, AK, pers. comm. January 2015], this thick ice grounded on Hanna Shoal in late winter of both 2012 and 2013. Eicken and Mahoney (2015) argue that the source of this ice is, in general, not pack ice that drifts southwestward from the polar basin, but heavily deformed ice displaced westward after detaching from the stamukhi zone of the Alaskan Beaufort Sea. . (Other potential sources for this thick ice would be from Ellesmere and Banks Island regions of the Arctic Ocean, where the thickest multi-year ice of the Arctic Ocean is traditionally found.)

The reasons for these year-to-year differences in ice retreat are not readily apparent, but they do not appear to be related to August and September winds (Figure 10). In both 2011 (light ice year) and 2013 (heavy ice year) the winds were persistently from the northeast (and moderately strong). In contrast, the winds in August 2012 (heavy ice year) were from the south and southwest. By fall in all years the winds strengthened and were generally northeasterly.

On an even more local level Figures 11 and 12 show the evolution of sea ice as detected by the upward-looking ADCPs at each mooring location for the 2012 – 2013 and the 2013 – 2014 deployments, respectively. In 2012 ice concentrations increased very rapidly in late October at all locations simultaneously. This appears to have been largely due to advection of the pack ice from the basin onto the shelf due to northerly winds. Later we show that the stratification over this portion of the shelf is shallow, very strong and persistent. As such, the stratification may enhance the onset of ice formation by confining ocean heat loss to the atmosphere to a very shallow surface layer. Figure 13 shows the SSMI ice concentrations, which indicate open water was present over all mooring sites in late October 2012, but that 100% coverage had developed by mid-November. Ice concentrations of ~100% persisted through June 2013, although it appears that the springtime decrease in ice concentrations began earlier at the HSNW moorings than at the HSNE moorings. This is consistent with the late June and early July 2013 ice concentrations maps (Figure 8), which indicates lower ice concentrations on the western and northwestern sides of Hanna Shoal compared to the eastern side.

Sea ice concentrations also increased more or less simultaneously at all locations in late October 2013 as well. The ice cover developed much more erratically than in 2012, however, as ice concentrations varied between 0 and 100% between late October and mid-November before uniform concentrations of 100% set in by late November. The ice concentration time series in Figure 12 indicates that the ice actually set up later at the HSNW moorings than at the HSNE moorings. This asymmetry in the timing of ice setup is also evident in the SSMI fall ice concentration maps for 2013 (Figure 13). The mooring time series ended too early in summer 2014 to tell if there was an asymmetric retreat of the ice on either side of Hanna Shoal. SSMI imagery from summer 2014 (not shown) indicates that ice concentrations decreased more rapidly on the western side of the Shoal compared to the east, at least through mid-July. Thereafter, the ice retreat appeared to progress more uniformly on either side of the Shoal.

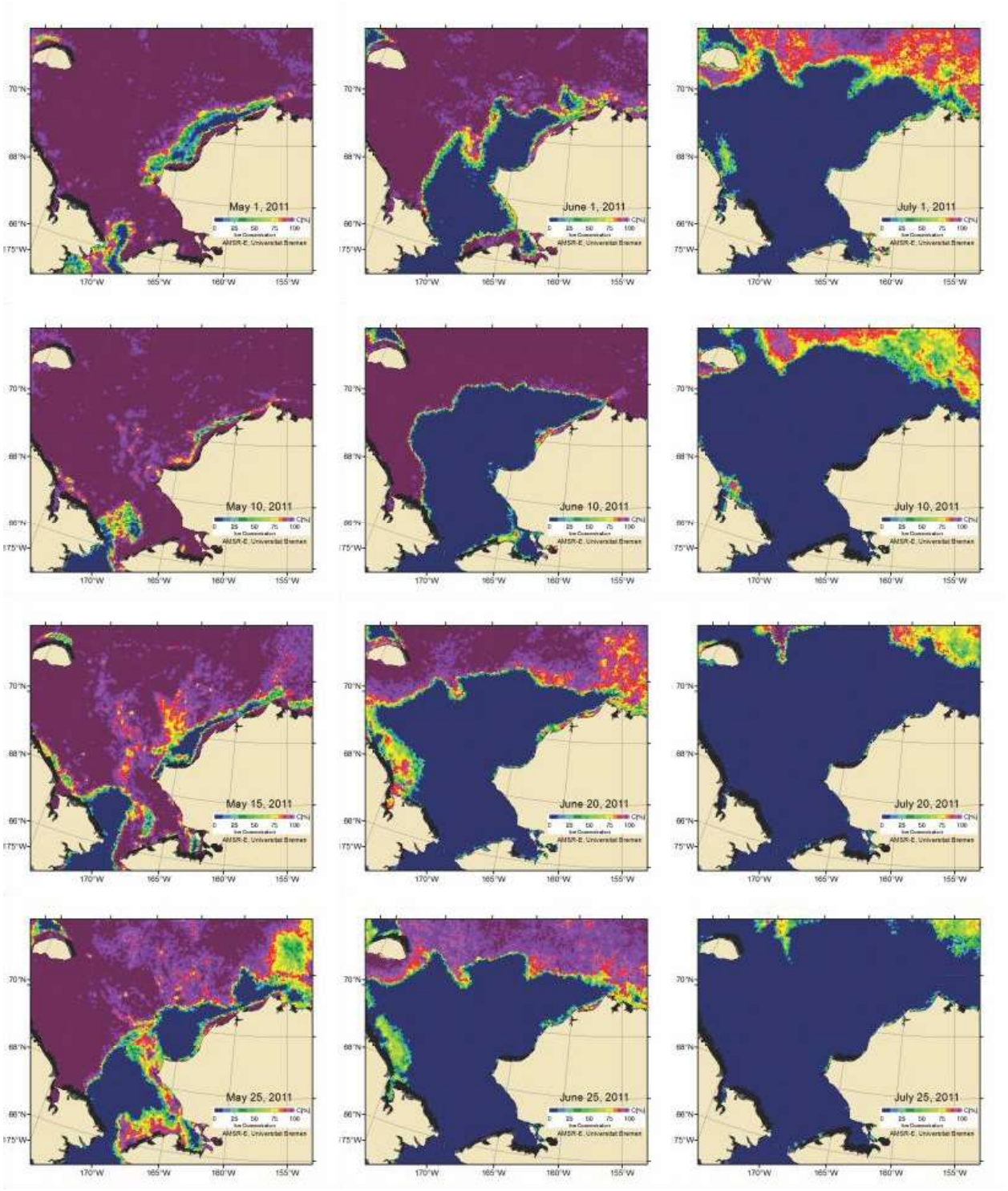

Figure 6. SSMI sea ice concentration maps for the Chukchi shelf in 2011: May (left column), June (middle column) and July (right column).

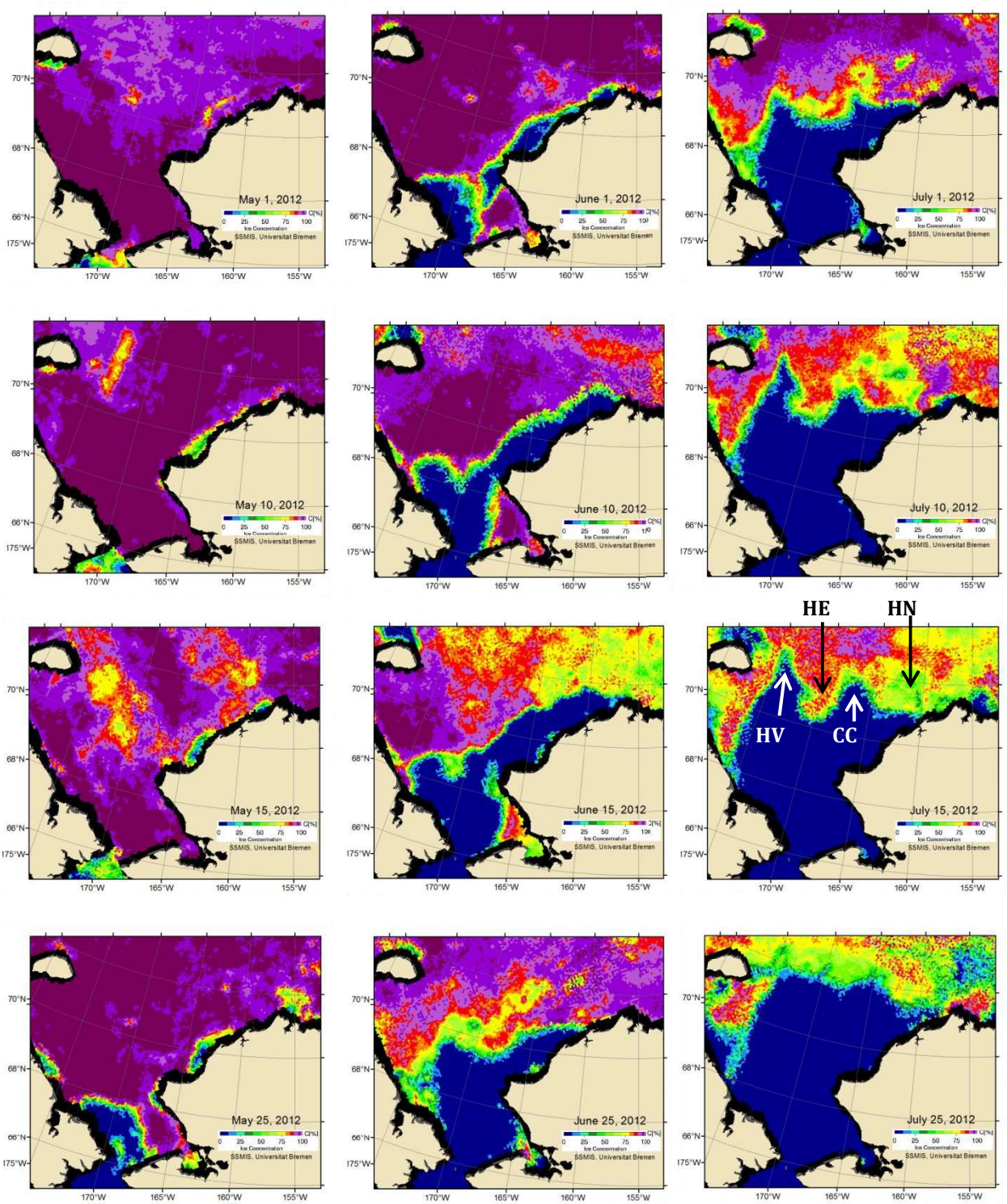

Figure 7. Sea ice concentration maps in 2012 for May (left), June (middle), and July (right). The labels on the July 15 map refer to Hanna (HN) and Herald (HE) shoals, the Central Channel (CC), and Herald Valley (HV).

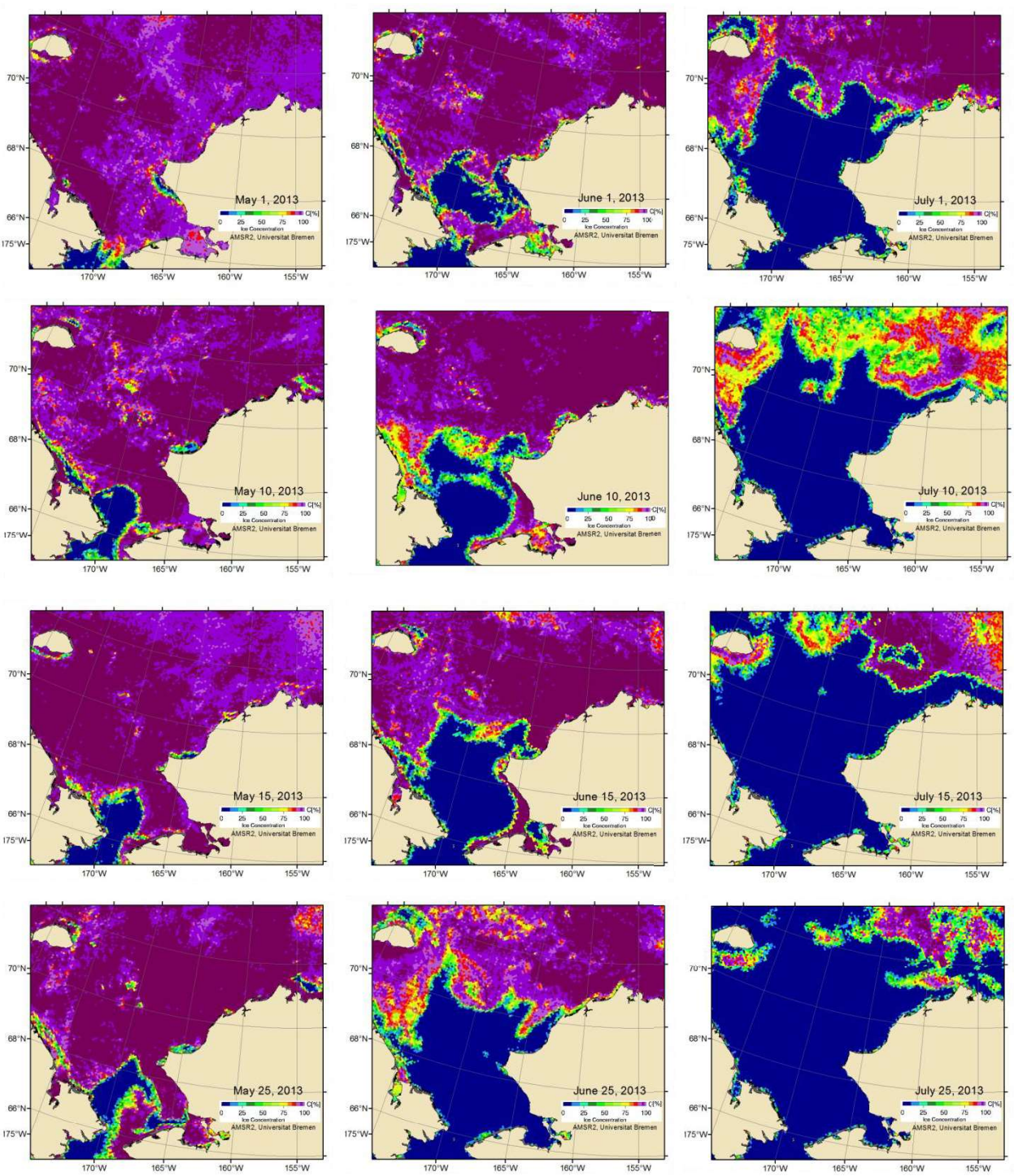

Figure 8. Sea ice concentration maps in 2013 for May (left), June (middle), and July (right).

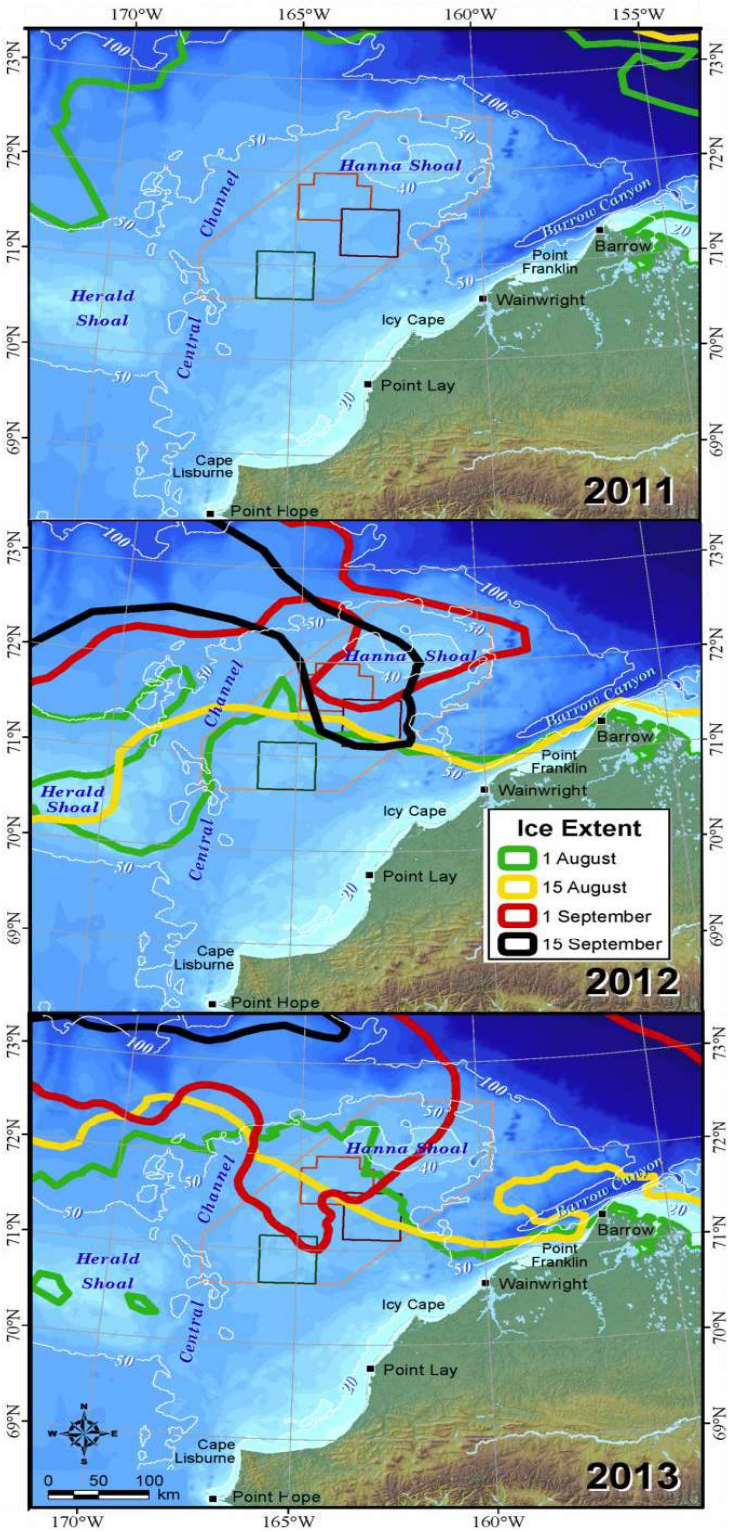

Figure 9. Locations of the ice-edge (15% ice concentration contour as determined by the NSIDC) on August 1 and 15 and September 1 and 15 for 2011 (top), 2012 (middle), and 2013 (bottom).

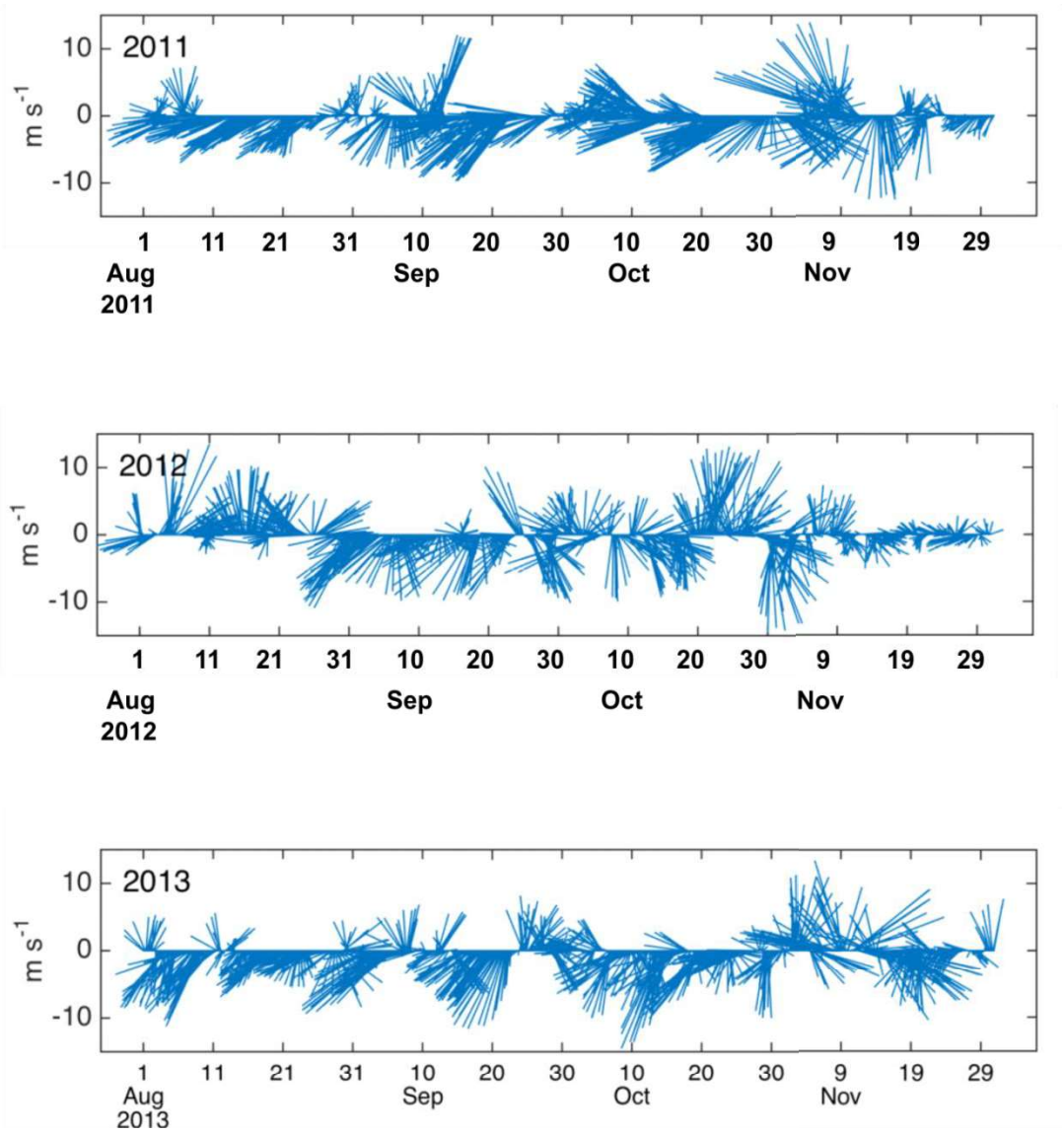

Figure 10. Time series of wind vectors over the northeastern Chukchi Sea for the August – November periods of 2011 (top), 2012 (middle), and 2013 (bottom).

The interannual and spatial differences in the timing of autumn ice set-up will result in different patterns of air-sea heat flux because sea-ice is an effective insulator of the ocean. Spatial differences in these heat fluxes may well leave spatial signatures in the fall distribution of ocean surface temperatures and salinities.

The bottom-tracking capability of the ADCP instruments enabled measuring sea ice velocities and the ice drift is summarized in Figure 14. In both years, the mean ice drift was westward at 2 - 5 cm s^{-1}. The variance ellipses indicate that the standard deviations are 2 – 4 times the magnitude of the mean. The ellipse orientations are approximately zonal, implying that the variability in ice drift is primarily in the east-west direction, although for the most part these ellipses are not strongly polarized. Interestingly the ellipse orientations with the largest polarizations are at HSNE50-13 and at HSNE60-13; the former was zonally polarized while the latter was meridionally-polarized. The drift was spatially coherent and, at all sites, directed approximately

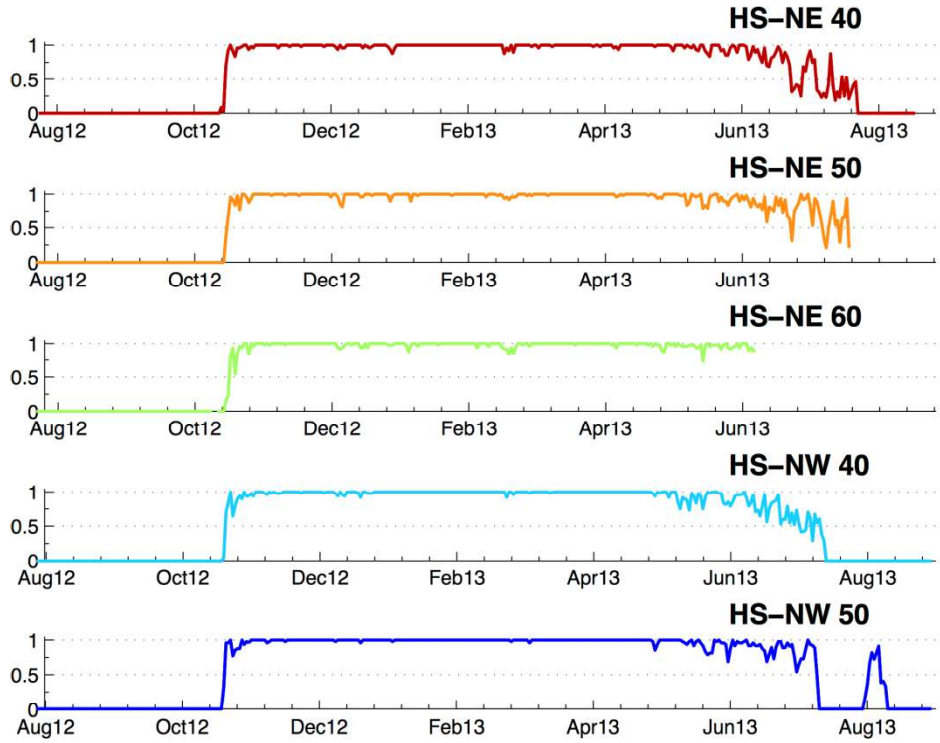

Figure 11. Ice concentration time series for 2012 – 13at each mooring location based upward-looking ADCPs.

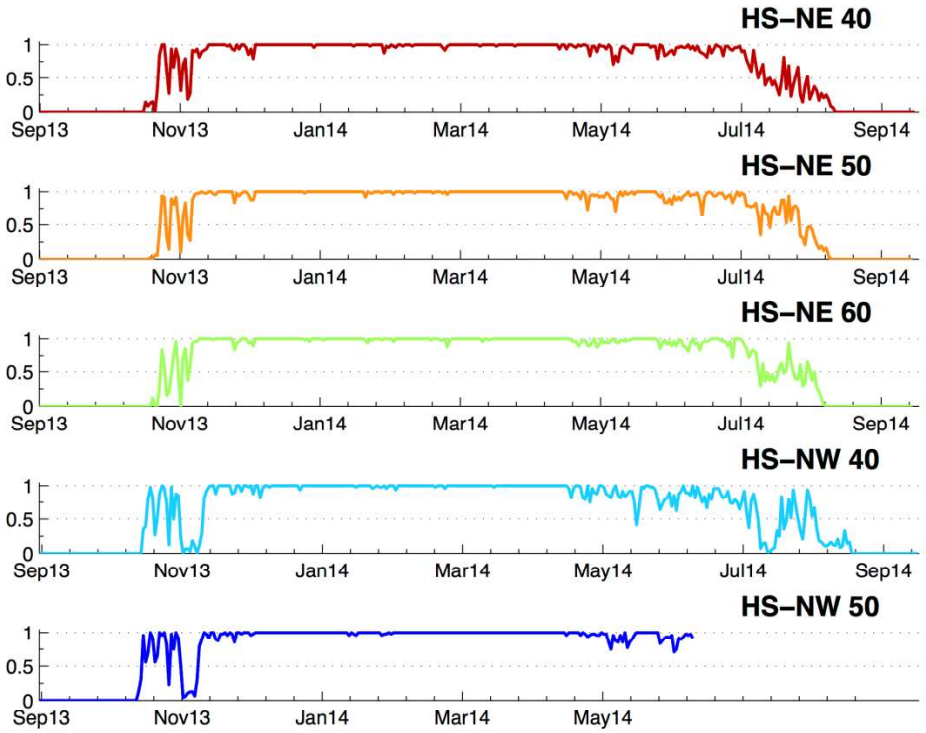

Figure 12. Ice concentration time series for 2013 – 14 at each mooring location based upward-looking ADCPs.

45° to the right of the wind. Note that the winds in both years were from the northeast with the mean speed in 2012 – 13 being about 3 m s^{-1} and in 2013 – 14 the mean speed was ~1.5 m s^{-1}.

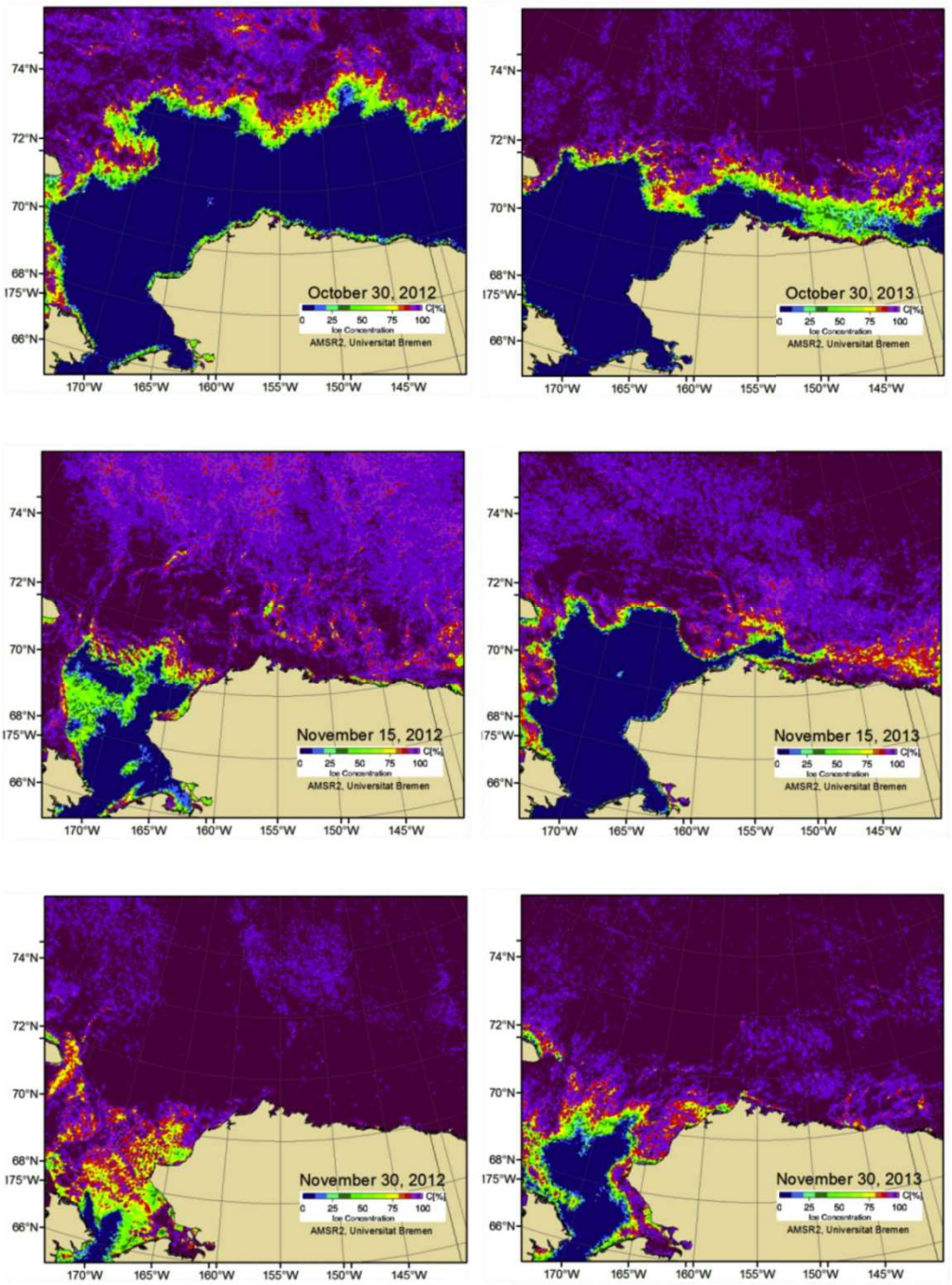

Figure 13. The evolution of sea ice concentrations as seen on 30 October top), 15 November (middle), and 30 November (bottom) for 2012 (left column) and 2013 (right column).

Finally, the mean 2013 – 14 ice velocities at the HSNW moorings were about half those at the HSNE moorings. Although the scales over which we view these differences are large, the means suggests that the ice drift may have been convergent over Hanna Shoal in 2013 – 14. Such convergence could lead to deformation of the ice pack and grounding. Based on the mean ice velocities, there was no evidence of convergence over the 2012 – 13 deployment.

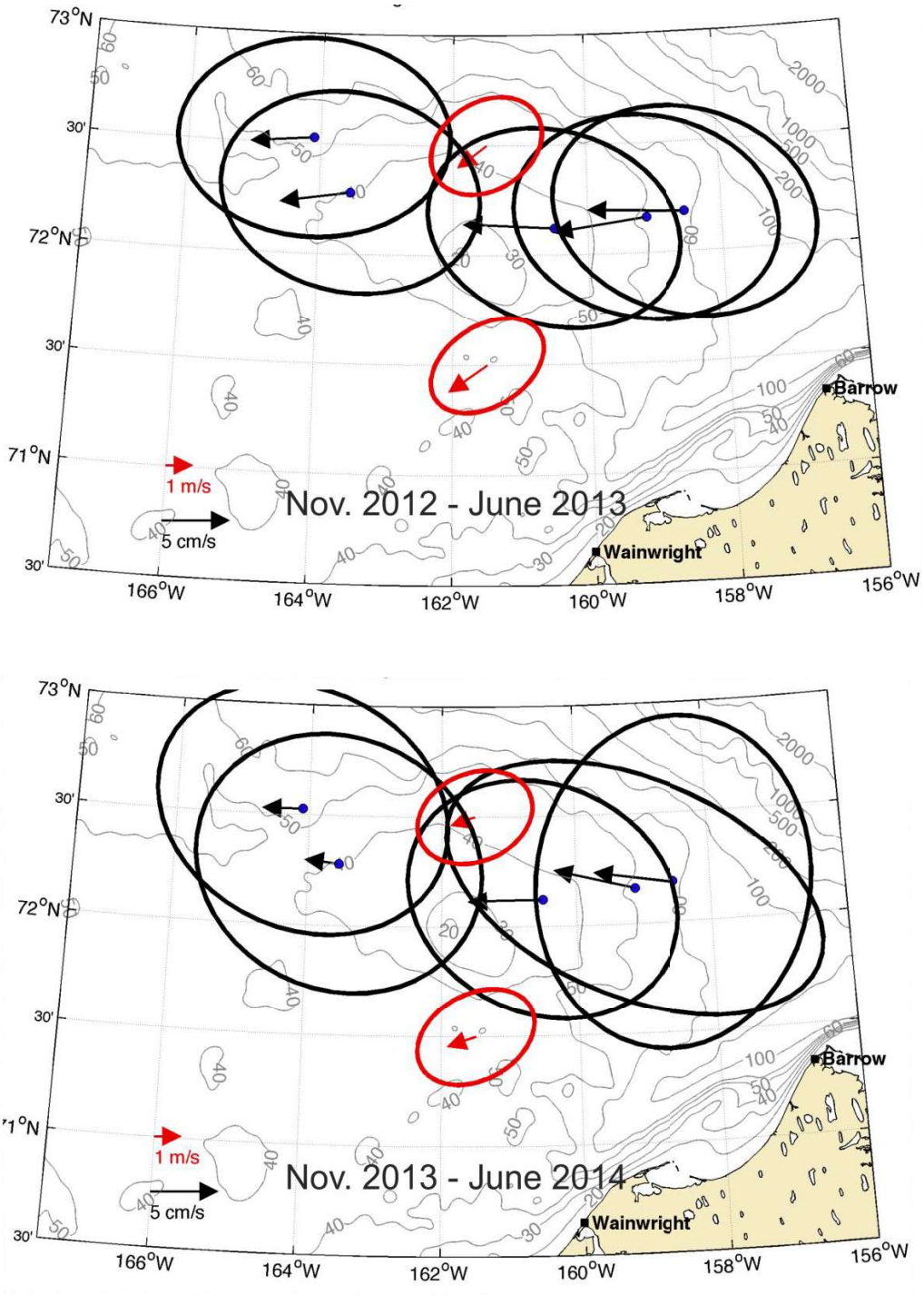

Figure 14. Mean vectors and variance ellipses for sea ice (black) and winds (red) for the periods of November 2012 – June 2013 (top) and from November 2013 – June 2014 (bottom).

3.2 Sub-inertial Currents

In this section we examine the current variability at both long and short periods; long periods are the sub-inertial motions of 3 days or longer. The shorter period current variations of interest are inertial (~12 hour) and the subject of Section 3.3. The sub-inertial currents were formed by low-pass filtering the original time series with a 40-hr cutoff period. Figure 15 shows the low-pass filtered current components at each site in both years for the 40 and 50 m moorings. Figure 16 shows the same data sets for both years from HSNE60. Several general observations emerge from these figures. First, in both years the currents at the NE moorings had greater vertical shear than those at the NW moorings. Second, in 2012 – 13 the flow at both HSNW50 and HSNW40 was mainly eastward, whereas in 2013 – 14 there were more westward flow events, with these occurring primarily in winter. Third, there were also more westerly flow events in the NE moorings in 2013 – 14 compared to the 2012 – 13. Fourth, the velocity data at the NW mooring do not appear to be strongly correlated with the velocities at the NE moorings. This last impression was confirmed by computing the rotary coherences among mooring pairs. Although not shown, we have done this for the currents at the near-surface, the mid-depth (22 m), and bottom (10 m above bottom). Over the low-frequency portion of the current spectrum (e.g., periods > 3 days), the rotary coherence squared values vary from 0.4 to 0.6 for moorings within ~60 km of one another, but decrease to ~0.3 or less at distances >60 km.

Using the same plotting convention as applied to the ice drift, Figure 17 summarizes the record length means and variances for the near–surface currents for both deployment periods. The means and ellipses for these currents were very similar to the ice drift. In both years the near-surface drift was nearly westward with current speeds averaging ~3 cm s^{-1} at the HSNE moorings in 2012 – 13 and about half that at the HSNW moorings for the same deployment period. For the 2013 – 14 deployment, the record-length means were approximately twice as large as those from the corresponding sites in the previous year. Upper ocean current ellipses were large and isotropic.

The near-surface record-length average currents were consistent with the trajectories of satellite-tracked drifters released at the time of deploying the HSNE50-13 and HSNW50-13 moorings (Figures 18 and 19, respectively). The cluster-averaged speeds were ~5 cm s^{-1} although maximum sustained speeds were ~40 cm s^{-1}. In both cases the clusters drifted ~200 km westward in less than 2 months under the prevailing northeasterly winds. Although the winds are the presumable causative agent for this drift, we note that the winds only explain about 30% (20%) of the current variability for the HSNE (HSNW) cluster.

Figure 20 shows the record-length means and ellipses for the vertically-averaged currents. In both years the vertically-averaged flow was eastward on the northwest side of Hanna Shoal at speeds of from 3 to 7 cm s^{-1}. On the east side of the Shoal the mean flow was negligible for the 2012 – 13 deployment but westward at ~2 cm s^{-1} for the 2013 – 14 average. The current ellipses tend to be oriented parallel to the isobaths and their semi-major and –minor axes indicate that the standard deviations are many times the magnitude of the mean. These results have major implications on the along-isobath continuity of the flow field around the north side of Hanna Shoal for they imply that the flow is convergent between the northwest and northeast sides of Hanna Shoal. How that convergence arises is unclear, but it implies a cross-isobath transport,

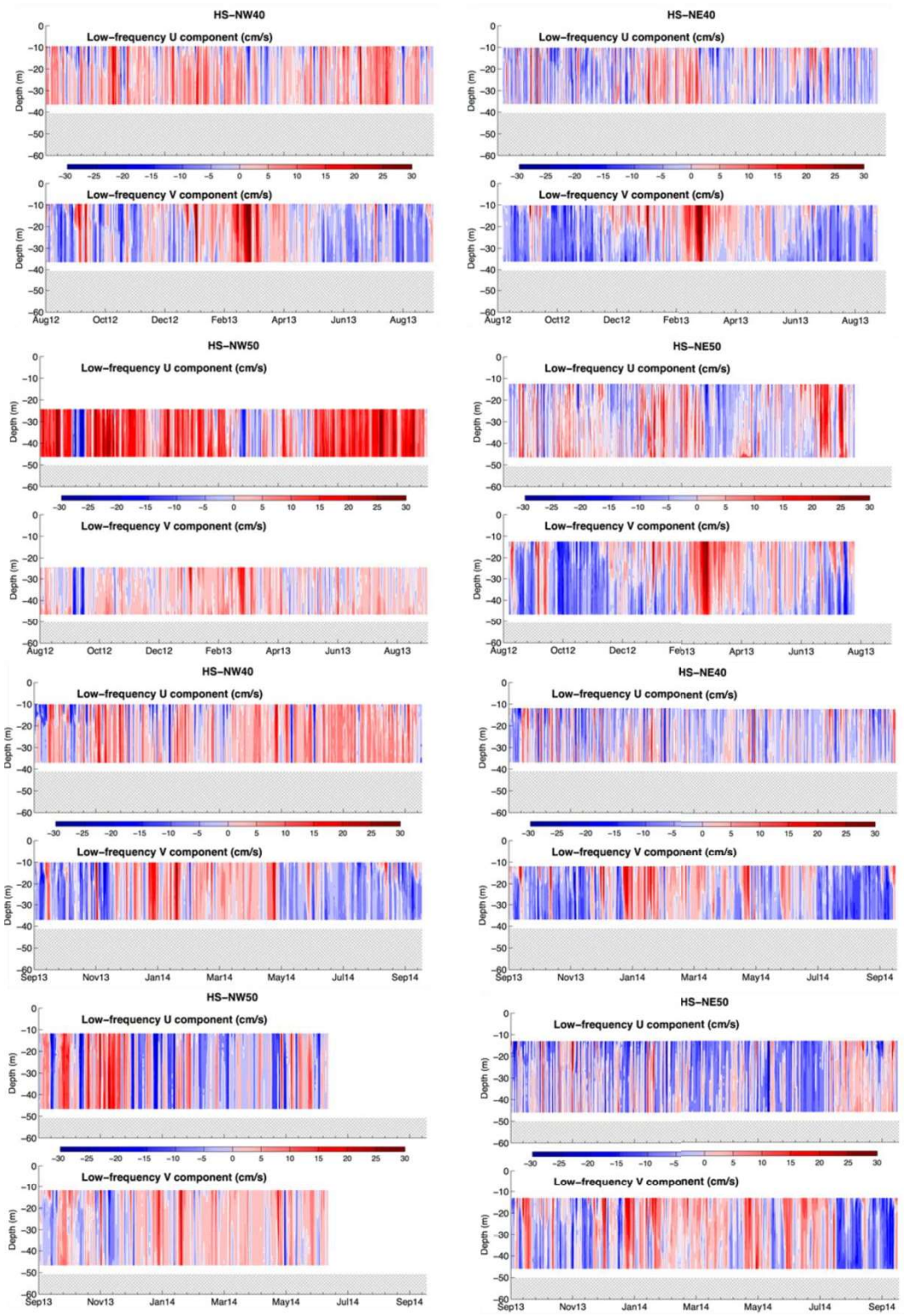

Figure 15. Zonal (U) and Meridional (V) components of velocity as a function of depth and time for moorings HSNW40, HSNW50, NSNE40, HSNE50 for both the 2012 – 13 and 2013 – 14 deployment periods.

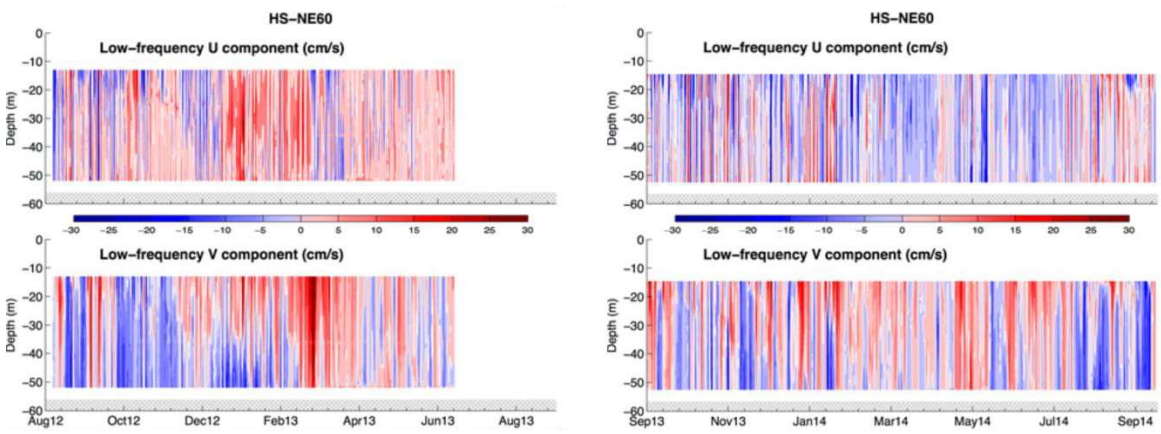

Figure 16. Zonal (U) and Meridional (V) components of velocity as a function of depth and time for moorings HSNE60 mooring for both the 2012 – 13 and 2013 – 14 deployment periods.

which presumably would be directed toward the shelfbreak and deeper water rather than southward and onto Hanna Shoal.

We next examine the near-bottom currents (e.g., 10 meters above bottom; mab) in Figure 21. Northwest of Hanna Shoal the currents were eastward and in the same direction as the vertically-averaged flow and opposite in the direction of the near-surface flow. Turning to the east side of Hanna Shoal the bottom currents were southward in 2012 – 13 and, although not shown, were somewhat stronger in summer and fall than in winter. In 2013 – 14, the bottom currents were considerably weaker east of Hanna Shoal, but nevertheless showed a southward tendency at least at HSNE40 and HSNE60.

In summary, the record-length means from both mooring deployments indicate a westward drift of sea ice and surface waters on either side of Hanna Shoal. The vertically-averaged flow was convergent on the north side of the Shoal, with an eastward flow on the northwest side of Hanna Shoal and weak or westward flow on the eastern side of the Shoal. The bottom water followed a clockwise circulation pattern with swifter flow on the northwest side of the Shoal and weaker and southward flow on the eastern side of the Shoal.

As noted previously in our description of the drifters, the local winds did not account for a large fraction of the current variations. A particularly good example of the loose connection between the winds and currents is evident upon comparing the mean February and October 2013 current vectors and ellipses (Figure 22). The mean winds in both of these months were quite similar; ~5 m s^{-1} from the northeast. In February 2013 the bottom water flowed northward on average at ~ 5 cm s^{-1} at all locations. By contrast in October 2013 the mean bottom water flow was southward at all locations except HSNW50, where the flow was eastward. These differential responses to similar "local" winds suggest that the circulation around Hanna Shoal is, at least, in part remotely forced. The exact nature of this forcing is uncertain at this time, but a more inclusive analysis, which includes a large amount of additional mooring data, may resolve this issue.

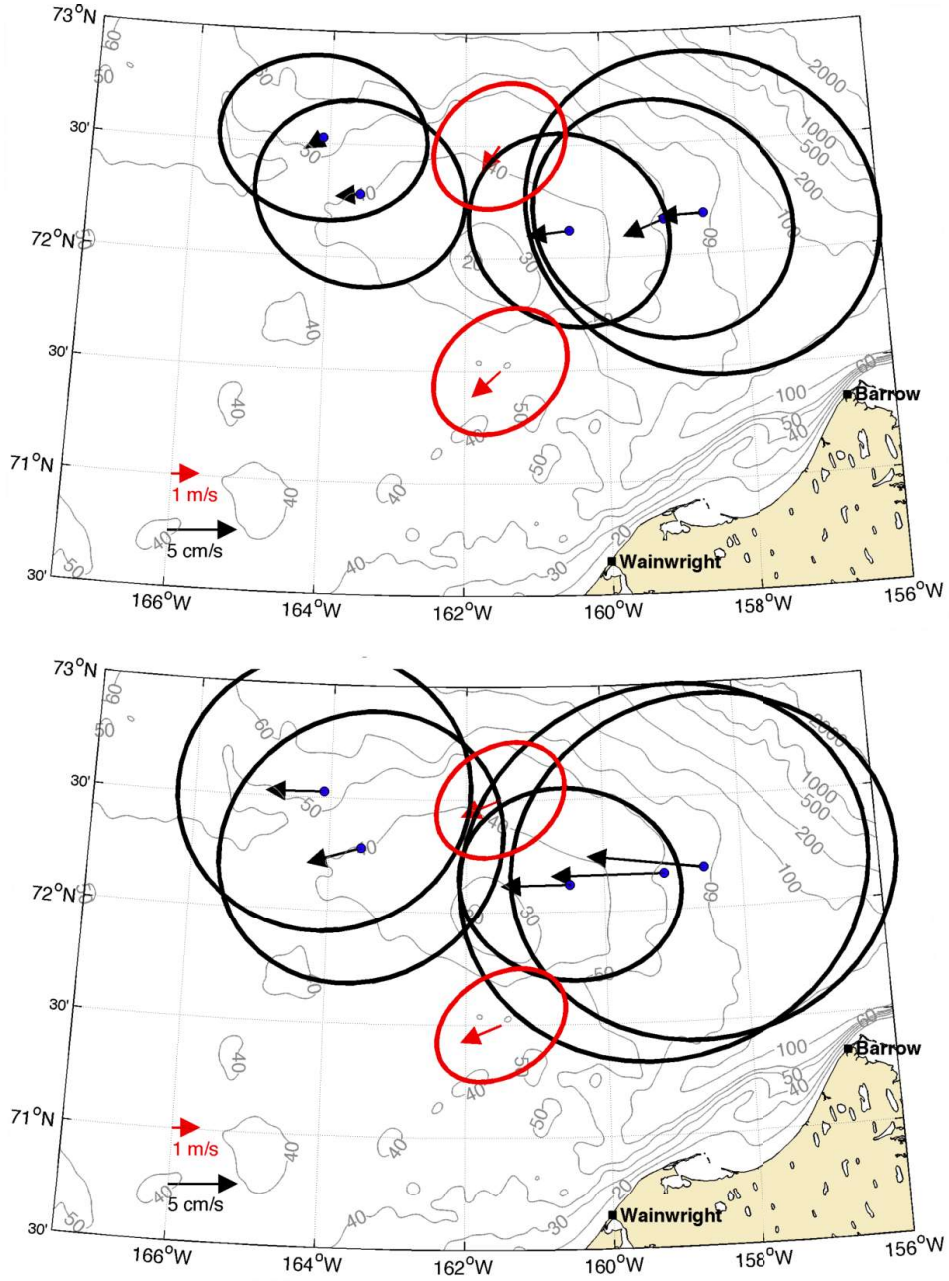

Figure 17. Mean vectors and variance ellipses for the uppermost ADCP bin (black) and winds (red) for the 2012 – 2013 deployment (top) and the corresponding period in 2013 – 2014 (bottom).

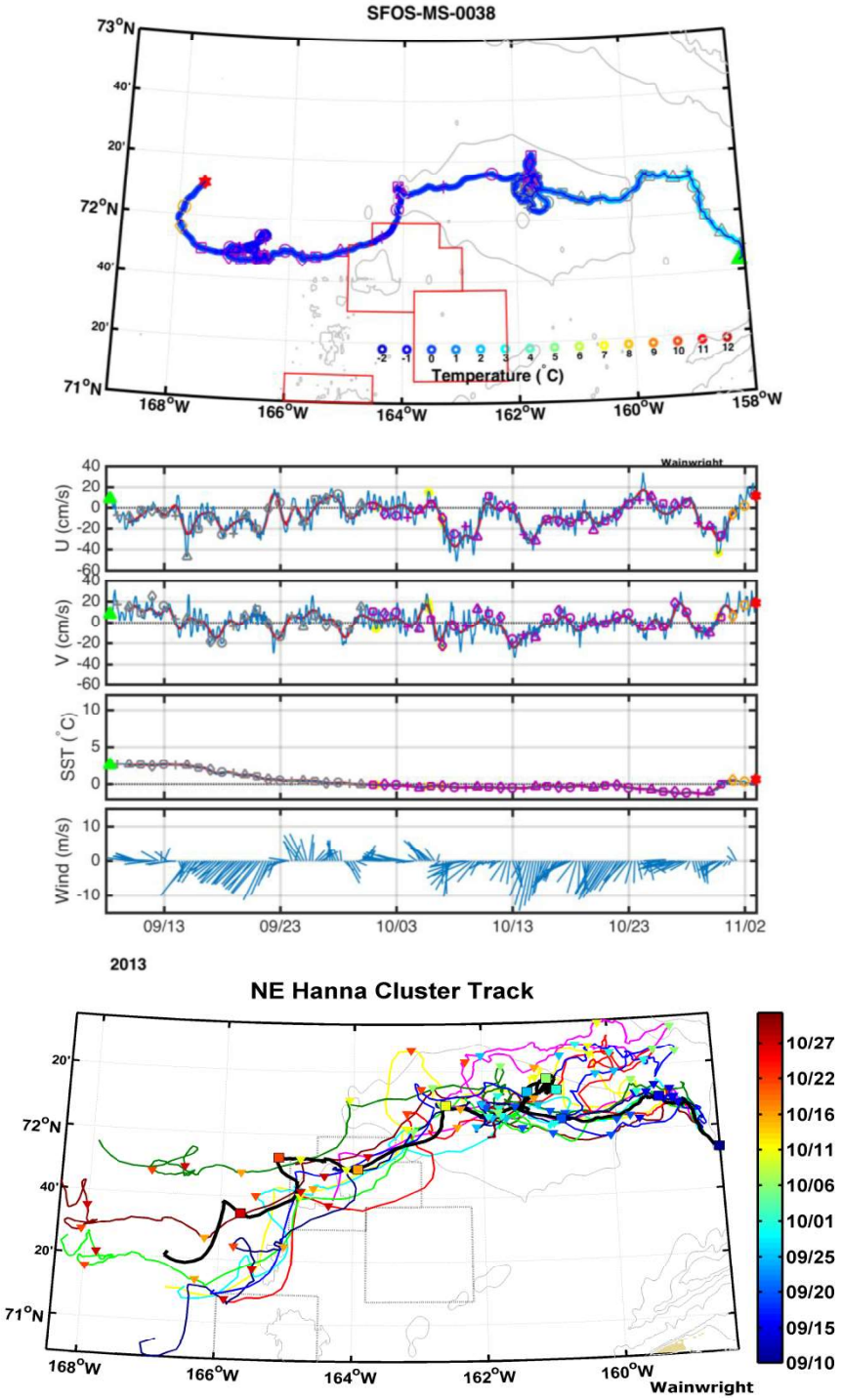

Figure 18. The trajectory of one of nine satellite-tracked drifters released during deployment of the HSNE50 in September 2013, along with time series of the drifter velocity components, SST, and winds along the drifter track. The thick lines on the velocity plots are low-pass filtered currents. The bottommost panel shows the cluster's centroid trajectory and the individual trajectories of the drifters comprising the cluster.

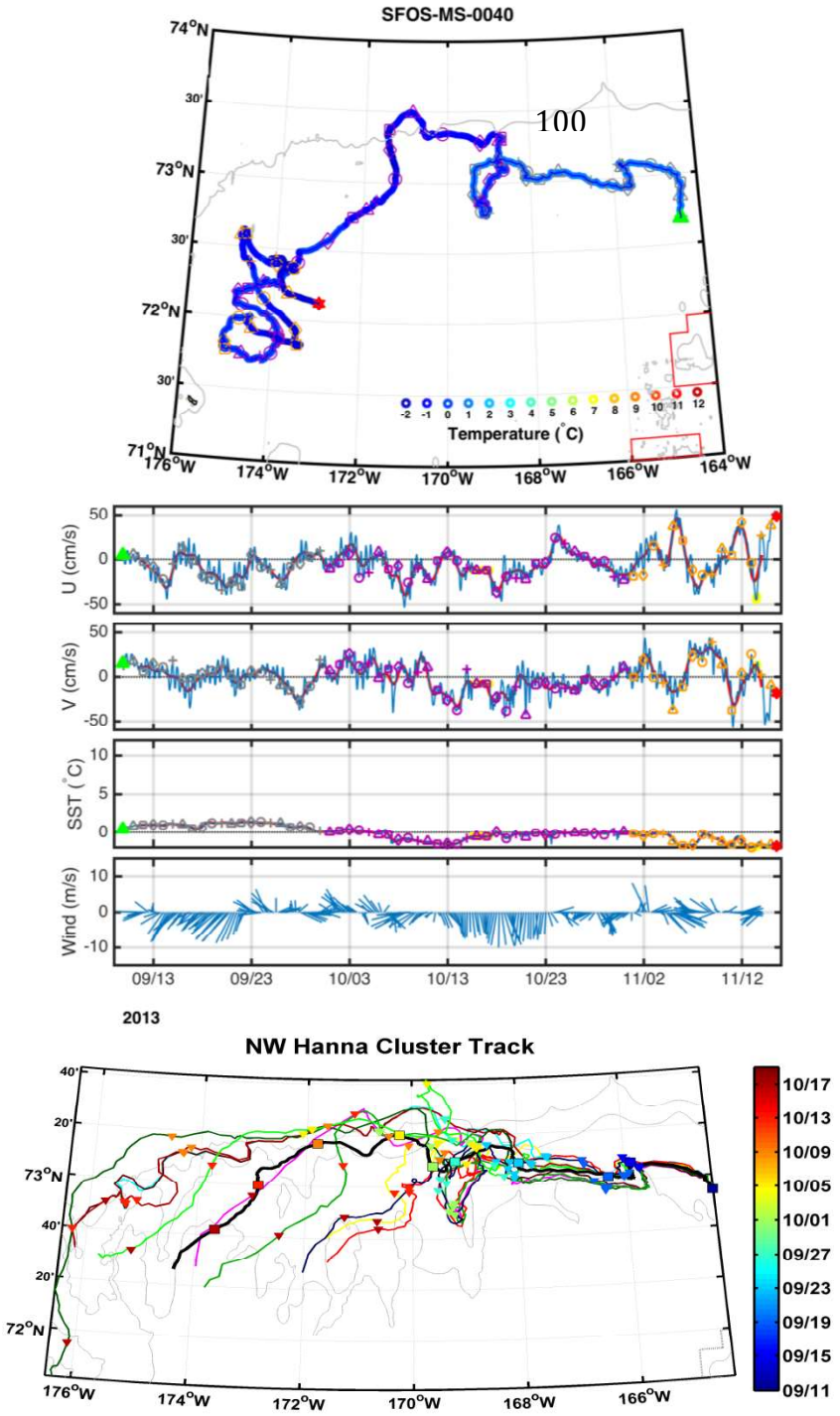

Figure 19. The trajectory of one of nine satellite-tracked drifters released during deployment of the HSNE50 in September 2013, along with time series of the drifter velocity components, SST, and winds along the drifter track. The thick lines on the velocity plots are low-pass filtered currents. The bottommost panel shows the cluster's centroid trajectory and the individual trajectories of the drifters comprising the cluster.

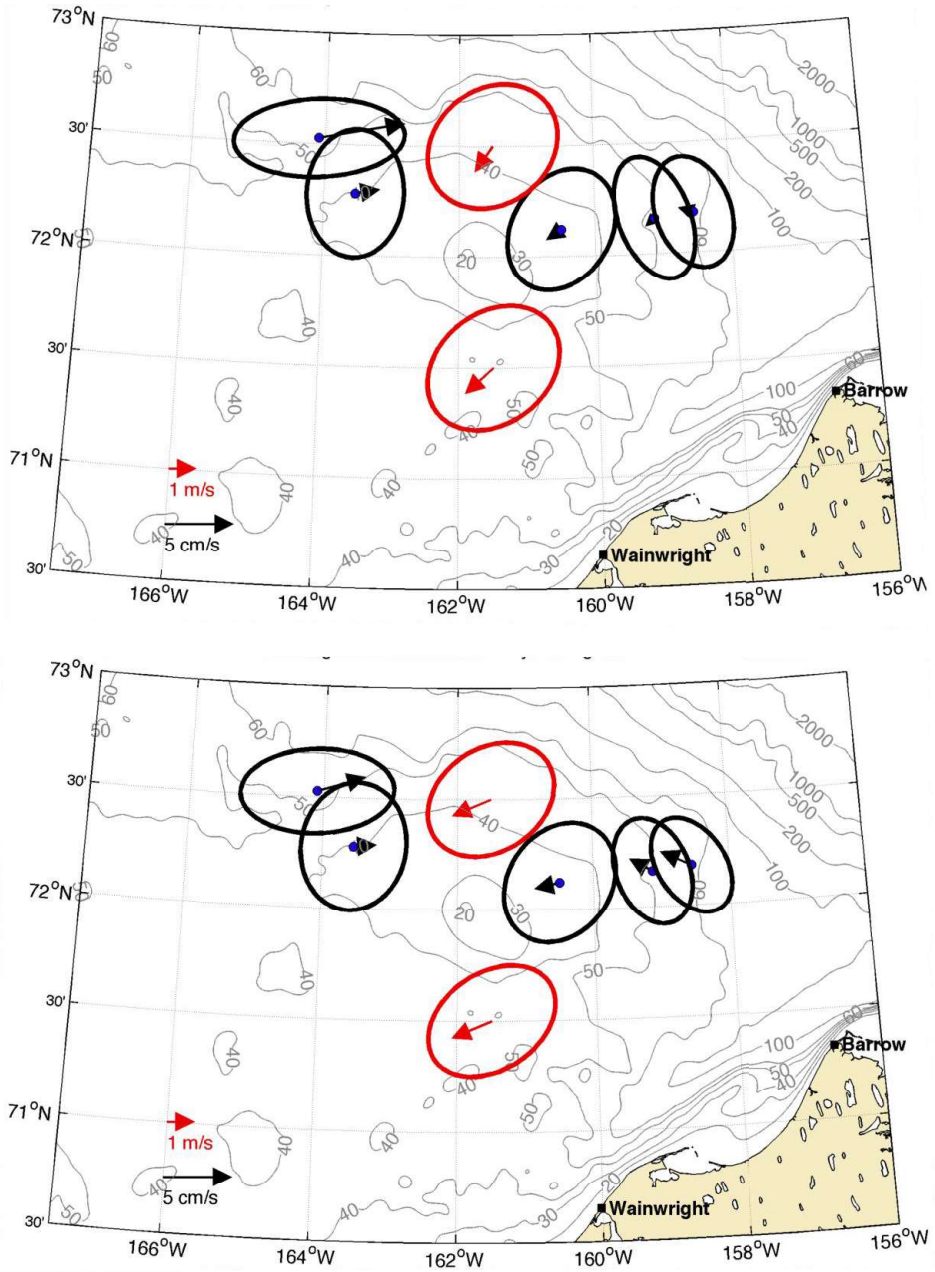

Figure 20. Mean vectors and variance ellipses for vertically-averaged currents (black) and winds (red) for the periods of November 2012 – June 2013 (top) and the corresponding period in 2013 – 2014.

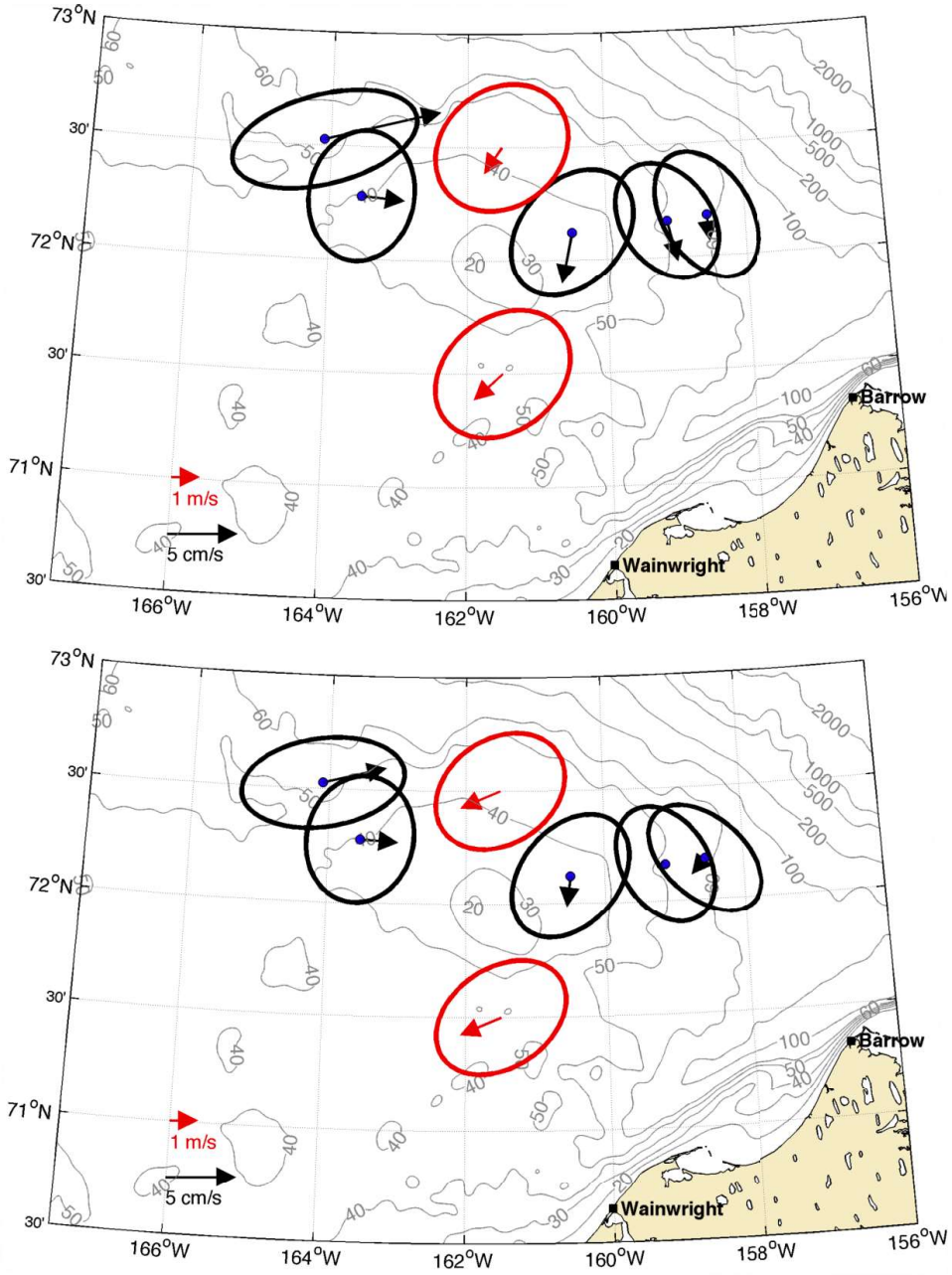

Figure 21. Mean vectors and variance ellipses for currents at 10 mab (black) and winds (red) for the periods of November 2012 – June 2013 (top) and the corresponding period in 2013 – 2014 (bottom).

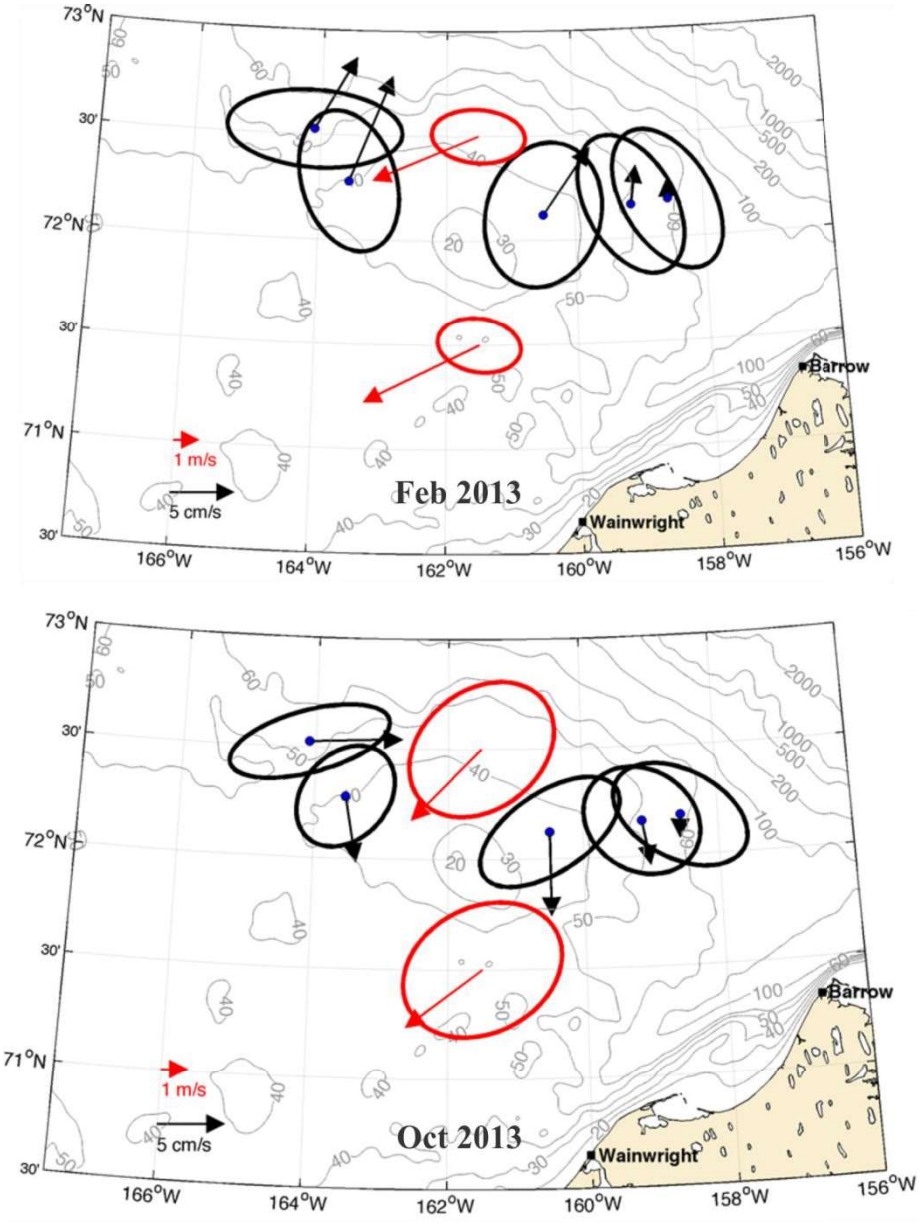

Figure 22. Mean vectors and variance ellipses for currents at 6 mab (black) and winds (red) for the periods of February 2013 (top) and October 2013 (bottom).

We conclude this section by comparing the seasonal changes in vertically-averaged currents and temperature and salinity at HSNW50-12 (Figure 23) with the corresponding time series at HSNE50-12 (Figure 24). The latter figure includes the time series of temperature and salinity from both the ISCAT moored at 23 below the surface and the MicroCat at 43 m depth. At HSNW50-12, the vertically-averaged flow was eastward generally; there was a reversal to the southwest in September 2012 and a burst of northward flow in March 2013. The record-length average flow was ~7 cm s^{-1} westward. At the beginning of the record in August bottom temperatures were close to the freezing point (~-1.8°C), but they then increased to ~-0.5°C in late September. This increase was followed by a brief cooling event in early October and then a

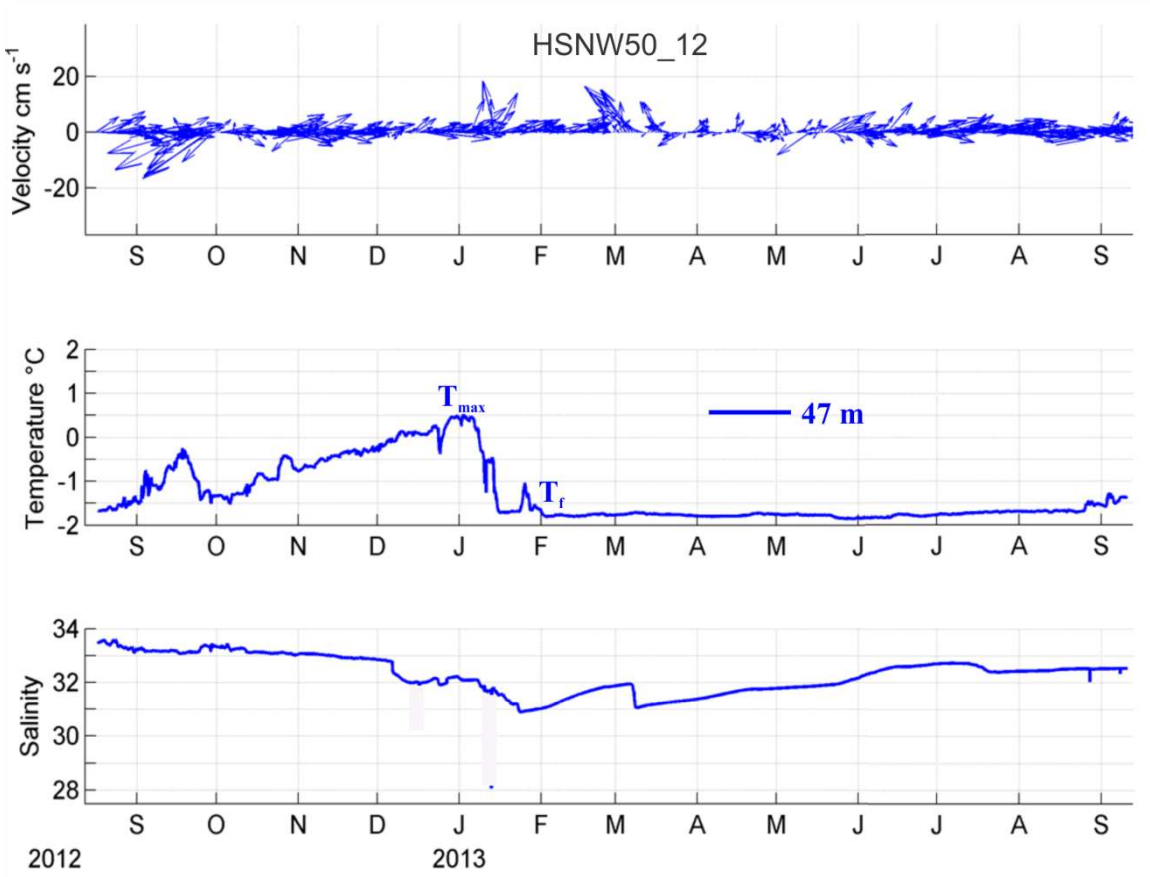

Figure 23. Time series of vertically averaged current vectors (top), and temperature (middle) and salinity (bottom) at 47 m depth from mooring HSNW50-12. The timing of the temperature maximum (T_{max}) and the descent to the freezing point (T_f) are noted.

monotonic increase to a maximum of 0.5°C by late December. In January, the temperature decreased rapidly until it reached the freezing point by 1 February. Salinities were initially ~33.5 in September but gradually decreased to a minimum of ~31 in mid-January. Over the remainder of the record the salinity increased very slowly and attained ~32.5 by September 2013. The December-January transition in bottom waters consisted of a change from being cool and saline to warm and fresh is of particular interest. For reasons outlined later, we believe that this transition was primarily associated with vertical mixing.

At HSNE50-12 the vertically-averaged velocity was quite variable through time, and over the record averaged to 0 cm s^{-1}. In fall the flow was primarily south-southeastward but with the exception of the strong northward flow event in March, the flow was weak and variable from December to August. Consider next the salinity records at 23 and 47 m, which provide an index of the bulk vertical stratification because of the density dependence upon salinity. In fall the vertical salinity difference between was ~1, but this increased to ~5 by mid-December. This change came about primarily because of freshening at 23 m even though the bottom salinity had also decreased slightly through fall! The shallow salinity decrease was associated with increasing temperatures, which were a maximum of ~1.5°C in mid-December. Salinities then increased at 23 m through February, but continued to decrease at the bottom. In March, the salinity difference was a minimum of <1. This change in stratification was associated with northward flow and an

increase in salinity at both depths, which suggests that the change reflects the advection of a less stratified water column from the south rather than local mixing.

After March, the stratification increased again, due primarily to a slight salinity increase (decrease) at the bottom (mid-depth). Bottom and mid-depth salinities both increased in July and remained nearly constant into August. The salinity record indicates that the vertical stratification over this portion of the Chukchi Sea shelf remains intact throughout the year, which is a remarkable and unexpected finding!

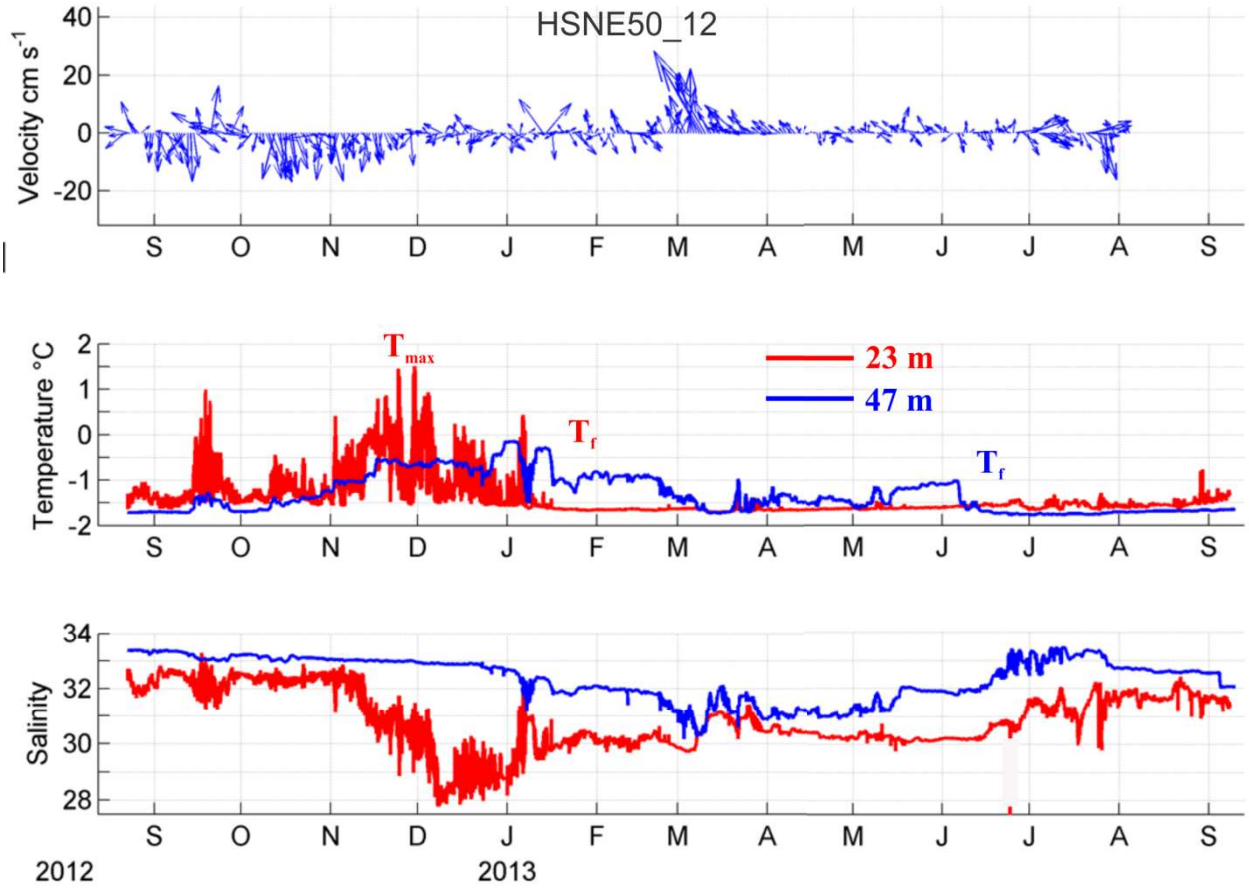

Figure 24. Time series of vertically averaged current vectors (top), and temperature (middle) and salinity (bottom) at 23 m (red) and 47 m (blue) depth from mooring HSNE50-12. The timing of the temperature maximum (T_{max}) and the descent to the freezing point (T_f) are noted.

Bottom temperatures at HSNE50-12 increased slowly through fall and reached their maximum (<~0°C) in January. They remained fairly constant through the first week of June, with the exception being the decrease to the freezing point (T_f) during the northward flow event in March. The decrease to T_f coincided with a bottom salinity increase, further suggestive that these winter-formed waters were advected into the area. Bottom temperatures decreased again to the freezing point (and salinity increased in conjunction with the temperature decrease) in the second week of June.

This change occurred well after the onset of spring ice melt and bottom conditions remained that way through the end of the record. Again, advection has to account for the presence of these winter waters at this time of the year. The mean flow from August through September at both HSNE50 and HSNE60 was to the southeast at this time indicating that the source of this winter water was from the northern side of Hanna Shoal.

The mid-depth temperature record reached its maximum in December and then decreased to the freezing point in early January. That decrease was most likely due to local freezing at the surface and convective mixing. Nevertheless, the mixing was insufficient to penetrate entirely to the bottom. Mid-depth temperatures remained at the freezing point through early June but began to increase at about the same time that the bottom temperatures collapsed to the freezing point. We speculate that the mid-depth temperature increase may be associated with penetrating solar radiation as sea ice begins breaking up and meltponds allow solar radiation to penetrate through the ice and into the water column (Light et al., 2008).

An important feature of the mid-depth temperature and salinity records is the signature of very high-frequency oscillations. These were present throughout fall, and especially from November through early January. We contend that the MicroCat at 23 m depth was very likely in the midst of a strong pycnocline and that these high frequency fluctuations are internal wave signals.

The bottom temperature and salinity records from the 2013 – 14 HSNE deployments (Figure 26) show the same basic seasonal evolution in temperature and salinity as was observed in 2012 – 13. However, the seasonal evolution was quite difference at the HSNW moorings (Figure 26). The annual maximum in temperature occurred in mid-November 2013, nearly two months earlier than in the previous year. Temperatures then dropped to the freezing point in early December and remained at the freezing point into July. These differences may be related to the differences in ice concentration between fall 2012 and fall 2013 as discussed in relation to Figures 11 – 13. In 2012, we surmised that the northerly winds rapidly advected ice over the both northeastern Chukchi Sea with coverage being spatially uniform at ~100% by mid-November. In 2013 by contrast, the development of 100% ice cover was slower and included episodic advance and retreats before finally setting up. Moreover, 100% ice cover developed sooner on the east side of the Shoal than in the Central Channel and northwest side of the Shoal. These differences in ice cover (in conjunction with the assumed differences in stratification) on either side of the Shoal would lead to earlier cooling at the HSNW moorings compared to the HSNE moorings.

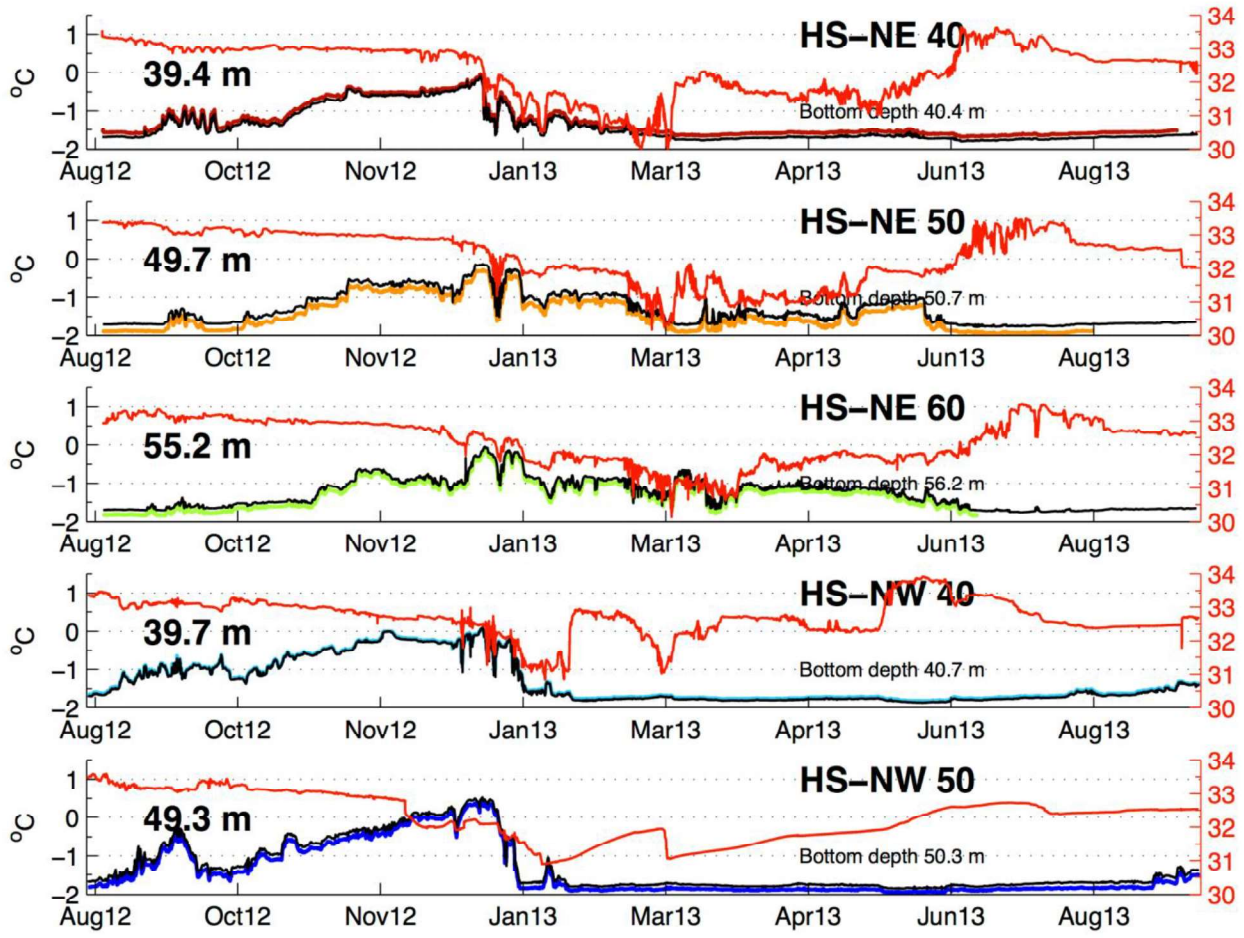

Figure 25. Time series of bottom temperature and salinity from the COMIDA 2012 – 13 mooring array.

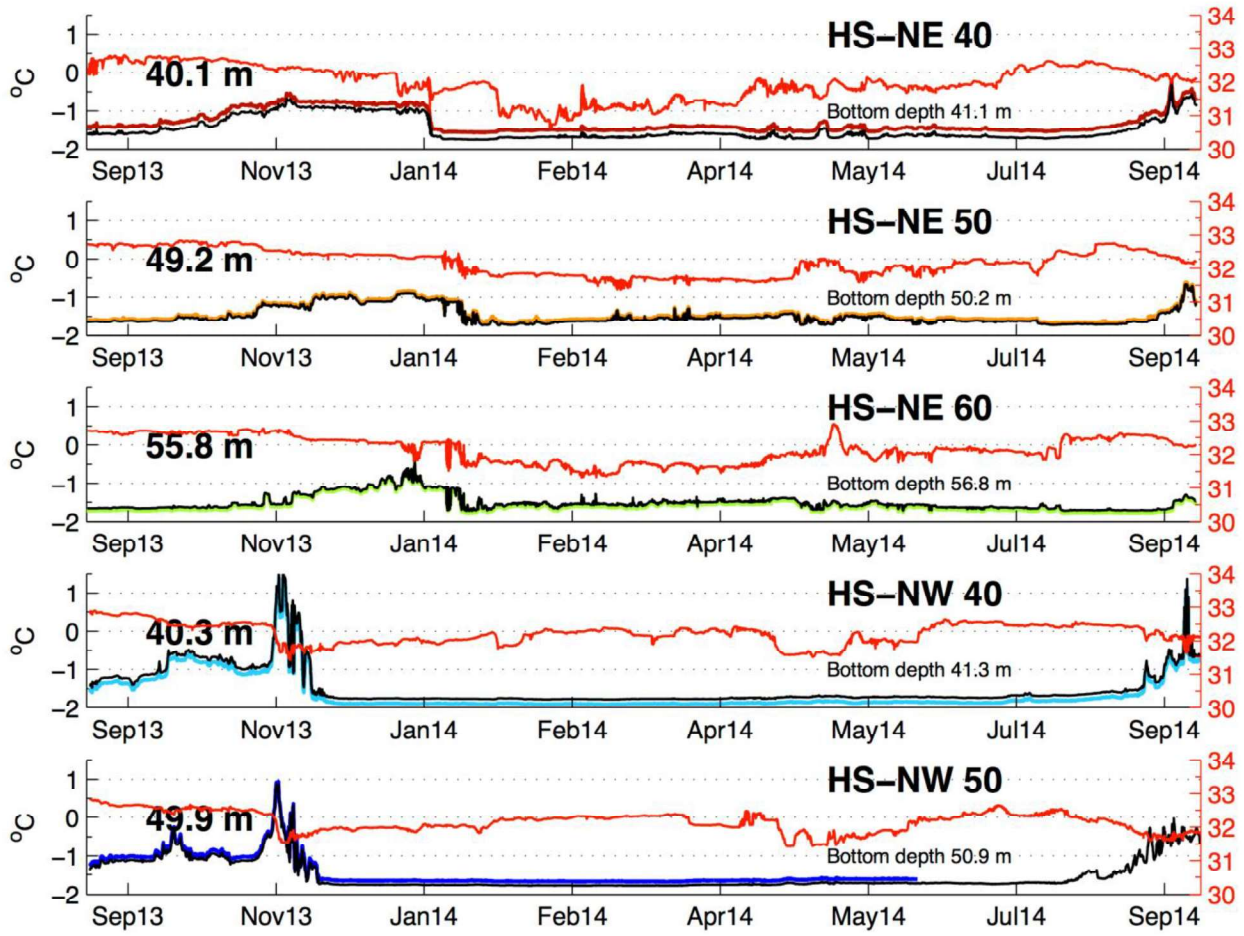

Figure 26. Time series of bottom temperature and salinity from the COMIDA 2012 – 13 mooring array.

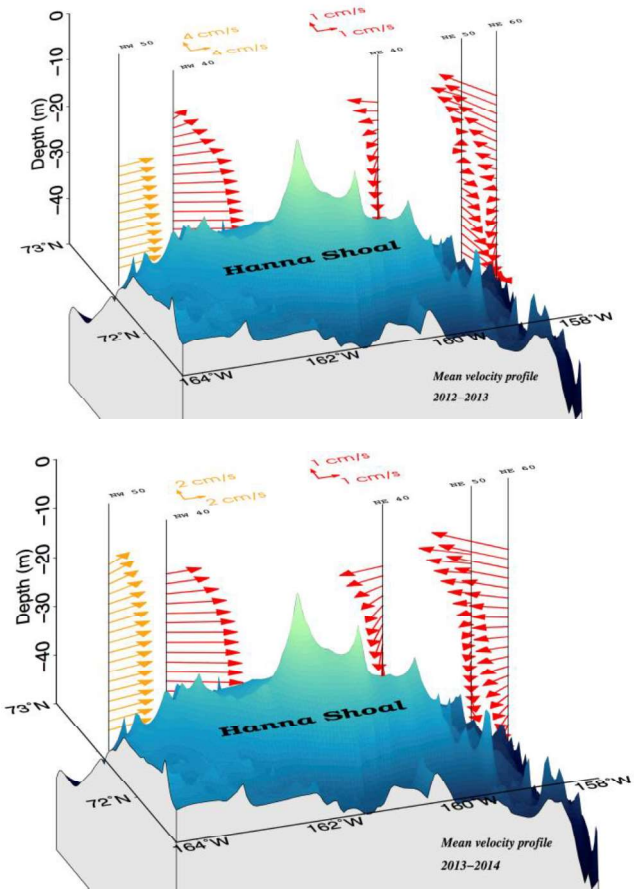

Figure 27. Mean vertical profiles of velocity for the 2012 – 13 (top) and 2013 – 14 (bottom) deployments.

We conclude this section with two summary figures that show the mean velocity profiles at all HS mooring sites for 2012 – 13 and 2013 – 14 (Figure 27). These show that the velocity shear was greater on the eastern of Hanna Shoal than on the western side in both years. On the eastern side of the Shoal, the surface flow was generally westward and the velocity vectors veered counterclockwise with depth. This veering amounted to ~180° at HSNE50-12 but closer to 90° at the other HSNE moorings. On the western side of the Shoal the flow tended to be more unidirectional with current magnitudes increasing with depth. Note that the large shear on the northeastern side of the Shoal explains the weak vertically-averaged flow. There may be several reasons for the difference in mean shear on either side of the Shoal. First, some of the shear differences may be associated with differences in surface stress, especially if the ice at the NWHS moorings was less mobile than the ice on the eastern side of the Shoal. Horizontal density gradients, associated with either fronts and or sloping isopycnals, will produce a geostrophic shear via the thermal wind (with the degree of veering proportional to the strength of the horizontal density gradients.) The counterclockwise veering at HSNE50 implies that water densities increased moving westward toward the Shoal. This implies the existence of baroclinic pressure gradients that, on their own, would drive a vertically-sheared counterclockwise, flow around the eastern side of Hanna Shoal. If this baroclinic pressure field exists, then it works in opposition to the barotropic (and geostrophic) motion associated with the clockwise flow around Hanna Shoal.

3.3. High-frequency current variations

Thus far we have emphasized the low-frequency current variations and differences in the circulation on either side of Hanna Shoal. There are also important spatial and seasonal differences in the higher-frequency currents, especially those associated with near-inertial motions. Figure 28 shows the rotary spectra at 45 m depth from HSNE50-12, which is typical of the rotary spectra at other locations. At low-frequencies the variance is equally distributed between clockwise (CW) and counterclockwise (CCW) current components. At periods <1 day, CW energy dominates the spectrum, especially at the inertial (*f*) and semi-diurnal (M_2) tidal frequencies. Our sampling rate was insufficient to resolve the inertial and semi-diurnal tides. Consequently harmonic analysis for the purposes of isolating the M_2 tide will be biased by contamination from inertial motions. Inertial energy is intermittent, however, whereas the semi-diurnal barotropic tide is periodic and deterministic. Wavelet analysis allows determining how energy in a particular frequency band changes through time. We applied rotary wavelet analyses to our data to distinguish periods of enhanced inertial energy from periods when inertial motions were absent or subdued. We focused on the CW component (because inertial and M_2 currents rotate clockwise) and identified periods when inertial motion was statistically different from background energy levels.

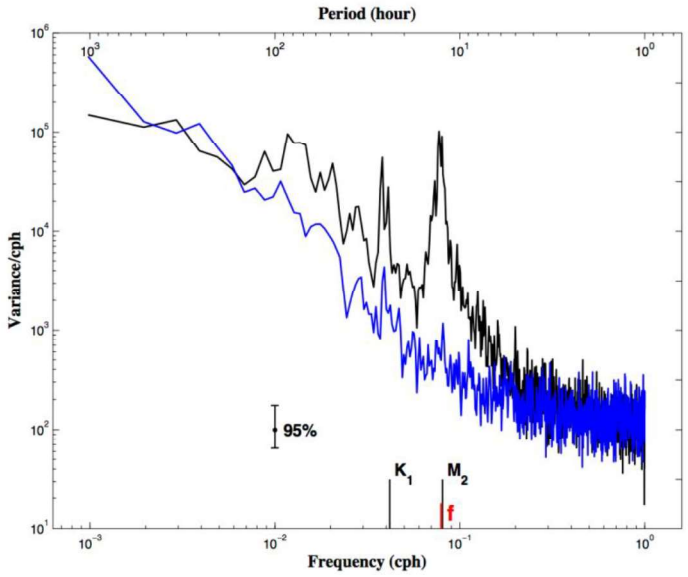

Figure 28. Rotary spectra of currents at 45 m depth from HSNE50-12 consisting of clockwise (black) and counterclockwise (blue) spectral components. The symbols K_1, f, and M_2 denote the diurnal tide, inertial, semi-diurnal tide frequencies, respectively. The width of the 95% confidence interval (95%) for the spectral estimates is included.

Figure 29 shows an example of the wavelet analyses for several depths for HSNE50-12. Inertial energy, contained within the 8 – 16 hour period band, was observed at all depths, and while highly intermittent varied seasonally and was a maximum in fall.

Figure 30 shows examples of the wavelet analyses from HSNE40 and HSNW40 for the 2012 – 13 deployment and from and HSNE 50 and HSNW50 for the 2013 – 14 period. Two key results of these analyses are that a) the near-inertial energy tends to decrease when sea ice is present on both sides of Hanna Shoal and b) there is more inertial energy on the northeast side of Hanna Shoal than on the northwest side of the Shoal. These results are common to both years. The general reduction in inertial wave energy in the presence of ice may be due to the ice containing most of this energy and perhaps dissipating it through ice-ice interactions. It is not clear why

there are differences in inertial wave energy on either side of Hanna Shoal, although we noted earlier that the mean ice velocities were smaller at the HSNW moorings than at the HSNE moorings. If the ice on the NW side of Hanna Shoal was less mobile than the ice on the east side of the Shoal, then the reduction in ice mobility could impede inertial wave generation.

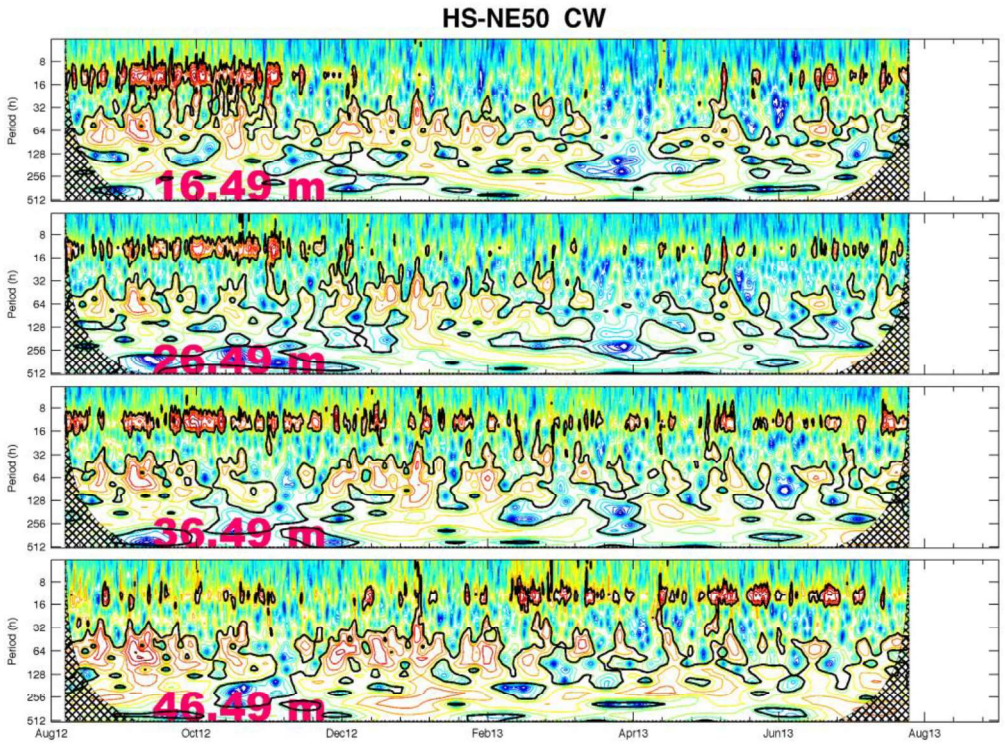

Figure 29. Wavelet analysis results for the clockwise (CW) spectral component at HSNE50-12. The inertial band lies within the 8 – 16 hour period. Periods when the energy levels are significantly greater (at the 95% level) than background are enclosed by black contours.

3.4 Hydrography

The presentation of shipboard hydrographic data relies on two different sources: the data sets collected under the auspices of the COMIDA program from the USCG *Healy* and data sets collected by other programs including those supported by BOEM and the oil industry. We supplement the *Healy* data with that from other programs, because the *Healy* sampling approach did not permit acquiring data to form quasi-synoptic hydrographic sections, which are most helpful in understanding the circulation and water mass distribution.

The *Healy* CTD stations occupied in August 2012 and 2013 are shown in Figures 31 and 32. Note that in 2013 the sampling extended across the shelf and shelfbreak to the northeast of Hanna Shoal. We constructed potential temperature-salinity (θ/S) diagrams for each cruise (Figures 33 and 34) as an aid in identifying the various waters masses that were present based on the Coachman et al., (1975) nomenclature. There were four water masses present in both years: Alaskan Coastal Water (ACW), Bering Sea Water (BSW), meltwater (MW) and winter water (WW). In addition Atlantic Water (AW) was observed in 2013 only.

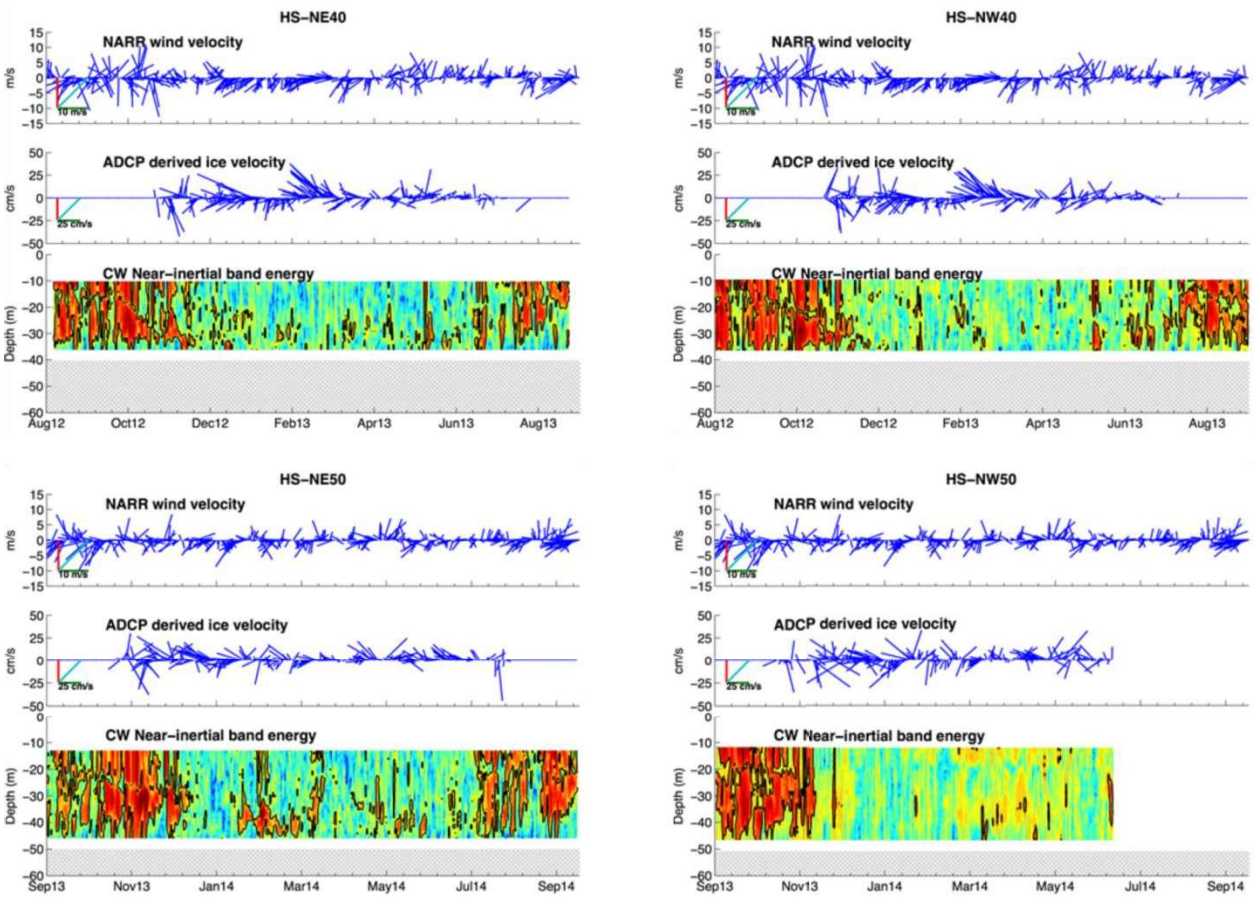

Figure 30. Wavelet analysis from the 2012 – 13 deployments of HSNE40 (upper left) and HSNW40 (upper right) and HSNE50 (lower left) and HSNW50 (lower right). In each panel the time series includes the wind the ice velocity vectors. The lowest panel consists of the time series as a function of depth of clockwise (CW) energy in the near-inertial wave band (8 – 16) hours.

ACW is fresh (<31.5) and the warmest (≥ 5°C) water mass. In general it occurred closest to the coast and within Barrow Canyon. BSW is saltier (31.5 – 32.5) and cooler (≤ 5°C) than ACW and was generally found in the Central Channel and south of Hanna Shoal. Both ACW and BSW are water masses that have flowed northward from Bering Strait during the summer. MW is cool (<1°C) and is the freshest (<30) water mass. It is a result of ice melt and was found at the surface of nearly all stations. The freshest and coldest MW fractions were at stations with melting ice. WW is very salty (≥32.5) and the coldest water mass with temperatures at or very close to the freezing point. WW is formed in winter due to salt rejection from growing ice. Finally, AW is the saltiest water mass having salinities >33.2 and temperatures >-1.5°C. AW spans a range of temperatures from -1.5°C to ~1°C. As is evident from the figure, each of these water masses tend to blend with one another to form intermediate products. Mixing occurs either vertically through the action of the winds or through horizontal exchange processes (e.g., Lu et al., 2015). The exceptions are the ACW in 2013 and the AW in 2014. The former was observed only in the surface waters in Barrow Canyon where it resided at depths shallower than the BSW and WW. The AW was located seaward of the shelfbreak and beneath the Arctic Ocean's halocline, which contains shelf-derived WW.

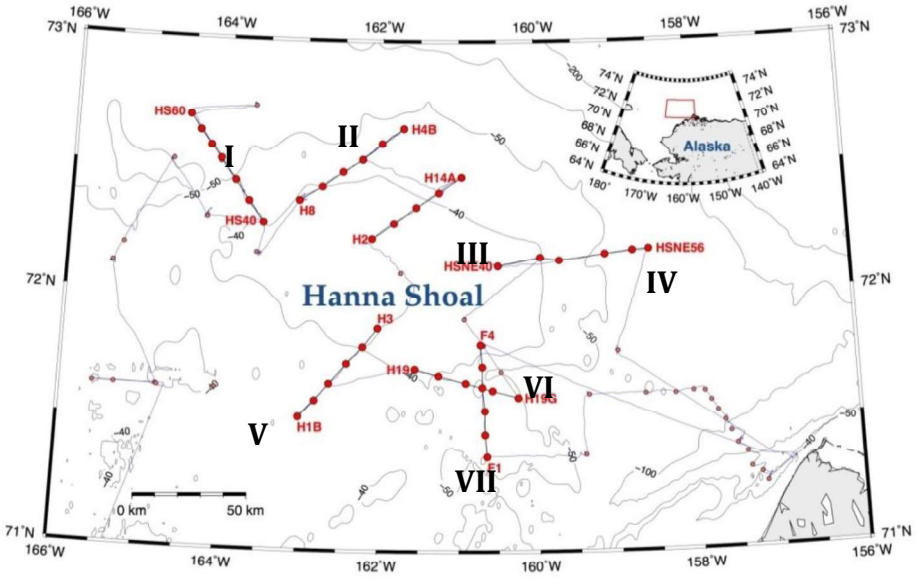

Figure 31. COMIDA CTD stations occupied in August 2012. Roman numerals denote the transects used to construct vertical sections shown in separate Figures 34, 36 – 38.

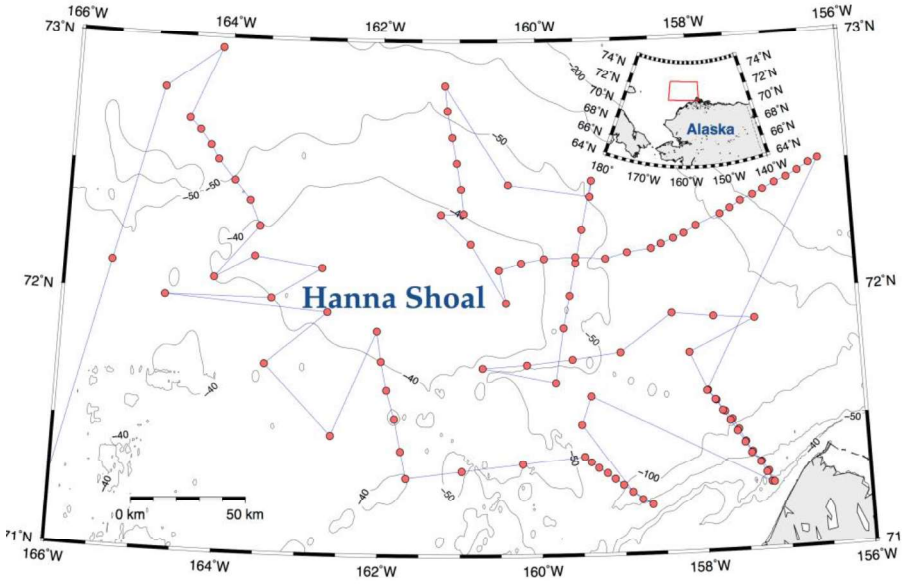

Figure 32. CTD stations occupied in August 2013.

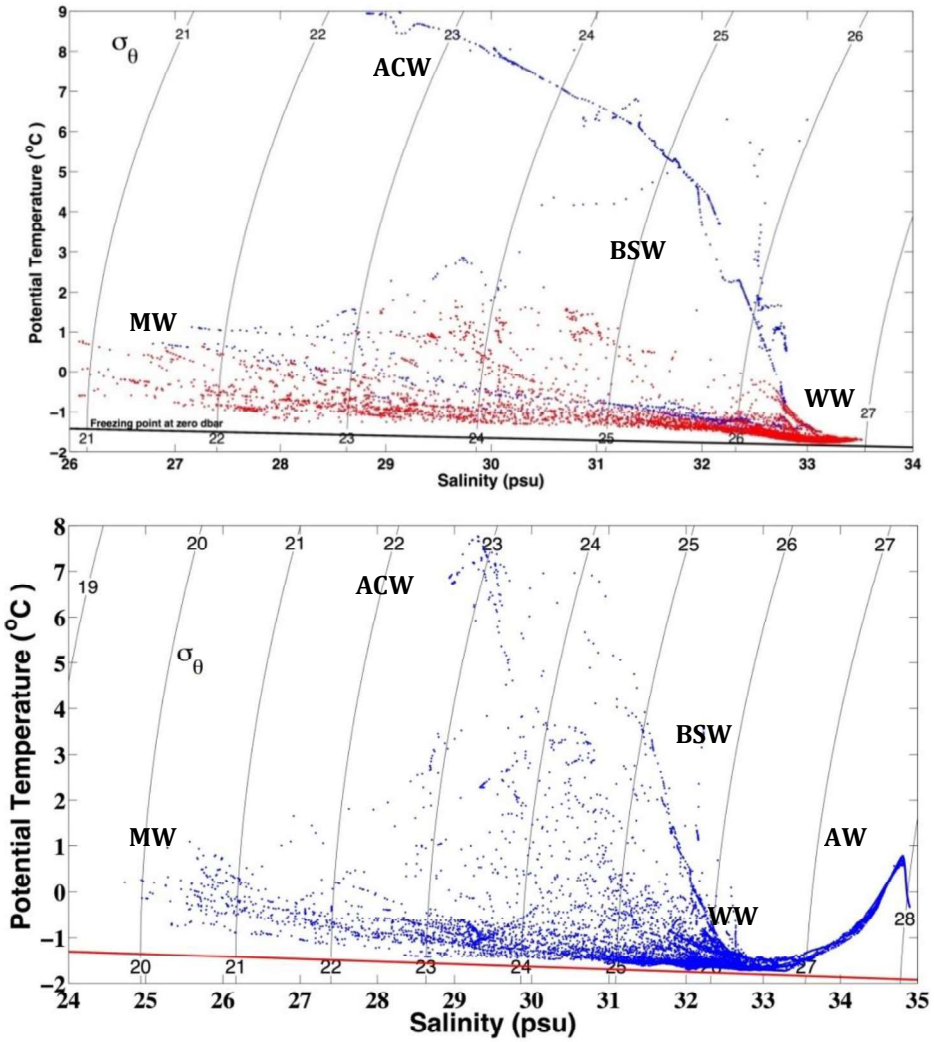

Figure 33. θ/S diagrams from 2012 (top) and 2013 (bottom).

From the 2012 CTD survey we constructed seven hydrographic vertical sections along transects that surrounded the Shoal (Figure 31). Three of the sections (I, II, and III) were from transects occupied on the northwestern and northern sides of the Shoal (Figure 34), a fourth section (IV) was from the eastern side (Figure 36) and the remaining three sections (V, VI, and VII) were from transects distributed along the southern flanks of the Shoal (Figure 37). Several features are common to all sections. First below ~20 m depth the water column consists entirely of WW with salinities >32.5 and temperatures <-1.6°C. The most saline waters (>33.3) were found along transects VII and IV, south of and east of Hanna Shoal, respectively. Second the surface waters were all <30 and quite cold (≤0°C) indicating that these waters were from melting sea ice.

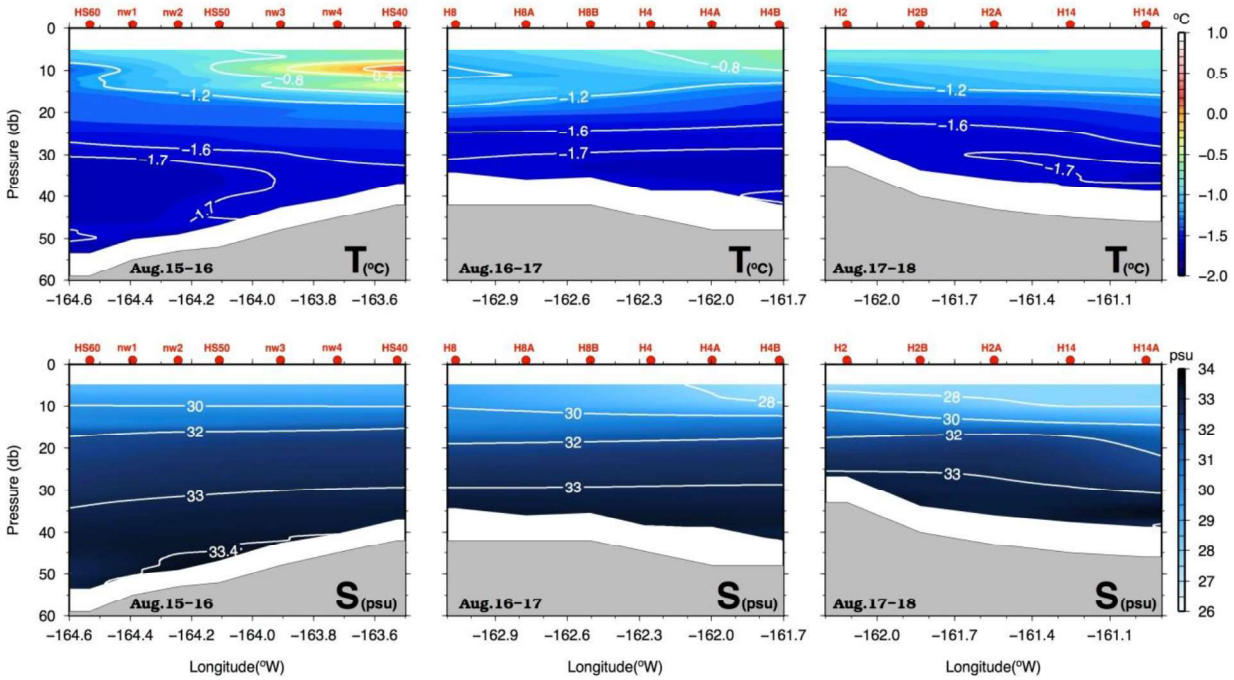

Figure 34. Vertical sections of potential temperature (top row) and salinity (bottom row). The sections are from Transects I (left), II (middle), and III (right; see Figure 31 for transect locations). Typical ice concentrations on these transects were 50 – 90%.

Third, the water column was strongly stratified due to the large vertical differences in salinity. The halocline was thin, amounting to a salinity change of ~4 over 10 m depth, which corresponds to a density difference of 0.4 kg m^{-4} across the pycnocline. Fourth the isohalines (and isopycnals) tend to slope downward and away from the Shoal. Fifth, surface fronts, manifested as large horizontal salinity changes, were evident only along Transects II, V and VII, although these fronts were not well-resolved because of the coarse station spacing. Subsurface fronts were also present particularly on the east (Figure 36) and south sides (Figure 37) of Hanna Shoal along Transects IV and VII, respectively. In both cases these subsurface fronts were associated with the most saline winter waters observed during the cruise.

Surface waters showed considerably more variability in their temperature and salinity properties than deeper waters. Along Transects I – III (Figure 34) temperatures decreased moving northward and away from the Shoal. For example the maximum temperature (~0°C) was observed closest to the Shoal and below the surface along Transect I. On the other two transects the temperature maxima were observed at the northernmost stations at the surface and were smaller. For example, the temperature maximum along Transect III was ~-1°C. Coincident with the decrease in the temperature maximum was a decrease in salinity, suggesting that these changes coincided with an increase in ice melt along the path of the temperature maximum. If this is the case, then the horizontal pathway of this warm water is eastward along the north side of Hanna Shoal and consistent with the mean eastward flow observed at moorings HSNW50 and HSNW40. It is also consistent with the VM-ADCP data at 20 m depth (Figure 35), which shows

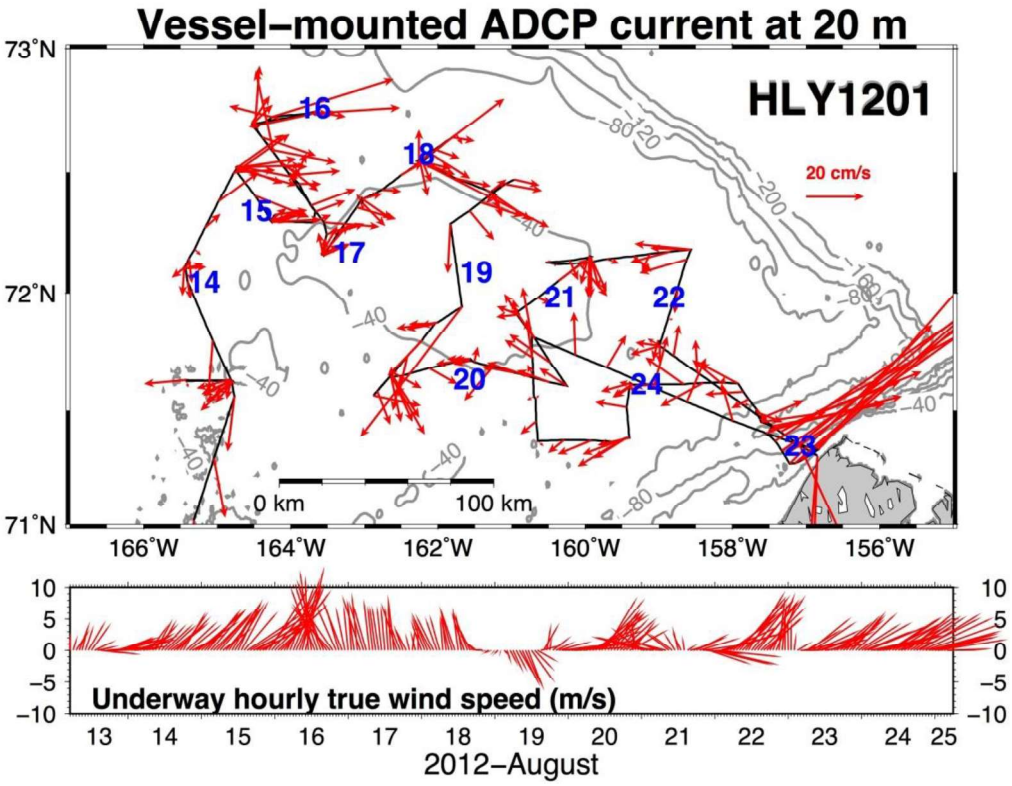

Figure 35. VM-ADCP vector at 20 m depth in August 2012. Blue numbers indicate the day in August when the data were collected. The bottom panel shows the wind vector.

a clockwise circulation of ~0.15 cm s^{-1} around the northwest side of Hanna Shoal. A rough approximation of the heat flux divergence over the upper 20 between Transects I and III is 50 W m^{-2}, based on the temperature changes between the sections and the VM-ADCP data. This assumed ocean-to-ice heat eat flux is roughly half the clear sky net solar radiation flux of 120 W m^2. Much of the region in which we operated, however, was subjected to dense fog, so that the ocean heat flux to the bottom of the ice may have been equivalent to the radiative flux at the ice surface.

The warm surface waters observed along the other transects were warmer than those along Transects II and III. These stations were occupied later in the cruise, however, and their elevated surface temperatures most likely reflect the effects of increased solar radiation.

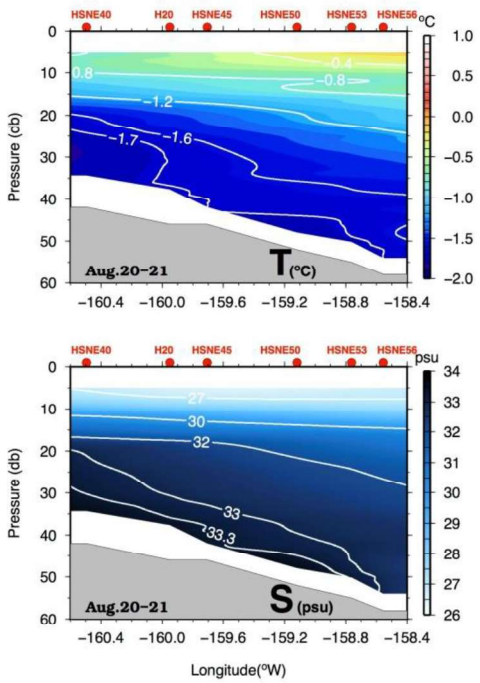

Figure 36. Vertical sections of potential temperature (top) and salinity (bottom) constructed from Transect IV (see Figure 31 for transect locations). Ice concentrations along this transect ranged from 30 – 70% ice cover.

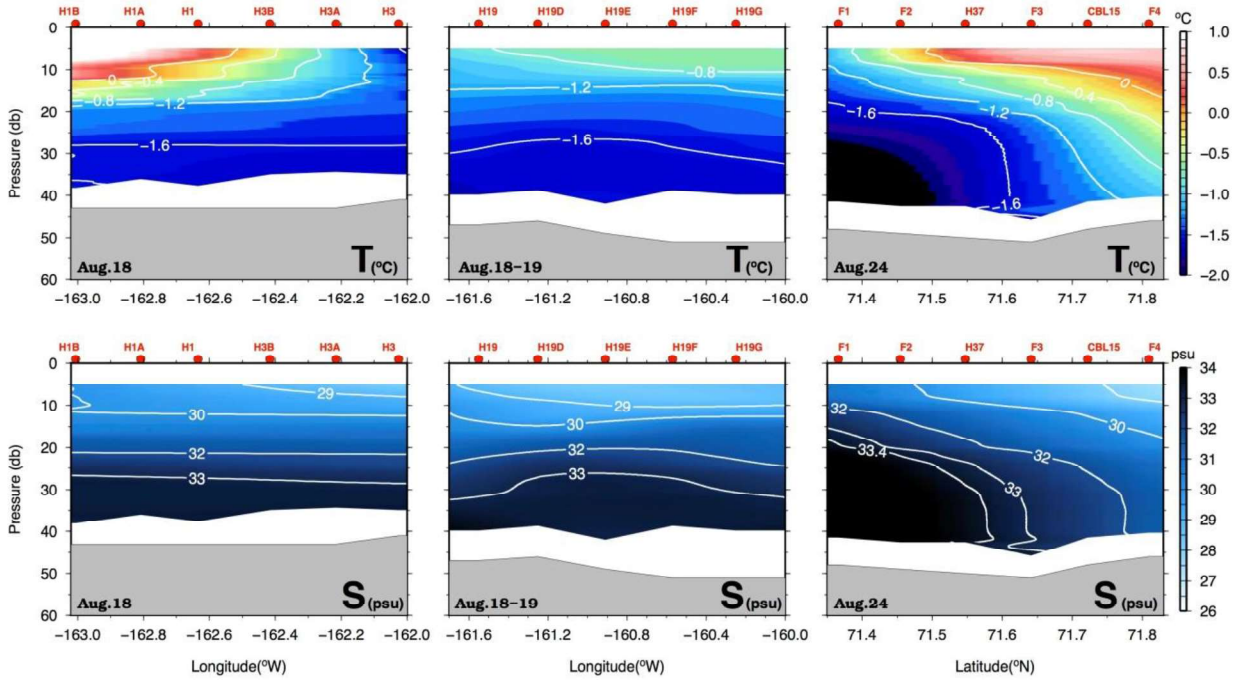

Figure 37. Vertical sections of potential temperature (top row) and salinity (bottom row). The sections are from Transects V (left), VI (middle), and VII (right; see Figure 31 for transect locations).

In 2013, schedule constraints limited us to two transects for synoptic sampling. The first of these was similar in location to Transect I from the 2012 survey. Two important features emerge upon comparing the vertical sections from both of these occupations (Figure 38). The first is that the wedge of warm, surface waters occurred at identical locations, e.g. close to the northwest side of the Shoal. These waters, with a salinity of 30 – 31, are probably a mixture between warm, moderately salty Bering Sea Water (BSW) and meltwater (MW). The origin of the BSW is the northward flow in the Central Channel. This notion is consistent with the northward and preferential erosion of sea ice in the Central Channel (cf. Figures 7 – 9) compared to the shelf regions immediately to the west and east of the Channel. The second point of interest is that the bottom waters in 2012 were considerably saltier (by ~0.5) than those in 2013. The reason for this is not completely clear, although when grounded ice occurs atop Hanna Shoal in winter, latent heat polynyas may form in the lee of the grounding (typically over the south side of the Shoal). The very heavy and broad distribution of grounded ice over Hanna Shoal in the winter of 2012 likely led to extensive polynya development in that year. In that case, vigorous ice growth would have led to salinization of the waters over and around the Shoal. If this was the cause for the salinity differences between these years then the summer observations imply that dense winter water tends to be trapped to the Shoal.

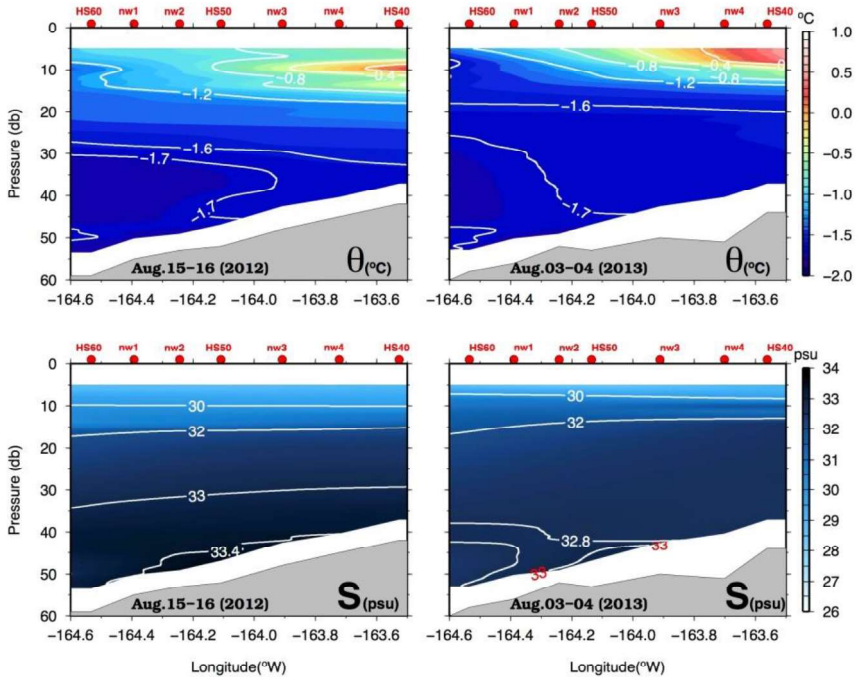

Figure 38. Vertical sections of potential temperature (top row) and salinity (bottom row) from along Transect I in 2012 (left) and 2013 (right).

During the August 2013 COMIDA cruise, we occupied a CTD transect that crossed the shelfbreak along the northeast side of Hanna Shoal. The shelf and slope were partially ice-free at this time (Figure 9). In July 2014, Dr. Robert Pickart completed a CTD survey in roughly the same area. The temperature and salinity sections from each of these surveys are compared in Figure 39. In August 2013, the near-surface waters were strongly stratified (more so than in July 2014) due to low salinity (<30) waters. Upper ocean temperatures were > -1.0°C except offshore where surface temperatures were >0.0°C but <1.0°C. (We will address the possible sources of

this warm water below.) Shelf salinities beneath the pycnocline were ~32 in both years and temperatures were <-1.5°C. The hydrographic structure also differed between these sections seaward of the shelfbreak (~80 m isobath) and at depths greater than 100m. In 2013, warm (>0.0°C) salty (>33) water was confined to depths greater than 180m and the deep, warm isotherms were relatively flat or sloped downward toward the bottom. In July 2014, the isotherms and isopycnals had a pronounced upward tilt over the slope with warm (~0.5°C), salty (>33.1) Atlantic Water observed at ~140 m depth. The sloping of the isotherms and isohalines at this time are suggestive of active shelfbreak upwelling. Upwelling favorable winds occurred in June 2014, but winds were weak and variable in July. Hence the upwelling-structure observed in 2014 might not have been a local response to the winds, but rather the signature of an upwelling-coastal trapped wave that was propagating eastward along the slope. The July 2014 section also indicates that the 32 isohaline bows upward and the 33 isohaline bows downward suggesting an anticyclonic eddy centered at ~157°W and within the Arctic Ocean's halocline. Such eddies are not unusual features along the continental slopes of the Chukchi and Beaufort seas (Weingartner et al. 1998; Spall et al. 2008; von Appen et al. 2012).

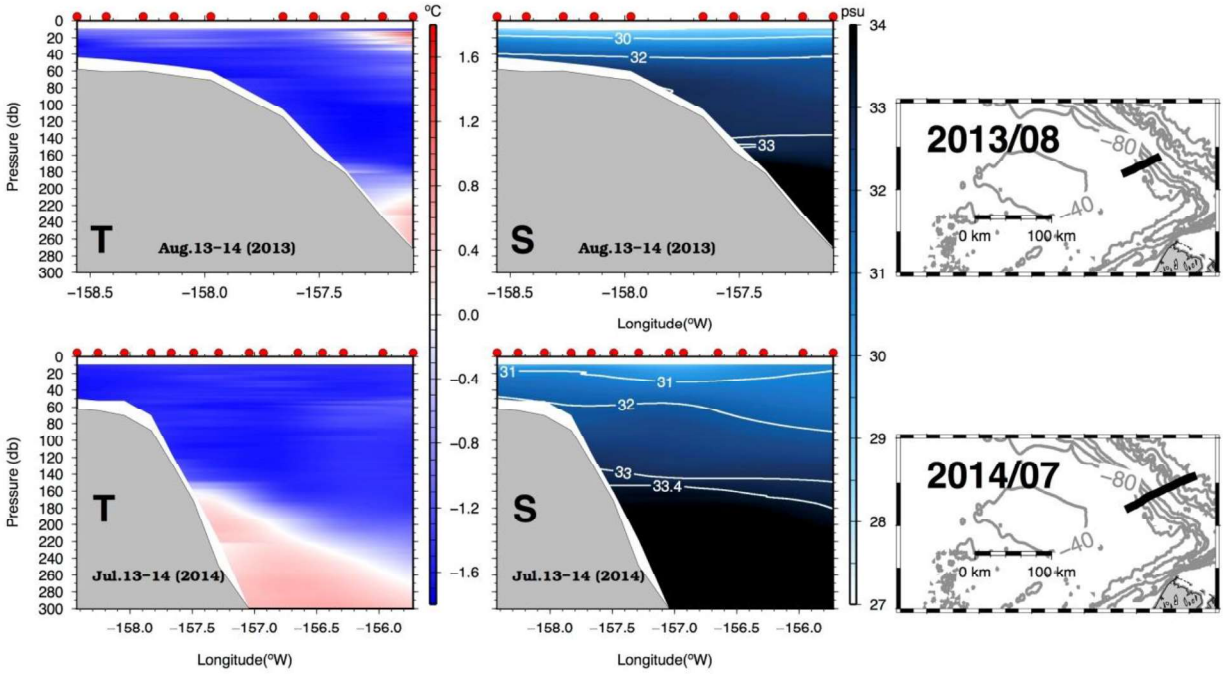

Figure 39. Vertical sections of temperature (left) and salinity (right) in August 2013 (top) and July 2014 (bottom) along the sections shown on the maps to the right of each section.

The source of the warm surface waters observed seaward of the shelfbreak in August 2013 is of some interest. We doubt that it was formed locally as a consequence of solar radiation. If that was the case, then we would have expected surface temperatures along the entire section to be nearly as warm. Instead we believe that this water is ACW advected westward from the mouth of Barrow Canyon. We base our speculation on the behavior of a cluster of 13 drifters released near Icy Cape, Alaska, at the head of Barrow Canyon on 11 August 2012. Two of the trajectories

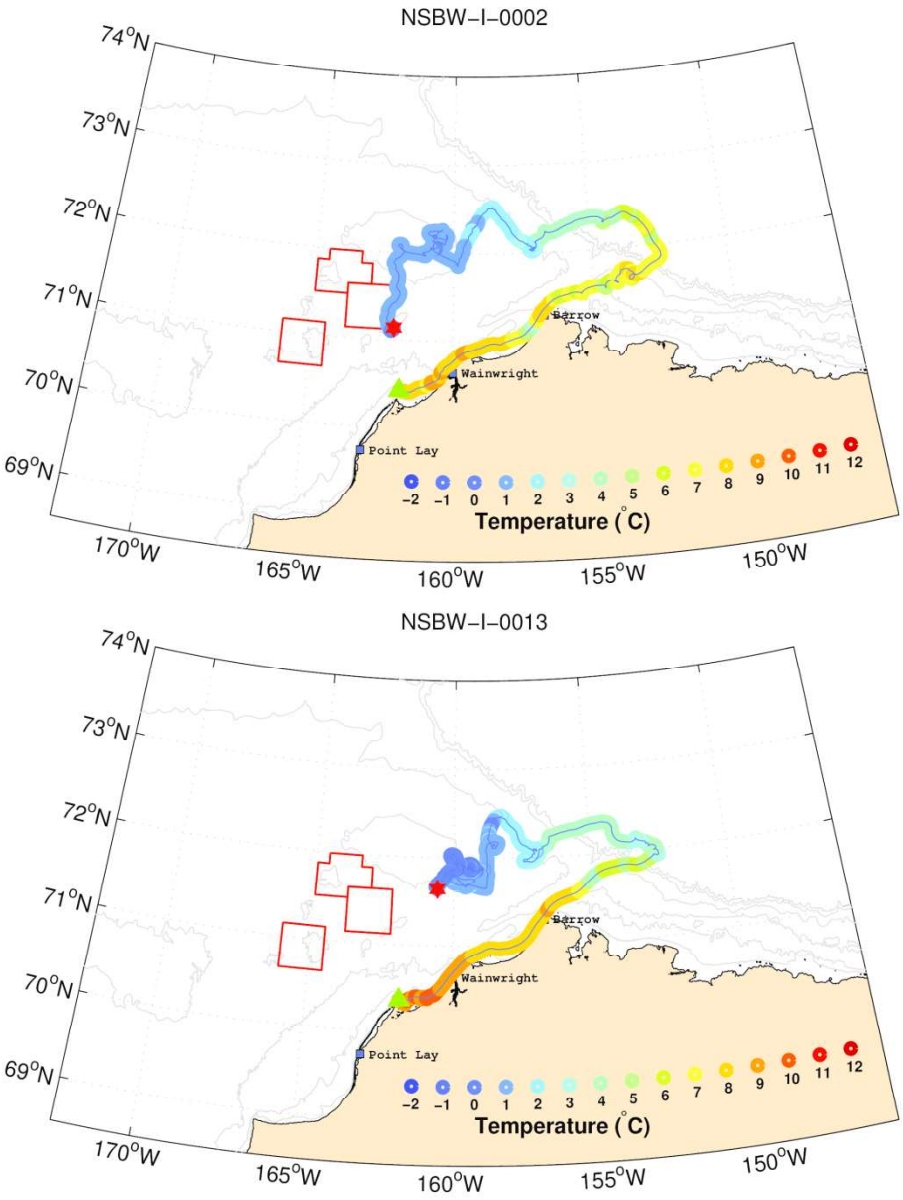

Figure 40. The trajectories of two of 13 drifters released near Wainwright Alaska on 11 August 2012. The trajectories are color-coded according to the sea surface temperatures measured by the drifter and given by the scale on the map.

are shown in Figure 40 (and the other trajectories can be found at University of Alaska, School of Fisheries and Ocean Sciences web site (http://dm.sfos.uaf.edu/chukchi-beaufort/data/drifters/drifter_map_2012.php). During the first week the drifters moved ~400 km northeastward to the mouth of the canyon.

During this time the temperatures decreased from ~10 to 5°C. During the next week they drifted westward along the Chukchi continental slope and temperatures decreased to ~3°C. Over the next month, several of the drifters moved back onto the shelf to the east of Hanna Shoal where they slowly meandered over this portion of the shelf before dying. It is clear from both the trajectories and the drifters' SST records that ACW water is at least occasionally advected

westward from Barrow Canyon along the Chukchi shelfbreak and onto the shelf east of Hanna Shoal. Aside from the heat brought onto this portion of the Chukchi Sea shelf, the ACW also carries relatively fresh water so this flux may also impact the local salt budget.

Time constraints prevented us from conducting extensive CTD surveys south of Hanna Shoal in both years. In order to place the COMIDA CTD data in a broader spatial and temporal context, we use hydrographic data from other BOEM-supported studies and the industry-supported CSESP program to show that the region south of the Shoal is different in several noteworthy respects from the shelf to the north of the Shoal. We will also use these data sets to outline some of the large interannual variability in hydrography that can occur around Hanna Shoal (and presumably the Chukchi Sea shelf).

We begin by examining plan views of the vertical average of the upper and bottom 10 m of the water column in both August and September 2012 (Figure 41). In August the surface waters between 70° - 71°N, and 164° - 165°W were warm (6°C) and moderately salty (31 – 32). Bottom waters were slightly colder and saltier, but both water masses are consistent with this being BSW. North of this location and over the south flank of Hanna Shoal, the surface waters were cooler and fresher, suggesting mixing between MW and BSW. In contrast the bottom waters were WW as these were very cold and salty. The more complete coverage from September 2012 underscores the broad spatial extent occupied by the MW at the surface. The BSW distribution was also quite broad as it extended northward in the Central Channel along 166°W as well as eastward toward the coast at Wainwright. Overall these data suggest a zonally-elongated front that ran eastward along about 71.5°N from the southwest edge of Hanna Shoal to the head of Barrow Canyon. The hydrography collected by the 2013 CSESP surveys was broadly similar to that of 2012 in terms of the distributions of water masses and locations of the MW/BSW frontal system (Weingartner et al., 2014).

In contrast, the situation in 2011 was quite different in several significant ways (Figure 42). In contrast to 2012, the surface waters in both August and September were horizontally homogeneous and consisted of BSW. The absence of MW is consistent with the very early retreat of sea ice over in 2011 (Figures 6 and 9) and also resulted in the absence of surface fronts. In August the bottom waters between 70° - 71°N and 164° - 165°W were BSW, while bottom waters north of that location and along the southern side of Hanna Shoal consisted of WW. In September, BSW protruded prominently northward in the Central Channel, occupied the shelf south of ~71°N, and occurred over the bottom atop the shallowest portions of Hanna Shoal. WW occurred elsewhere including within a prominent lobe that extended westward toward the Central Channel and along the south side of Hanna Shoal. A prominent frontal system delineates this lobe of WW from the BSW.

An alternative perspective on these data is provided in Figure 43 which shows two, 300-km long vertical sections occupied in September 2011 and 2012. The sections ran from the southwest (beginning at ~70.5°N, 166°W) to the northeast (ending at ~72.5°N, 160°W) along the northeast side of Hanna Shoal (their location is shown in the lower right panel of Figure 42). In 2011 warm, moderately salty BSW occupied the uppermost 20 m over the entire area, while WW was confined to either side of Hanna Shoal. Fronts (primarily associated with temperature gradients) separated the BSW along the bottom over the southern portion of the section (south of km 100) from the WW to the north. In contrast, the 2012 section consisted of a strong, frontal system

associated with the MW and BSW at km 140 in addition to weaker MW frontal systems at km 175 and km 200. Similar to 2011, the WW was primarily observed around Hanna Shoal. The sections also differ with respect to vertical stratification. In both years the stratification was dominated by salinity, however, in 2012 the stratification was twice as strong as in 2011. These interannual

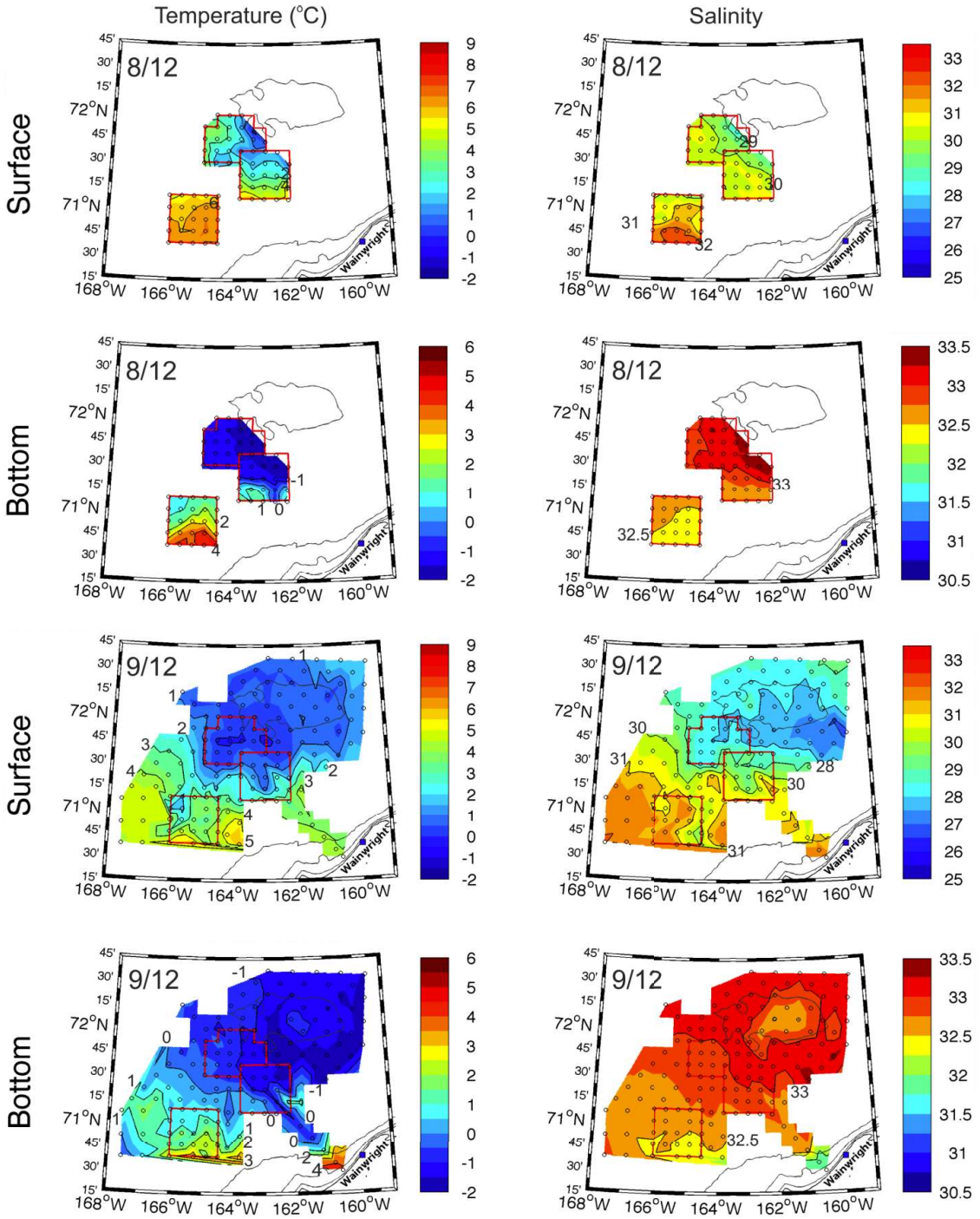

Figure 41. Plan views of temperature (left) and salinity (right) in August and September of 2012. The plan views are based on averages of the upper and bottom 10 m of the water column.

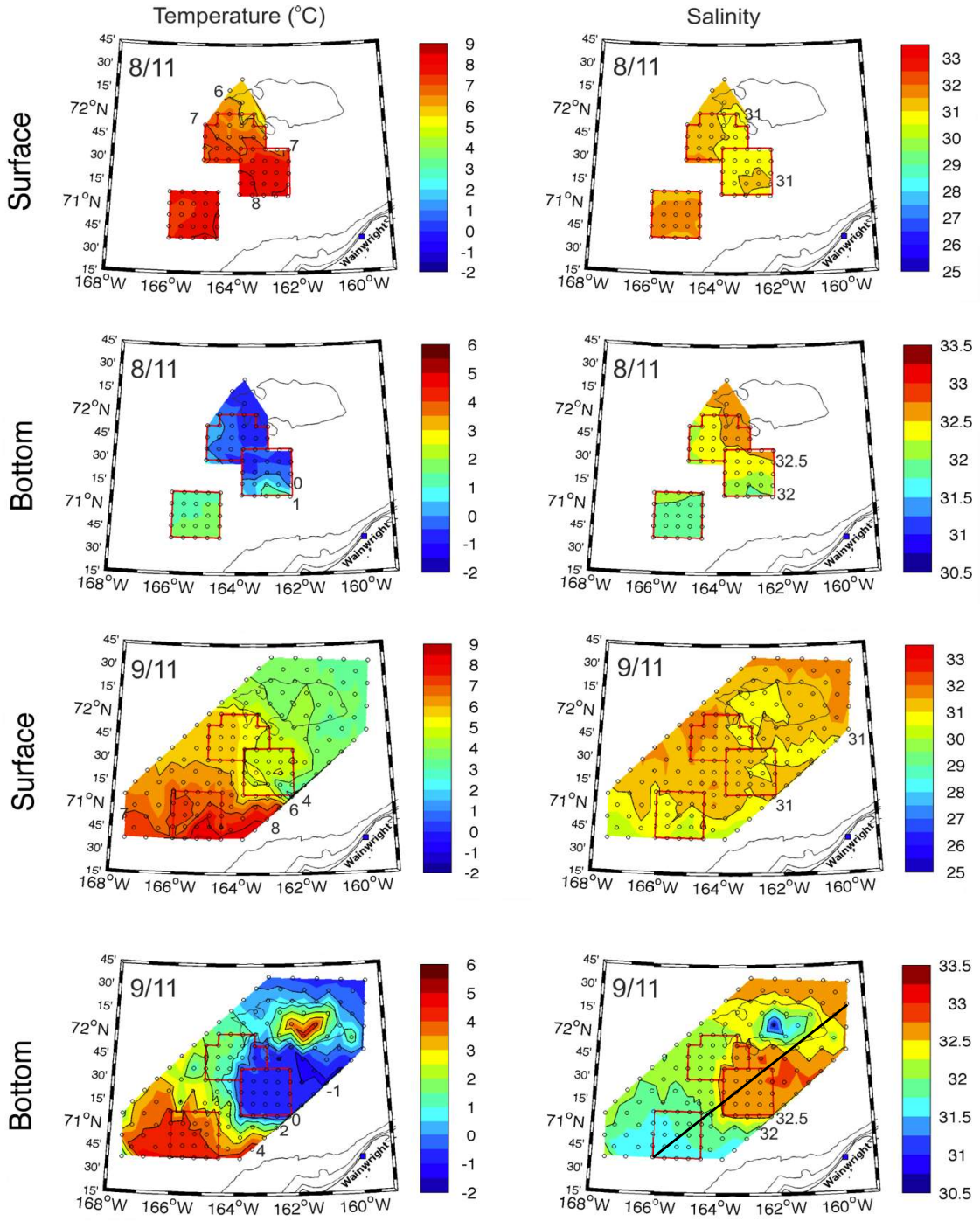

Figure 42. Plan views of temperature (left) and salinity (right) in August and September of 2011. The plan views are based on averages of the upper and bottom 10 m of the water column. The black line in the bottom right panel shows the location of the vertical sections shown in Figure 43.

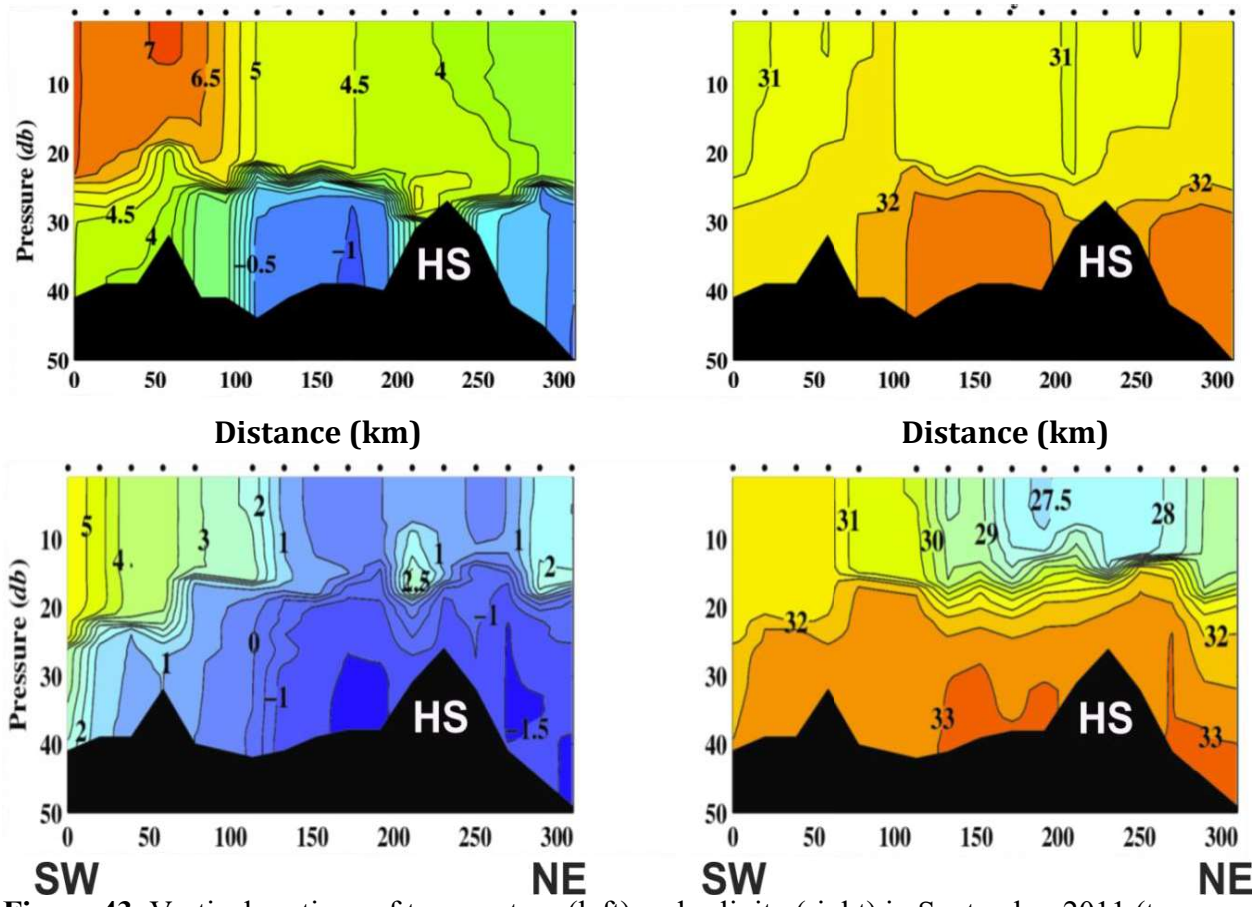

Figure 43. Vertical sections of temperature (left) and salinity (right) in September 2011 (top row) and 2012 (bottom row).

differences in stratification were due to the absence of MW in 2011 and its presence in 2012 (and in 2013).

Another important feature observed in the 2012 section was the presence, at km 225, of a "blob" of warm (~2°C) water, which was enclosed by the upward-bowing of the 29 isohaline above the blob and the downward-bowing of the 32 isohaline below it. This feature is probably an anticyclonic, intrapycnocline eddy that formed via a baroclinic instability of the MW/BSW front (Lu et al., 2015). The eddies appear to be common features of these frontal systems and are an important agent for lateral mixing and as a potential heat source for the underside of ice (Lu et al., 2015). The coarse resolution of the CSESP CTD sampling did not permit adequate horizontal resolution of these fronts. A more highly-resolved view of this front is shown in Figure 44, which was constructed from data obtained from the Acrobat towed-CTD data collected in September 2013 during the Norseman II recovery of the COMIDA moorings. The horizontal resolution of the hydrographic data on this section is ~250 m and more than adequate to resolve the ~10 km-wide MW BSW front centered at about km 30. Also included on the map to the right of the sections is a dotted line denoting the approximate location of the MW/BSW front as ascertained from CSESP data and other acrobat sections. We infer that the front is zonally-oriented and aligned along about the 71.5°N parallel. At its offshore end, the front very likely bends northward and parallels the Central Channel west of Hanna Shoal. It also bends northward along the western half of Barrow Canyon.

The figure also shows that there was a striking contrast in the chl *a* distribution to the south and north of the front. South of the front, the chl *a* concentrations were low and diffuse, but north of the front high chl *a* concentrations were compressed into thin sheets slightly below the pycnocline (the bottom of which coincides with the 26 σ_t isopycnal). These sheets were not horizontally continuous, but instead quite patchy. The lack of chlorophyll south of the front (associated with the BSW) is because these waters are nutrient-poor on the northeast self in August; phytoplankton having consumed the nutrients in these waters during their transport northward from Bering Strait. MW is devoid of nutrients whereas the WW is nutrient-rich (Codispoti et al., 2005). By residing at the base of the pycnocline phytoplankton growth was presumably aided by the availability of nutrient-rich water while residing within the euphotic zone. These thin patches embedded in the pycnocline may be very productive from summer through late fall, with much of this fixed carbon sinking to the bottom given the generally weak currents in this area.

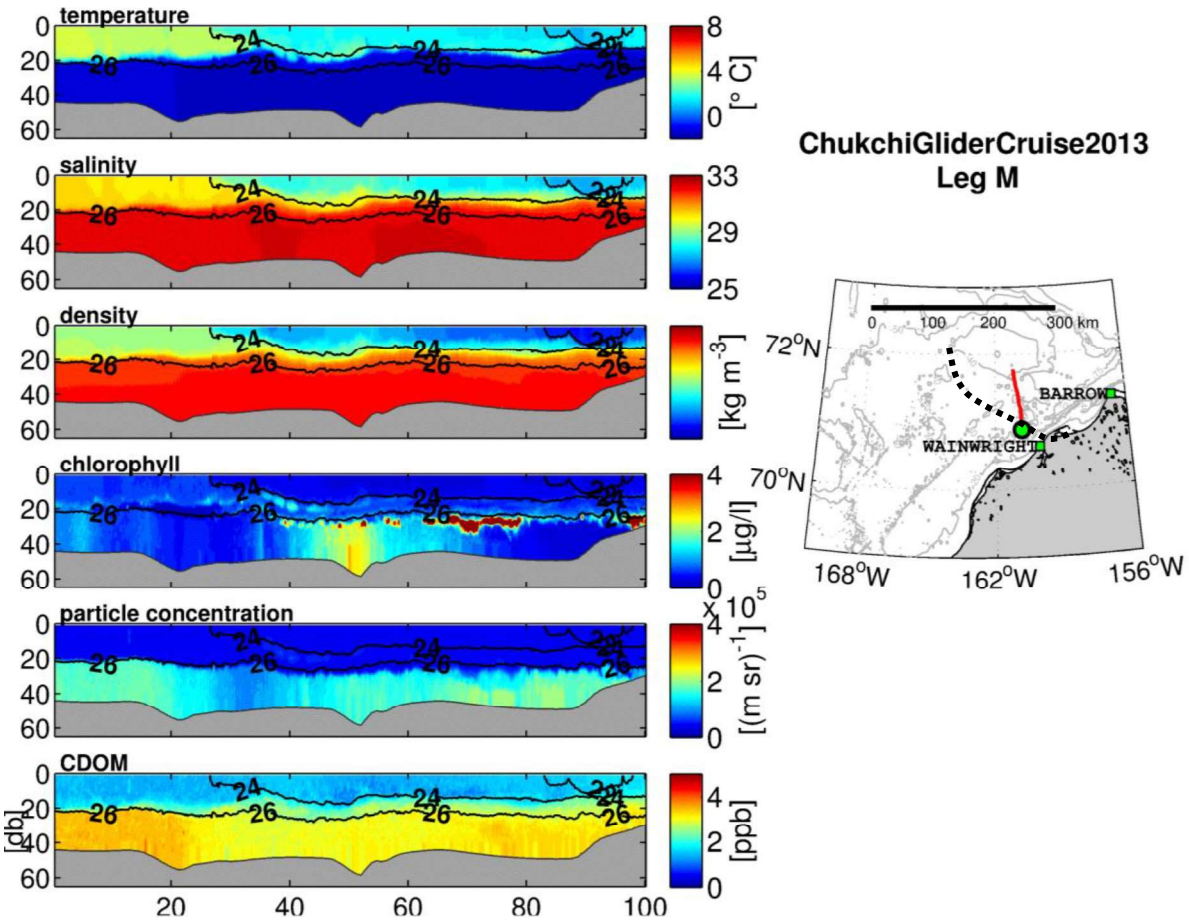

Figure 44. Vertical sections of (from top to bottom) temperature, salinity, density, chl *a*, particle concentrations, and CDOM (color dissolved organic matter) along the Leg M transect collected by the acrobat towed CTD unit in September 2013. The dotted line shows the approximate position of the MW/BSW front evident at km 30 on the section. The green dot shows the start of the transect, which corresponds to the left side of the section plots.

Figure 45 consists of vertical sections collected along the HSNW mooring line in September 2013 and provides another example of these eddy-like features. In this case several anticylcones were evident in the form of warm, intrapycnocline features encapsulated between the vertically-distended 30 and 32 isohalines. The temperature and salinity properties of these features clearly indicates a BSW source, because the waters above and below the pycnocline were MW and WW, respectively. Very likely these features arose due to frontal instability within the Central Channel.

We conclude with two other examples of these MW/BSW fronts. The first, shown in Figure 46, is a map of the weekly mean surface velocity vectors collected over the northeastern Chukchi Sea shelf during the week of 5 September 2012 from shore-based high frequency radars (HFR) in Barrow Wainwright, and Pt. Lay. The vector distribution suggests a convergence zone extending from west to east along about 71.5°N. North of this zone the surface flow is southward (and downwind based on the mean wind vector at Barrow during this time). South of the zone, the flow is northeastward. The convergence is roughly aligned with the positon of the fronts discussed previously and appears to extend eastward to Barrow Canyon.

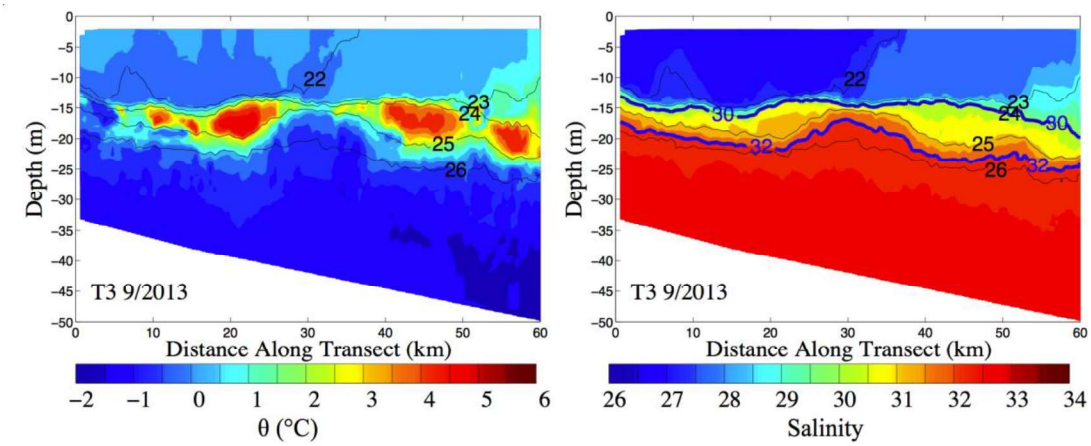

Figure 45. Temperature and salinity distribution along the HSNW mooring line in September 2013 (from Lu et al., 2015).

Surface current vector maps obtained in August and September 2011 showed no such features, which is consistent with the hydrography from that year. As might be expected the presence of mesoscale motions should yield differences in surface current variability. In 2011, the variance in both the zonal and meridional velocity components across the radar mask was half that for the same components in 2012. These differences cannot be attributed to differences in the wind regime between these two years for the variances in both wind vector components were identical in both years.

Figure 47 shows the trajectory of a 10-m drogued, satellite-tracked drifter that was released from the USCG *Healy* on 13 August 2012. Over its first 45 days the drifter's trajectory included a number of meanders and large excursions in SST, neither of which were associated with changes in winds. These variations in SST and trajectory path are suggestive (but not conclusive) that the drifter was entrained into mesoscale motions associated with frontal instability.

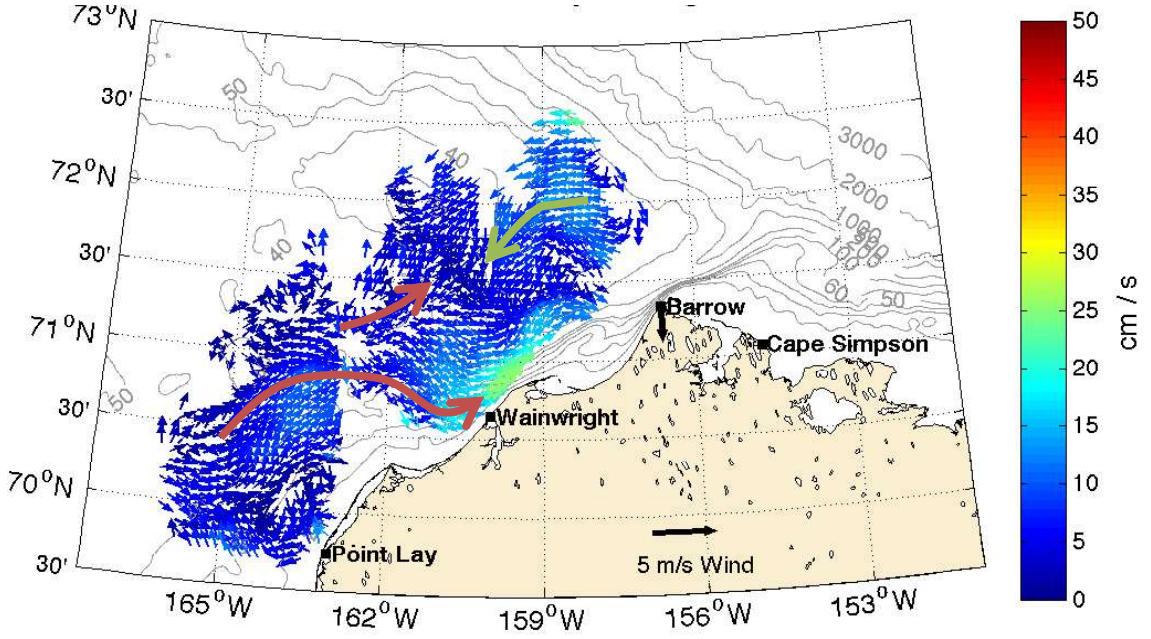

Figure 46. Mean surface current vectors for the week of 5 September 2012, as estimated from HFRs.

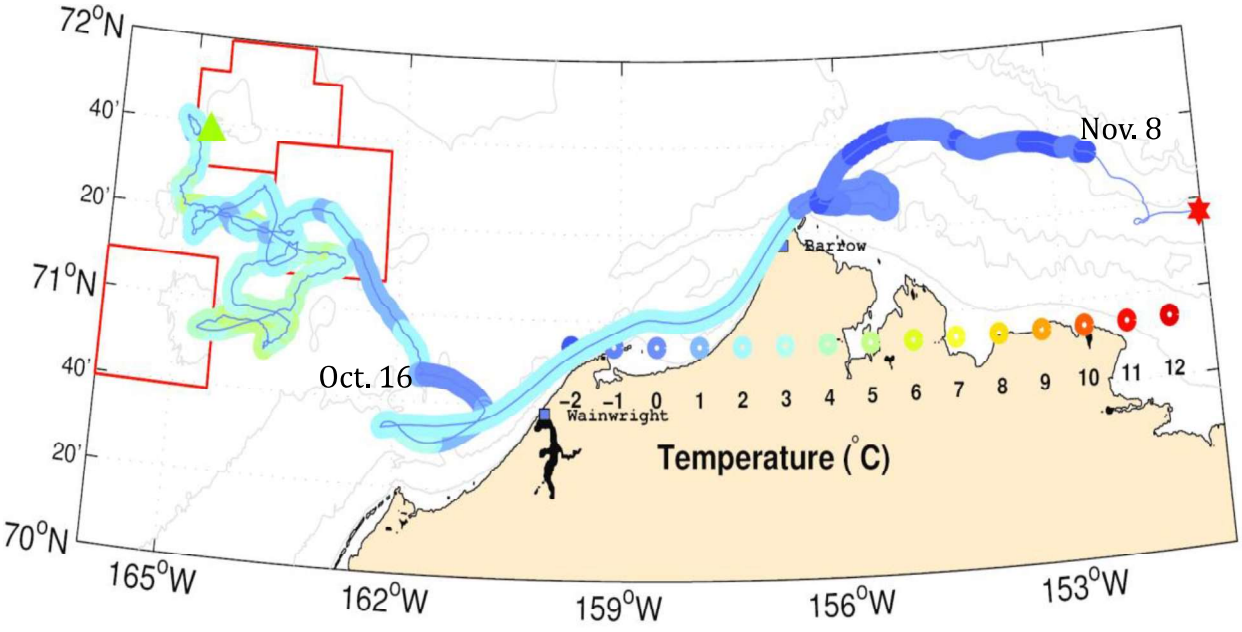

Figure 47. Color-coded (by SST) trajectory of a satellite-tracked drifter released at the location of the green triangle on 13 August 2012. The drifter's last reported position was on 15 November at the location of the red star.

4. Discussion and Conclusions

The goals of the physical oceanography component of the COMIDA program were to understand the time-varying circulation and water mass properties of the Chukchi shelf surrounding Hanna Shoal and to provide the physical context for the biological and chemical components of the program. In part our measurements were meant to address the results from numerical ocean circulation models (e.g., Winsor and Chapman, 2004; Spall, 2007) that suggested that mean circulation is clockwise around Hanna Shoal. We found that the ice and surface meltwaters are transported westward on average in response to the prevailing northeasterly winds. The vertically-averaged flow was eastward and parallel to the isobaths northwest of Hanna Shoal, in agreement with the models. Over the shelf to the northeast of Hanna Shoal the vertically-averaged flow was negligible or westward, in contrast to the models. These observations imply that there should be, on average, zonal convergence in the flow field north of Hanna Shoal. Presumably this convergence is associated with an off-shelf deflection of the eastward flowing water observed to the northwest of Hanna Shoal. Finally, in agreement, with the numerical models, the near-bottom circulation appears to be clockwise around the northwest and northeast flanks of Hanna Shoal. Other differences in the circulation characteristics between the northwestern and northeastern sides of Hanna Shoal included the enhancement in inertial energy and the greater vertical velocity shear of the sub-inertial flow in the east compared to the west.

There are several possible reasons for the differences in the circulation characteristics between the east and west sides of the Shoal. First the strong geostrophic, barotropic flow along the northwest side of the Shoal must weaken (although the transports should not change) proceeding clockwise around the Shoal because the isobaths diverge on the eastern side of the Shoal. Note that this weakening in the circulation implies a longer residence time for the waters east of the Shoal. This difference may be reflected in the chemical and biological composition of the water column and sediments. Second, the weaker geostrophic flow will be more susceptible to wind-driven reversals. In particular, these reversals will be confined primarily to the strongly, stratified surface layer. Recall that we inferred that the stratification eroded in early winter on the northwest side of Hanna Shoal, but remained strong and intact year-round over the shelf east of the Shoal. Third, the fall CTD data sets suggested that there may be horizontal density gradients, with less dense water moving eastward from the eastern side of Hanna Shoal. These density gradients will impel a counterclockwise baroclinic, geostrophic flow, via the thermal wind relationship, over the shelf east of the Shoal. If these density gradients prevail year-round they will compete against the clockwise barotropic flow.

The strong stratification, the deep clockwise barotropic motion, and persistent baroclinic pressure gradients should lead to greater velocity shear on the east side of the Shoal compared to the west side. Indeed, we found that the mean velocity profile on the shelf east of the Shoal had substantial shear, whereas the profile to the northwest of the Shoal had little shear.

These findings have significant implications on the disposition of various shelf water masses. The bottom waters to the northwest and northeast of Hanna Shoal vary seasonally in their composition. In late fall and early winter their temperatures were a maximum of from -1°C to 1°C and their salinities were a minimum of 31 – 32.5. Shelf waters south of Hanna Shoal typically reach the freezing point temperature in October or November (Weingartner et al., 2005). The fact that the bottom temperatures north of Hanna Shoal were well-above the freezing

point indicates that these bottom waters had 1) originated earlier in the summer from south of Bering Strait and 2) had minimal exposure to the surface waters during their northward transit in fall. There are two possible pathways by which these waters reached the northwest side of Hanna Shoal: via the Central Channel or Herald Valley. The latter is the more circuitous route (see Figure 1) as it involves westward flow across the Hope Sea Valley, northward flow in Herald Valley, and then eastward flow across the outer shelf north of Herald Valley. We tentatively suggest that Herald Valley is the source of this warm water at depth (Woodgate et al., 2005; Pickart et al., 2010) in late fall and winter, because previous (albeit limited) measurements indicate that temperatures are at or near the freezing point in the Central Channel by mid-fall (Weingartner et al. 2005).

During our summer and fall CTD surveys the bottom waters around Hanna Shoal consisted of dense winter-formed waters. The mooring time series shows that these winter waters appeared northwest of Hanna Shoal in late January when the observed ice cover of 100% effectively insulated the ocean. Winter waters occurred northeast of Hanna Shoal only in the following summer, well after melting had commenced. This implies that at both locations dense water was advected into the region from elsewhere; either from ice formation regions well to the south of Hanna Shoal or from around the immediate periphery of Hanna Shoal when latent-heat polynyas form in the lee of grounded ice on the Shoal. Our summer CTD observations indicated that very salty (>33) and near-freezing waters were trapped around the Shoal in both summer surveys. According to A. Mahoney (University of Alaska, August 2015), satellite images indicate that grounded ice was atop the Shoal during the winters of both 2012 – 13 and 2013 – 14 and that there were (at least) occasional polynyas formed in the lee of the grounded ice. This dense winter water and the meltwater released from ice the following summer are key ingredients in the formation of the strong regional stratification. We argued that this stratification eroded in late January northwest of Hanna Shoal, some 2 – 3 months later than the breakdown of stratification on the shelf south of the Shoal (Weingartner et al., 2005). A surprising finding was that heavy stratification remained intact year-round on the shelf to the east of the Shoal.

Our understanding of the hydrographic conditions around Hanna Shoal was aided by the inclusion of hydrographic data obtained by surveys undertaken by other programs around Hanna Shoal, including those well to the south of Hanna Shoal and much later in the fall to the northwest and northeast of Hanna Shoal. These data sets showed that Bering Sea summer waters (Alaskan Coastal Water and Bering Sea Water) were often found south of ~71.5°N in 2012 and 2013, with this approximate boundary defined by a strong, surface front (and a sub-surface front, not necessarily contiguous with the surface front) that separates the Bering summer waters from the meltwater. Although a complete characterization of this front was not achieved, it appears to extend zonally from the southwest side of Hanna Shoal eastward to the head of Barrow Canyon. We further surmise that the front extends northward and parallel to the eastern side of the Central Channel along the west side of Hanna Shoal. This supposition is based on three lines of evidence: the summer sea ice concentration maps, which effectively delineate the northward path of the Bering Sea Water in the Channel, both COMIDA CTD sections collected along the northwest side of Hanna Shoal in August, which captured waters clearly influenced by BSW, and the September 2013 acrobat section that detected intrapycnocline eddies along the HSNW mooring line.

These MW/BSW fronts appear to be baroclinically unstable, a process which leads to the formation of intrapycnocline, anticyclonic eddies that propagate across the front and that contain Bering summer waters. The existence of these fronts (and the associated frontal processes) and the strength and depth of the pycnocline in the COMIDA sampling area depends upon the meltwater distribution and its juxtaposition with winter water and Bering summer waters. In contrast to 2012 and 2013, there was no evidence of surface fronts in 2011 and the shelf stratification in that year was much weaker. These differences were attributed to the dearth of meltwater on the northeastern Chukchi shelf in 2011.

In addition to the meltwaters north of this front, cold, salty, winter-formed waters persist over the shelf bottom around Hanna Shoal throughout most of the year. This sub-surface front was present in all years and is likely a perennial feature of the shelf. Both the surface and sub-surface fronts are somewhat pliable boundaries that effectively divide the southern and northern portions of the northeastern shelf. South of the front, shelf water properties vary seasonally due to the annual influx of Bering Sea summer waters. The front constrains the northward movement of these summer waters (except through frontal instabilities). North of the front, the shelf has more of an arctic-flavor insofar as it is heavily stratified due to surface meltwater and very dense winter waters over the bottom. The circulation also changes on either side of the front. South of the front the summer waters are carried northward over the shelf from Bering Strait and then into Barrow Canyon. Here the shelf circulation is engaged in the meridional transfer of Pacific Ocean waters into the Arctic Ocean. North of the front the exchange appears to be primarily zonal. Meltwater and sea ice are advected westward and dense bottom waters are transported eastward.

We have begun processing the recently acquired industry data sets and while we are not in a position to discuss these in detail, two summary figures further substantiate some of the conclusions thus far stated and others reveal additional information on the circulation around Hanna Shoal. Figure 48 shows record length mean currents and variance ellipses for all moorings over the 2011 – 2012 deployment period in the northeastern Chukchi Sea. Maps were prepared for the vertically-averaged currents as well as those near the surface, mid-depth, and near bottom.

During the 2011 – 2012 deployment, the currents northwest of Hanna Shoal were eastward at all depths. With the exception of the surface currents, this result is identical to that obtained from the COMIDA moorings. The single mooring to the east of Hanna Shoal revealed negligible flow at all depths except at the bottom where the mean currents were eastward at ~1 cm s^{-1}. Along the southern flank of Hanna Shoal the flow was southeastward on average at ~3 cm s^{-1}. This flow would have transported waters from the southwest side of Hanna Shoal and the northern end of the Central Channel toward Barrow Canyon. These current vectors, as well as those closer to the canyon, also indicate that there is no net exchange between the shelf to the east and south of Hanna Shoal. (This contrasts with Spall's [2007] model prediction that on average some of the water east of Hanna Shoal flows over the shelf south of Hanna Shoal.) This supports our contention that the shelf east of Hanna Shoal is isolated from the shelf to the immediate south of the Shoal. Perhaps not surprisingly, these vectors are aligned roughly parallel to the sub-surface front that forms in summer between BSW to the south and WW to the north.

Consider next the currents measured by the three moorings south of 71.5°N. Within the Central Channel (~71. 2°N, 167.5°W) the flow was northward at all depths at ~ 5 cm s^{-1}. The two

moorings to the east of the Channel registered a mean eastward current of 2 – 3 cm s^{-1} implying that this flow would carry water from the Central Channel toward Barrow Canyon. Northeastward flow occurs only in Barrow Canyon.

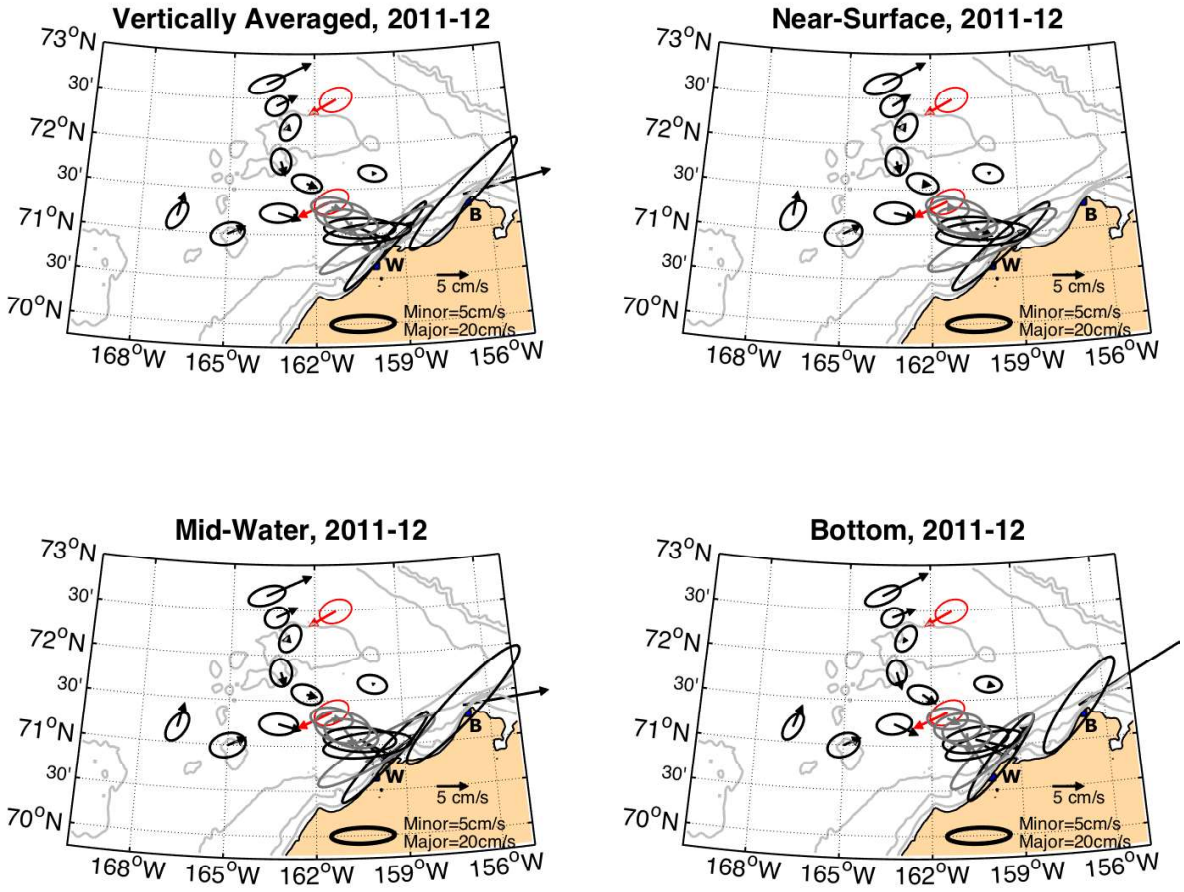

Figure 48. Record-length mean currents and current ellipses for all moorings in the northeast Chukchi Sea, 2011 – 2012. Red vectors and ellipses are for winds, grey indicate statistics based on less than one full year of data.

Figure 49 consists of similar maps for the 2012 – 2013 deployment. Although the mooring locations differ somewhat between the two years, there is remarkable similarity between the two deployments insofar as there is northward flow in the Central Channel and eastward flow south of Hanna Shoal toward Barrow Canyon. The mooring east of Hanna Shoal and south of the HSNE array shows results similar to the preceding year, i.e., very weak vertically-averaged flow, but a bottom flow that was eastward at ~2 cm s^{-1}.

These and additional mooring data from the northeastern Chukchi Sea are presently being analyzed to assess flow variations on shorter time and space scales and to examine potential forcing mechanisms. We will also be exploring the circulation coherence over this portion of the Chukchi shelf. Our measurements underscore the critical role that meltwater plays in this region.

In summer, the amount of meltwater present on the shelf depends upon the rate of sea ice retreat from Hanna Shoal and the adjacent northeastern shelf. We found no compelling evidence

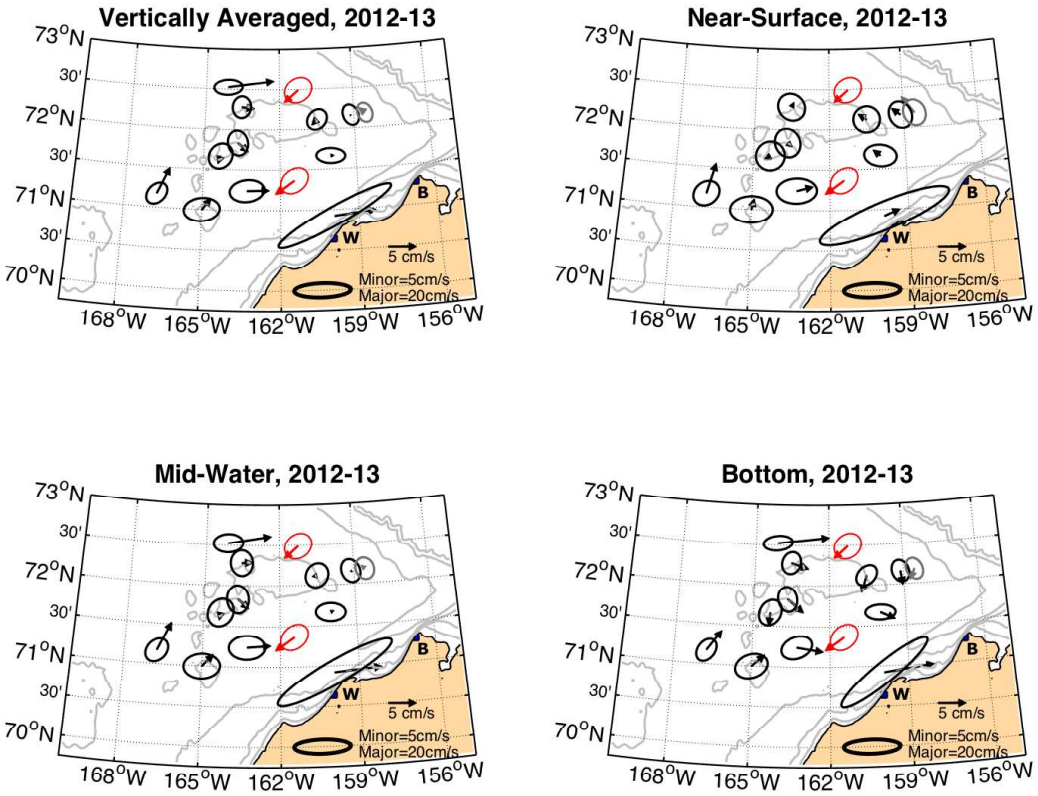

Figure 49. Record-length mean currents and current ellipses for all moorings in the northeast Chukchi Sea, 2011 – 2012. Red vectors and ellipses are for winds, grey indicate statistics based on less than one full year of data.

that the local winds controlled the August sea ice distribution over the COMIDA sampling domain. Nor have we found strong evidence that the winds from May through June affect the amount of summer ice cover in the Hanna Shoal region. We suggest that local and remote (in both time and space) processes are involved in determining the summer ice distribution. Recall that the COMIDA summer sampling occurred following winters when extensive grounded ice covered Hanna Shoal. Eicken and Mahoney (2015) contend that the thick ice that grounds on Hanna Shoal derives primarily from the highly deformed seaward edge of the landfast ice of the Alaskan Beaufort Sea. There are two requirements for this to happen. The first is that sufficiently thick (e.g., deformed) ice be produced by detachment from the seaward edge of the landfast ice zone. The second ingredient is that the detached ice drifts westward. Our ice drift measurements from the moored ADCPs show a mean westward ice drift and surface flow under northeasterly winds, which is the vehicle for transporting ice from the Alaskan Beaufort Sea to Hanna Shoal. We speculate that once grounded on Hanna Shoal, the ice may serve as a barrier to pack ice drifting over the Shoal that promotes additional deformation, grounding, and ice accumulation. We further hypothesize that if there is sufficient accumulation (and grounding) then the ice

remains intact well into summer. Hence, both a local process (e.g., grounding due to the local bathymetry) and remote processes (ice deformation, breakout, and the trajectory of thick ice floes during the winter) may be important in regulating the summer ice distribution over the Hanna Shoal region.

As an additional comment, we note that the interannual variability in ice concentrations over Hanna Shoal do not appear to be closely tied to variability in ice concentrations over the Arctic basin. For example, the heavy sea ice concentrations in the northeastern Chukchi Sea in summer of 2012 occurred when the arctic-wide sea ice extent was the third lowest in record (the other summers being 2007 and 2011) since the onset of satellite-based sea-ice record in 1979 (National Snow and Ice Data Center).

Interannual variations in the northward flux of heat through Bering Strait may also affect year-to-year differences in ice concentrations on the northeastern shelf. This heat flux increased nearly twofold between 2008 and 2011, primarily due to an increase in the mass transport through the Strait (Woodgate et al. 2012). The heat flux subsequently decreased to 2008 levels in 2012 before slightly increasing again in 2013 (Woodgate et al., 2015). A key difference amongst these years was that the sea-surface height difference between the Aleutian Basin in the Bering Sea and the Chukchi Sea shelf was much greater in 2011 than in the later years (Danielson et al., 2014) so that the large-scale pressure gradient that forces flow northward through the Strait and over the Chukchi shelf was stronger in 2011 than in 2012 and 2013. Interannual changes in this pressure gradient also will affect the magnitude of the wind-forced response of the shelf flow field. The interannual differences in heat flux from 2011 through 2013 roughly correspond to similar variations in the ice cover. The processes by which this oceanic heat flux may influence ice melt may depend upon more local processes, however, and include the wind-driven circulation, the degree of stratification of the summer waters moving northward from the Strait, and mesoscale processes associated with the marginal ice zone (Lu et al., 2015).

Summer sea ice concentration maps (including those presented here) consistently show an ice-edge embayment extending northward in the Central Channel and along the west side of Hanna Shoal. That indentation has been ascribed to the northward flow in the Central Channel (Weingartner et al., 2005 and see Figures 48 and 49) as well as the Taylor-column effect ascribed to Hanna and Herald shoals (Martin and Drucker, 1997). Our CTD measurements showed warm water moving clockwise around the northwest side of Hanna Shoal, consistent with inferences from satellite-imagery that the Central Channel is this heat source. We estimated that the ocean heat flux convergence (approximate at best and assumption dependent) was ~50 W m^{-2}, which must represent a substantial contribution to ice melt especially when dense fog (as was common on the August COMIDA cruises) scatters and absorbs the incoming solar radiation. Figures 48 and 49 indicate the mean northward flow in Central Channel. Our preliminary inspection of the Central Channel mooring time series (from 2008 – 2015) suggests that this northward flow varies but little from year-to-year and rarely reverses. As noted earlier, we do not believe that all of the water flowing along the northwest side of Hanna Shoal derives from the Central Channel. Rather we posited that some fraction of this transport derives from Herald Valley.

The COMIDA mooring data indicates that there must be flow convergence on the north side of Hanna Shoal. How this convergence arises is unclear, but one candidate mechanism is associated with the counterclockwise pressure gradient due to the inferred baroclinic pressure gradient on

the east side (at least) of Hanna Shoal. Regardless of the mechanism the observations imply that there is a cross-isobath transport, which would direct the flow northward toward the shelfbreak and deeper water rather than southward toward Hanna Shoal. If our contention is correct then it means that Chukchi shelf waters are being transported into the basin north of Hanna Shoal.

4.1 Recommendations

The results from the physical oceanography component of the COMIDA program have yielded an abundance of new information and insights on the Hanna Shoal portion of the northeastern Chukchi Sea. There are, however, a number of key issues that have emerged from our analyses that deserve future study. These are:

There is a strong eastward flow along the northwest side of Hanna Shoal, which extends to at least as far to the northwest as the 60 m isobath, but very likely even farther. This flow likely consists of water emanating from both the Central Channel and the mouth of Herald Valley farther to the west. Information is needed on how much water is flowing eastward from Herald Valley. This can be determined by deploying an array of moorings from south to north slightly east of the Russian-US Convention Line. We recommend that a meridional array of moorings be deployed between the 50 and 100 m isobaths to assess this transport.

Closely coupled to this issue is the need to quantify better the transport in the Central Channel. We believe that this could be done be deploying 2 – 3 moorings at the southern end of the Channel and 2 – 3 at the northern end to the west of Hanna Shoal. The moorings in recommendation 1 and 2 should include T/C/P recorders at multiple depths in order to assess the stratification.

We hypothesized that flow convergence occurs over the shelf to the north of Hanna Shoal. This possibility should be explored by conducting a zonal sequence of meridionally-oriented synoptic transects to examine water properties and the circulation here. This survey would benefit from concurrent VM-ADCP data and consideration should be given to deploying deep-drogued (i.e., 35 m) satellite tracked drifters to assess the deep circulation on the north side of the Shoal.

Two surprising and related observations were the year-round presence of heavy stratification and the inferred year-round counterclockwise baroclinic pressure tendency on the shelf east of Hanna Shoal. We surmised that the baroclinic pressure field opposed the barotropic pressure field in the upper half of the water column. These competing pressure fields are critical to establishing the weak circulation, the inferred convergence north of the Shoal and the water properties east of the Shoal. Verification of this baroclinicity could be done easily with carefully deployed array of moorings using ISCATS (which were deployed successfully in COMIDA) and/or a string of T/C/Ps. This deployment could be done in conjunction with the Chukchi Environmental Observatory (Danielson, pers comm.)

The persistence of sea ice (or lack thereof) in summer on Hanna Shoal has a profound influence on the regional circulation and hydrography. In addition, it also affects the regional biology through control of stratification and as habitat for walruses and other marine mammals. It may also play a key role in governing sources and sinks of carbon and the structure of the benthos. A prudent area of investigation would be to determine the sources of ice on Hanna Shoal, the mechanisms controlling these sources and those that affect its persistence or its ablation.

5. Acknowledgements

This study was funded by the US department of the Interior, Bureau of Ocean Energy Management (BOEM), Alaska Outer Continental Shelf Region, Anchorage, Alaska under BOEM Cooperative Agreement No. M11AC00007 as part of the Chukchi Sea Offshore Monitoring in Drilling Area (COMIDA).

6. References

Coachman, L., Aagaard, K., Tripp, R.B., 1975. Bering Strait: The Regional Physical Oceanography, Univ. of Washington Press, Seattle, 172 pp.

Codispoti, L., Flagg, C., Kully V., Swift J.H., 2005. Hydrographic conditions during the 2002 SBI process experiments. Deep-Sea Res. II, 52 (24-26): 3199 – 3226.

Eicken, H., Mahoney, A.R., 2015. Sea ice: hazards, risks, and implications for disasters. In: Ellis, J.T., Sherman, D.J. (Eds.), Sea and Ocean Hazards, Risks, and Disasters. Elsevier, Oxford, United Kingdom, pp. 381–401. doi:10.1016/B978-0-12-396483-0.00013-3.

Light, B., Grenfell, T.C., Perovich, D.K., 2008. Transmission and absorption of solar radiation by Arctic sea ice during the melt season, J. Geophys. Res., 113, C03023, doi:10.1029/2006JC003977.

Lu, K., Weingartner, T., Danielson, S., Winsor, P., Dobbins, E., Martini, K., Statscewich, H., 2015. Lateral mixing across ice meltwater fronts of the Chukchi Sea shelf. Geophys. Res. Lett., 42, 6754–6761, doi:10.1002/2015GL064967.

Martin, S., Drucker, R., 1997. The effect of possible Taylor columns on the summer sea ice in the Chukchi Sea. J. Geophys. Res., 102 (5), 10473 – 10482.

Mesinger, F., 19 Coauthors, 2006. North American regional re-analysis, Bull. Amer. Meteor. Soc., 87, 343–360.

Nikolopoulos, A., Pickart, R.S., Fratantoni, P.S., Shimada, K., Torres D.J., Jones E.P., 2009. The western Arctic boundary current at 152°W: Structure, variability, and transport. Deep-Sea Res. II, 56, 1164-1181.

Paquette, R.G., Bourke, R.H., 1981. Ocean circulation and fronts as related to ice melt-back in the Chukchi Sea. J. Geophys. Res., 86, 4215-4230.

Pickart, R.S., 2004. Shelfbreak circulation in the Alaskan Beaufort Sea: Mean structure and variability. J. Geophys. Res., 109(C4), C04024 10.1029/2003JC001912.

Pickart, R.S., Pratt, L.J., Torres, D.J., Whitledge, T.E., Proshutinsky, A.Y., Aagaard, K., Agnew T.A., Moore G.W.K., Dail H.J., 2010. Evolution and dynamics of the flow through Herald Canyon in the Western Chukchi Sea. Deep-Sea Res. II, **57**, 5-26.

Spall, M.A., 2007. Circulation and water mass transformation in a model of the Chukchi Sea. J. Geophys. Res. 112, C05025, doi:10.1029/2005JC002264.

Spall, M., Pickart, R.S., Fratantoni, P., Plueddemann, A., 2008. Western Arctic Shelfbreak Eddies: Formation and transport. J. Phys. Oceanogr., 38, 1644-1668.

Spreen, G., Kaleschke, L., Heygster, G., 2008. Sea ice remote sensing using AMSR-E 89 GHz channels. J. Geophys. Res. *113*, C02S03, doi:10.1029/2005JC003384.

University of Alaska School of Fisheries and Ocean Sciences. http://dm.sfos.uaf.edu/chukchi-beaufort/data/drifters/drifter_map_2013.php

von Appen, W-J., Pickart, R.S., 2012: Two Configurations of the Western Arctic Shelfbreak Current in Summer. J. Phys. Oceanogr., 42, 329–351.

Weingartner, T., Irvine, C., Dobbins, L., Danielson, S., DeSousa, L., Adams, B., Suydam, R., Neatok, W., 2015. Satellite-tracked drifter measurements in the Chukchi and Beaufort seas. Final Report, OCS Study 2015-022, Bureau of Ocean Energy Management. 171 p. http://www.boem.gov/Alaska-Reports-2015/

Weingartner, T., Danielson, S., Dobbins, L., Potter, R., 2014. Physical oceanographic measurements in the Northeastern Chukchi Sea: 2013. Technical report prepared for ConocoPhillips, Inc., Shell Exploration & Production Company and Statoil USA E&P, Inc. 52 p.

Weingartner, T., Winsor, P., Potter, R., Statscewich, H., Dobbins, E., 2013a. Application of High Frequency Radar to Potential Hydrocarbon Development Areas in the Northeast Chukchi Sea. Final Report to the U.S. Department of the Interior Bureau of Ocean Energy Management, Alaska Outer Continental Shelf Region, ConocoPhillips, Inc., and Shell Exploration & Production Company (Cooperative Agreement No: M09AC15207 as part of the BOEM Alaska Environmental Studies Program). 162 p.

Weingartner, T., Danielson, S., Dobbins, L., Potter, R., 2013b. Physical oceanographic measurements in the Northeastern Chukchi Sea: 2012. Technical report prepared for ConocoPhillips, Inc., Shell Exploration & Production Company and Statoil USA E&P, Inc., 64 p.

Weingartner, T., Dobbins, E., Danielson, S., Winsor, P., Potter, R., Statscewich, H., 2013c. Hydrographic variability over the northeastern Chukchi Sea shelf in summer-fall 2008–2010. Cont. Shelf Res. http://dx.doi.org/10.1016/j.csr.2013.03.012

Weingartner, T., Danielson, S., Dobbins, L., R. Potter, R., 2012. Physical oceanographic measurements in the Northeastern Chukchi Sea: 2011. Technical report prepared for ConocoPhillips, Inc., Shell Exploration & Production Company and Statoil USA E&P, Inc., 38 p.

Weingartner, T., Aagaard, K., Woodgate, R., Danielson, S., Sasaki, Y., Cavalieri, D., 2005. Circulation on the North Central Chukchi Sea Shelf. Deep-Sea Res. II 52: 3150-3174, doi:10.1016/j.dsr2.2005.10.015.

Weingartner, T.J., Cavalieri, D.J., Aagaard, K., Sasaki, Y., 1998. Circulation, dense water formation, and outflow on the northeast Chukchi shelf. J. Geophys. Res., 103: 7647 – 7661.

Winsor, P., Chapman, D.C., 2004. Pathways of Pacific Water across the Chukchi Sea: A numerical model study. *J. Geophys. Res.* 109, C03002, doi: 1029/2003JC001962.

Woodgate, R.A., Aagaard, K., Weingartner, T.J., 2005b. A year in the physical oceanography of the Chukchi Sea: Moored measurements from autumn 1990-1991, Deep-Sea Res. II, 52(24-26), 3116-3149.

Woodgate, R.A., Weingartner, T.J., Lindsay, R., 2012. Observed increases in Bering Strait oceanic fluxes from the Pacific to the Arctic from 2001 to 2011 and their impacts on the Arctic Ocean water column. Geophysical Research Letters 39, L24603. doi:10.1029/2012GL054092.

Woodgate, R.A., Stafford K.M., Prahl, F.G., 2015. A Synthesis of Year-round Interdisciplinary Mooring Measurements in the Bering Strait (1990-2014) and the RUSALCA years (2004-2011). Oceanography 28(3):46-67, doi:10.5670/oceanog.2015.57.

Trace Metals in Sediments, Water and Biota

John Trefry, Robert Trocine, Austin Fox

Department of Marine & Environmental Systems, Florida Institute of Technology,
150 West University Boulevard, Melbourne, FL 32901

jtrefry@fit.edu

Abstract

As part of the Hanna Shoal Ecosystem Study, concentrations of trace metals in sediments, seawater and marine biota were determined to establish a baseline for future reference and to explain observed spatial and temporal trends for selected essential or potentially toxic metals. This study was carried out during a period marked climatic change and increased human activity in the Arctic. Concentrations of 17 trace metals (Ag, As, Ba, Be, Cd, Cr, Cu, Hg, Mn, Ni, Pb, Sb, Se, Sn, Tl, V and Zn) in 44 surface sediments and 278 sediment core samples from the Hanna Shoal area of the northeastern Chukchi Sea (NECS) were essentially all at natural, background values. Ratios of metals/Al were used to determine background metal concentrations. All concentrations of the potentially toxic metals Ag, Cd, Hg, Pb and Zn were below published sediment quality criteria. No elevated Ba concentrations were found in contrast to previous studies in the NECS when sampling included historic drilling sites for oil and gas. Concentrations of As and Mn were high in some surface sediments and could be linked to subsurface, diagenetic remobilization of these metals with subsequent reprecipitation in surface sediments. Concentrations of dissolved trace metals in seawater were low and in close agreement with values for North Pacific surface water (As, Ba, Cr, Pb, Sb, Se and Tl) or North Pacific deep water for nutrient-type metals (Cd, Cu, Ni, and Zn). Concentrations of As, Sb and Tl varied by <10% in the NECS and followed salinity. Values for Cd, Ni and Zn were higher in bottom water; Cd correlated especially well with dissolved phosphate with a slope of 0.37 (Cd/P, mole basis) in close agreement with values of 0.34-0.40 for the northwest Pacific Ocean. Concentrations of Ag, As, Ba, Cd, Cr, Cu, Fe, Total Hg, MMHg, Mn, Ni, Sb, Se, Sn, V and Zn were determined for the following organisms and tissue types during 2012 and 2013: mixed zooplankton, whole clams (*Astarte borealis*), whelk muscle (*Neptunea borealis*), snow crab muscle (*Chionocetes opilio*) and arctic cod muscle (*Boreogadus saida*). The primary focus of this effort was on total Hg and monomethyl Hg (MMHg) in biota because of the keen interest and concern for Hg contamination in the Arctic. Concentrations of MMHg biomagnified from 4 ng/g (d. wt.) in zooplankton to 13 ng/g (d. wt.) in clams to 165 ng/g (d. wt.) in whelk. Despite this distinct biomagnification of MMHg, concentrations of inorganic Hg were relatively uniform at 20 ± 5 ng/g (d. wt.) across the food web with no discernible biomagnification. Results for other metals are also presented and discussed here to provide a baseline for future assessments.